November 2018

Materials and Methods to Fabricate Porous Structures Using Additive Manufacturing Techniques

Mohsen Ziaee
University of South Florida, m.ziaee99@gmail.com

Materials and Methods to Fabricate Porous Structures Using

Additive Manufacturing Techniques

by

Mohsen Ziaee

A dissertation submitted in partial fulfillment
of the requirements for the degree of
Doctor of Philosophy in Mechanical Engineering
Department of Mechanical Engineering
College of Engineering
University of South Florida

Co-Major Professor: Nathan Crane, Ph.D.
Co-Major Professor: Rasim Guldiken, Ph.D.
George Nolas, Ph.D.
Craig Lusk, Ph.D.
Thomas Weller, Ph.D.
Wenjun Cai, Ph.D.

Date of Approval:
September 10, 2018

Keywords: Binder Jet Printing, Fine Stainless Steel, Varied Density, Powder-Bed Fusion, Demineralized Bone Matrix, Shrinkage

DEDICATION

To whom my greatest debt belongs to; my lovely parents. Thank you for the altruism, love, encouragement and unwavering support you have provided me upon which my efforts rested.

To my brothers Mehdi O Milad for being with me in good times and in bad, and acting as my sounding board and safety net through the many battles we have shared.

ACKNOWLEDGMENTS

First of all, I would like to thank Dr. Nathan Crane, my wonderful advisor. You helped me to fulfill Ph.D. with the wealth of your knowledge and support. I wish you happiness and success in the years to come.

I would like to thank Dr. Ayesha Mahmood and Lifelink Tissue bank for fostering the idea of the second part of the project and subsequently funding it.

Thanks to my committee members for their fruitful feedback and contribution in evaluating the dissertation.

I would also like to take this opportunity to thank my teachers and my friends through my education whom are too numerous to be listed. You all helped me get where I am today.

Thanks to Matt for the sense of humor and all the help with my dissertation. Thanks to Efe for making the lab atmosphere friendly with entertaining conversations. Thanks to Justin, Clayton and all those who made a fun-learning work place here in IDRB-lab#207.

TABLE OF CONTENTS

LIST OF TABLES

LIST OF FIGURES

ABSTRACT

Additive Manufacturing (AM), as the name implies, produces three-dimensional objects by progressively adding material rather than cutting away unneeded material. Typically this is done by processing a series of cross-sections obtained from a Computer Aided Design (CAD) model of the object. AM systems can process liquid photopolymers and solid materials in form of powder, wire and laminates to create intricate geometries in a short lead time.

This superb capability of AM methods enables to locally suit the properties of the part for the desired function by incorporating the designed pores in the CAD model [2]. The pore gradient creation opens up a new route to a wide variety of properties such as varied density, optimized strain distribution, tuned thermal conductivity, etc. [3-5]. But, the minimum feature size of the AM systems restricts the lower limit of the pore size. So, as an alternative, temporary space holders are introduced to the base material to introduce stochastic fine pores [6].

Nevertheless, processing powders has been notorious for reduced mechanical properties as a result of the residual voids within the compact. Further, the voids may cause distortion in the part during the post-processing and can lead to a significant deviation from the intended CAD geometry.

The inter-particle voids could impose more problems in fabricating parts with varied density can be even more due to shrinkage variation. In spite of these drawbacks, the high demand of porous structures in industrial and medical applications propels the researches to explore new ways to fabricate the parts with compatible shrinkage.

The first part of the work studies that how processing of fine 316L steel powder would influences on density and shrinkage of the final parts. The agglomeration of the base powder and mixing in temporary space holders were practiced to treat the raw powder. The prepared powder stocks must meet the spreadability criteria to allow printing proceed successfully. After screening the final parts, the processing methodologies that result in nearly same shrinkage level but different final densities are promising to create a multi-level porous part. Of the printed parts in this study, the agglomerates treated at 185℃ reached ~95% full density whereas the 25Vol% Nylon mixture led to 30% less density. The similar shrinkage of these parts is a key step toward creating spatially-controlled porosity with compatible shrinkage in all directions.

The second part of the dissertation utilizes powder-based AM to process Demineralized Bone Matrix (DBM) particles for tissue engineering applications. We combined the geometric freedom of AM advantage with biological benefits of natural bone to fabricate scaffolds. The spreading behavior of the granulated bone and polycaprolactone (PCL) composite was studied to identify the spreading device and conditions to enhance the compaction level of powder bed which later on were used in sample creation step.

A novel AM method that projects visible light to selectively treat the powder bed i.e. Large Area Projection Sintering (LAPS), was the first approach assessed to process the bone based implants. The mechanical properties of the samples showed that the LAPS-fabricated composites of 45-55% bone particulates produced strength comparable to cast composites and demineralized cancellous bone as two conventionally fabricated methods. The LAPS had a rather short process time but showed limited capacity in defining fine features as the low absorptivity of visible light by PCL required long heating times.

In order to overcome the challenge and define a cleaner geometry, a CO_2 laser was utilized as the second candidate fabrication method. To retain bone biological features, the safe operation window of variables including laser scanning speed, line spacing and the power range were determined. The best power setting was selected to provide adequate strength without burning while maintaining flat layers after processing so that a new layer could be spread. Then the green samples were cured under different heat treatment conditions and, finally, the shrinkage level and mechanical properties of the as-manufactured samples were determined. The mechanical strength analysis suggested that the material ratio and the heat treatment conditions are the two critical factors that enable to tune the final mechanical properties of the parts to match up with that of the host tissue.

CHAPTER 1: INTRODUCTION

1.1 Abstract

This chapter provides an overview on additive manufacturing and goes into more details for the methods used in this dissertation. Furthermore, the strategies to incorporate porosity in additively manufactured parts will be discussed. At the end, the objective of each chapter will be summarized.

1.2 Additive Manufacturing (AM)

The first commercialized additive manufacturing machine emerged in 1988 from 3D Systems. Since then AM industry has grown; its market value surged to over $6 billion in 2017 and is forecasted to surpass $10 billion by 2021 [1, 7, 8]. Compared to the early models, however, the principle of the AM systems has remained the same. Any AM machine creates physical objects directly from Computer-Aided Design (CAD) models with virtually no geometric constraints through building successive layers [9].

By extending AM to different industries, the printing mechanism has been adapted to new material systems. From material perspective, AM systems are classified into two major categories each of which involves a number of minor classification explained in books [10-12].

In this dissertation, the discrete particles of solid materials were processed by means of chemical bonding and heat energy source which is the highlighted route in red color in Figure 1.1.

Despite AM boom over the past decades, the researchers are pushing boundaries of this technology to make this approach a mainstream fabrication method and perhaps someday in the future, majority of the objects around us are made by this evolving fabrication method.

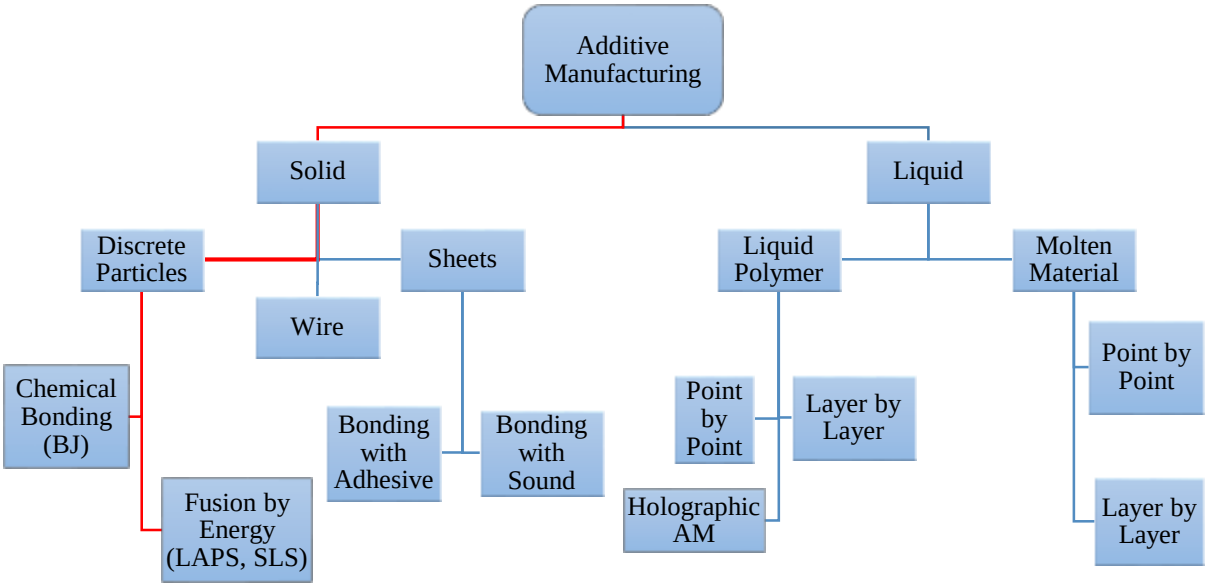

Figure 1.1. Classification of the AM systems based on physical state of the processing materials (adapted from Reference [1])

1.2.1 Powder-Based Additive Manufacturing

Powder is an attractive material for manufacturing. It is easy to handle and more importantly, many of the engineering materials can be turned into small particles. Moreover, the powder-based methods share the benefit of reusing the unbound particles and typically eliminate the need for sacrificial supports. In order to dispense the powders and create successive layers, a spreading tool, either roller or scraper (blade), delivers powder onto the building stage so that they selectively adhere to each other by means of heat or a chemical agent. But first, powders must form a defect free layer. Thus, flowability and spreadability are the initial criteria to select a suitable powder.

In this dissertation, three type of the powder-based machines were employed i.e. Binder Jetting (BJ), Large Area Projection Sintering (LAPS) and Selective Laser Sintering (SLS).

1.2.1.1 Binder Jet (BJ)

Typical Binder Jet (BJ) systems use adhesive liquids to bond the layers. The high rate of dispensing, excels the processing speed over the other AM methods. Further, thanks to applying glue to form the geometry, the method is versatile and can process polymers, metals and ceramics with fairly cheap equipment.

Yet, the deficit of the BJ printing lies in nature of the process where there are voids within the printed body. Therefore, the resultant body almost always requires further post printing operations-typically high temperature heat treatment and/or infiltration with a lower melting point material which adds on the cost and the lead time of this method. Additional challenge of the BJ-made parts is associated with dimension reduction during heat treatment operations. The pore gradient across a part complicates the challenge and may lead to a non-uniform shrinkage.

In this research the effort has been focused on identifying the pre-processing on the powdery material which yield to different final density yet compatible dimensional change. The results pave the way to create a multi-level dense part by binder jet printing.

1.2.1.2 Large Area Projection Sintering (LAPS)

The Large Area Projection Sintering (LAPS) is newly invented method by the University of South Florida. The LAPS system uses photonic energy in the visible range to provide the fusion energy. In this method, the whole image of a cross section is projected on the material and increases the processing rate. However, due to the technological limitations, aside from polymeric materials, it seems unpractical to directly build metallic or ceramic objects by using LAPS. Moreover, in the visible light range the color of the material plays an important role on energy absorption, so

processing translucent or bright-colored materials is quite challenging. This issue prolongs the processing time and reduces the resolution of printing for low absorption materials.

1.2.1.3 Selective Laser Sintering (SLS)

In Selective Laser Sintering (SLS), the heat is provided by a small laser beam to sinter the powders. SLS is able to process polymers, metals and ceramics. However, the processing variables for each material has to be optimized; the excess energy is more likely to leave residual thermal stresses in the construct and damages the dimensional accuracy while insufficient power leads to reduced cohesion within the layer. In addition, for metals, the high temperature of sintering spot necessitates using a protective inert gas such as argon or nitrogen to shield the material from unwanted oxidation.

1.3 Porous Structure Fabrication by Powder-Based Additive Manufacturing

The structural and functional characteristics of porous materials have created a high demand in different realms of industry. Porous structures offer light-weight, high surface area to volume ratio and good energy damping [13]. Examples of industries that broadly use porous structures include aerospace, filtration, purification, acoustic and medical to name a few [14]. Based on the application demand, the pores could be interconnected, closed-cell or both.

Where the geometry of the part gets complicated, AM is a potential solution to respond. Superior versatility of AM over the traditional methods, allows direct control on pore creation. The precise implementation of the 2D slices even offers optimization of the pore structures based on the loading conditions during part service life preventing premature failure of the construct. Another simple way to change void fraction is to use material of different morphology. The large particles tend to have more inter-particles voids and are favorable to produce parts with lower density.

The addition of pore forming agents or altering powder morphology has long history in powder metallurgy and has been practiced in AM-made parts as well [15]. The space holders are removed in a post-processing step. Depending on the chemistry of the agent it can be thermally decomposed or leached out by submerging in a solvent which would leave void spaces behind in the final product.

The coalescence level of the powders in powder bed fusion methods depends on thermal energy which makes the processing variables important in pore formation. The heat treatment during post processing may not be a crucial step for the produced structures of this method. In contrast, in the BJ, due to nature of the process, the weak bonding between the particles leaves a high fraction of porosity in the compact which, to some extent, can be transferred to the final part. However, since heat treatment is inevitable, the final pore structure within the end part largely depends on sintering/firing process.

1.4 Objective and Scope

This dissertation aims at fabricating porous structures by powder-based AM approaches and it can be divided into two main phases.

The first phase uses Binder Jetting (BJ) technique to process fine stainless steel particles. The objective of this part is to address processability challenge of fine particles and identify the treatment methods that result in varied density with compatible shrinkage. The result of this part has potential use in engineering applications.

The second phase of this dissertation pushes the boundaries of fusion based AM to process human bone/polymer composites. To retain the biological benefits of the bone particles, energy source of two different wavelengths within the non-ionizing range were utilized to thermally process the materials. The scaffolds are bio-absorbable, in a sense that they decompose in body as

the tissue repairs and thus there would be no need to another surgery to take out the implant. The results of this phase opens up a new window to fabricate temporary patient specific scaffolds which are expected to show superior bio-functionality.

1.5 Dissertation Outline

The next two chapters (Chapter 2 and 3) constitute the first phase of the work and are on fabrication of porous structures by binder jetting (BJ).

Chapter 2 gives an exhaustive review on BJ systems. As the first step of BJ processing, spreading methodologies of particles in both dry and wet state are reviewed. Then considerations in binder selection, a brief review on two main classes of print heads, and strategies for binder deposition are discussed. The interaction of binder and powder bed, as the key player in print quality, as well as the potential routes to mitigate the printing defects are reviewed. Then the papers on sintering, key materials and application of the BJ are presented.

Chapter 3 is on binder jet printing of fine stainless steel 316L powder with varied porosity fraction. The two material preparation procedures are explained and the required adjustments of printing variables to process each of the treated powder stock are discussed. After sintering the samples, the density variation and dimensional accuracy of samples of each treatment method are evaluated.

The second phase of the dissertation, chapter 4, chapter 5 and chapter 6, are related to fabrication of medical scaffolds by using LAPS and SLS.

Chapter 4 provides a literature review on additive manufacturing application in scaffolding. Then the potential of LAPS and SLS in medical field is discussed. The key concepts of bio-absorbable scaffolds and incorporating bone particles are presented. Final section of this chapter is devoted to creating porous scaffolds.

Chapter 5 is on utilization of LAPS method to process the bone/PCL composite. The experimental procedure including identifying the proper material ratios, layer formation and sample fabrication is presented. Then the resultant 3D parts were compared to the natural bone tissue and casted composites as the reference controls for tensile strength. In the last section of this chapter, the hydration effect on tensile strength of the samples was assessed.

Chapter 6 uses SLS to process the bone/PCL composite. This chapter starts with optimization of the processing variables to determine the safe operation window over which biological features of the bone are not altered. Then the samples are fabricated and tested to evaluate their ultimate tensile strengths.

Lastly, chapter 7 compiles the work's results and outlines the future plans.

CHAPTER 2: A REVIEW OF BINDER JETTING PROCESS

2.1 Abstract

Binder jetting is a low-cost AM method that can be applied to a very wide variety of materials. The binder jetting process brings together many different technologies to adapt the concept to different material systems. This chapter will address key concepts in each of the printing component and summaries the recent advancements in this areas.

2.2 Overview

Binder Jetting (BJ) was invented in 1992 at the Massachusetts Institute of Technology [16]. Two years later Z Corporation obtained exclusive license from MIT [17]. Several companies became successful machine developers such as ExOne, ZCorp (purchased by 3D Systems in 2012) and Voxeljet [10, 18]. As patents expire, additional companies will likely enter the marketplace including startup Desktop Metal [19]. BJ offers many potential advantages as an AM process. It can work virtually any liquid adhesives and powdered feedstock and can incorporate graded materials.

BJ has been adapted for different materials since its birth. It also has a relatively high build rate because it only needs to print the binder-a fraction of the total part volume. For example, a 100-nozzle print head can create parts at up to approximately 200 cm^3 /min [20]. Machines are available with large build volume such as 780 mm × 400 mm× 400 mm for metal parts and for sand casting machines are available for continuously manufacturing parts with width and height of 850 mm× 500 mm with no limitation on the length [21, 22]. However, the process produces a green part which must be post-processed to final properties. The quality of these final products

controls the application space for the process. These final properties depend on many process parameters including raw material, powder bed formation, build parameters, and post processing methods, much research has been and continues to be done to more fully realize the process's potential [23].

2.3 Binder Jetting Process

Figure 2.1 illustrates a typical binder jet system. For each layer of part, a layer of powder is spread—typically using a counter rotating roller. Afterwards inkjet print-head jets the liquid binding agent to the powder bed to create the 2D pattern for the layer. Some binder/powder systems may use heaters to help control moisture and curing, but heat is not a basic process requirement. After each layer, the build platform is lowered to make room for the next layer and the process is repeated. The powder-bed serves as a natural support material eliminating the need for printed supports. The as-printed parts are fragile and typically are post-processed to improve the mechanical properties [24, 25].

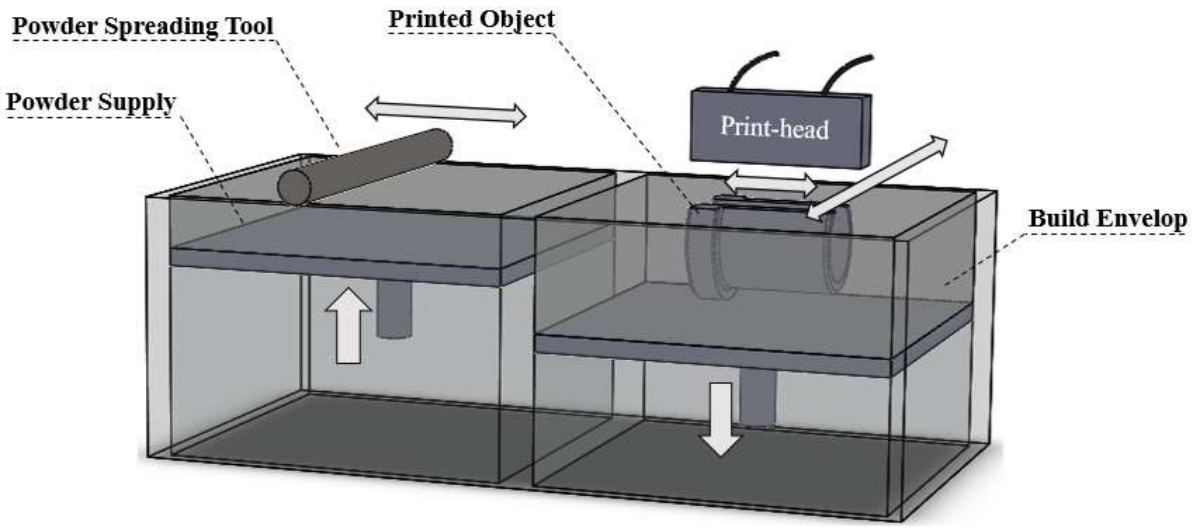

Figure 2.1. Schematic layout of a binder jet system.

Binder jetting has received less attention than low cost methods like fused deposition material and direct metal methods, but it has a strong potential for high speed and low cost manufacturing. This combined with the expiration of the early patents has generated an increased interest in this process from both industry and academia. This chapter summarizes the work on the aspects of this technique namely process, materials, methods and post processing. Finally, application of binder jetting in various industries is reviewed [26].

2.4 Powder Deposition

Powder is the foundation of BJ, therefore the proper deposition mechanism is a key component to building parts reliably and quickly. While powders can flow similar to fluids, their behavior is more complex. Inter-particle forces can vary with size, shape, composition, and humidity and may require different approaches to reliably form dense defect free layers. The powder flow characteristics determine the deposition method. For the standard powders around 30 μm have been processed in dry state while the smaller sized ones may require agglomeration or surface treatment. For the finest size ranges, the powder is often dispersed in a fluid to improve packing density and consistency.

One of the primarily concerns in BJ is how the powders lie when deposited. The importance resulted from the fact that in a less compact powder, intense shrinkages may cause defects. Besides, the arrangement of the particles in powder-bed fundamentally influence on the fired density. Typically for the monosized spherical powders, the powder-bed gets packed up to around 60% of the true density [27]. Theoretical studies on optimal packing configurations provide a helpful guidance on feasible limits [28-30], but typical powders deviate significantly from the ideal. For example, they are rarely monosized and may not be spherical or smooth.

BJ is perhaps more sensitive to powder packing than most other methods because the powder packing in the green body is directly related to the final structure. Discrete element modeling is a powerful tool to better understand powder packing and handling processes [31-35].

2.4.1 Dry Powder

Powder is very attractive as a raw material in AM because it can be handled plus many materials are available in a powder form. The ideal powder material will uniformly flow like a liquid with negligible force between the particles. Usually powders greater than 50 μm flow with small shear force but with declining the size, the challenges arise due to the acting forces between the powders and the free flow behavior weakens [36]. Flowability of a dry powder can be quantified via number of measurements e.g. static repose angle, Hausner ratio, mass flow through an orifice and powder internal cohesion [37-41]. Yet, depending on the powder storage and processing conditions the flowability characteristics may deviate from the predictions.

While flowability is a prerequisite for layer formation in BJ, it is insufficient to guarantee a successful printing. For instance Butscher et al. indicated that large calcium phosphate powder (with d50=51 μm) show excellent flow behavior but the layers displace during the process and the printing fails. They found the mean particle size in the range of 20–35 μm as the most promising size to have required flowability, powder bed surface roughness and maximum compaction rate [42].

2.4.1.1 Spreading Method

A proper deposition mechanism is a key to build the parts in a reliable and fast rate. A variety of early deposition methods were examined to lay down the uniform layers [43-45] but they were not able to meet the industry demands. In the commercial systems, the feedstock is placed next to the build platform in a feed piston that is raised to provide material for layer

formation. An alternative to the above mentioned way, is using the hopper feeding system. The reservoir in this case is above the powder-bed rather than beneath. To fluidize the powder, the hopper shakes and deposits the powder from the reservoir in front of spreading tool. The hoppers could be incorporated to change the material layer-by-layer enabling process of multi-material parts in a single print job [46].

Variations on these basic methods have been studied and shown to have some ability to improve powder spreading [47, 48]. Researchers have shown that the rotation rate and traverse speed has negligible impact on powder packing unless the spreading tool is vibrated to reduce the inter-particle shear force [48]. Seluga demonstrated an increase in spread density of coated 17-4PH steel powder from 39% to 51% by adding vibration to a roller. But that linear and angular speed of the roller ridged the layer surface and imposed a second pass with no rotation just to evenly level the layer surface [49].

The dry powder can be further compacted by performing double-smoothing method. Such procedure involves two levelling steps with dispensing an additional layer of powder in the interim. Shu reported a drastic improvement in green density of alumina from 43% to 70% by switching the spreading mechanism from vibrated rotational roller to double-smoothing method [50]. This method is advantageous over the conventional roller system in terms of the resultant green density, restricting layering defects and uniform structures within printed parts [50].

Further packing the materials can be achieved using mechanical vibrating compaction techniques and/or by applying acoustic energy to the deposited powder. Sachs et al. integrated an acoustic transducer system to supply acoustic energy to the surface layer into a BJ system. Vibration was used to vibrate the platen and blade to settle the powder therein [51]. However they

did not compare the density promotion using as-said spreading system. Recent advancement in powder deposition was achieved by double-smoothing the layer [50].

To increase spread density beyond the monomodal packing limits, one proven solution is the use of bimodal powder mixtures in which fine powders are added that fit in the spaces between the larger particles. The analytical evaluation of the particle packing are built upon two primary theories proposed by Furnas [52, 53] and Andreasen [54]. In these researches the models repeatedly have used four functions to evaluate porosity level in the packed particles; particle shape, modal size differences in multimodal distributions, mean particle size and size distribution [55-62]. For number of the monosized particles of different morphology, packing fraction has been computed or measured e.g. for discs [63], thin rods [64] and ellipsoids [65]. Computer modelling of various geometries of particles is addressed in references [66-73].

Due to the meager control on powder arrangement, the packing density of feedstock mixtures has been experimentally studied in many references [3, 74-78]. The results of the studies demonstrate that high packing density can be achieved when the volume fraction of fine powder is between 20-40 Vol.% [79, 80]. McGeary showed that for the spherical powders if the size ratio of fine to coarse powder is 1:7 then by mixing in 30% fine powders the packing level experience 30% increment. On the downside, employing fine particles (< 5μm) may cause clumping and spreading difficulties [81]. The experiments conducted on the Gaussian and log-normal size distribution bimodal mixtures proved that the packing density depends upon the compositions of the binary and packing density of the individual compositions. Maxima occur at compositions of 55-75% larger component and increasing mean-size ratios lead to greater packing densities [82].

In spite of the rich source of analytical and empirical works on powder packing, these principals are barely applied in powder selection of layer-wise AM methods since adding fine

material is associated with a risk of poor flowability and size separation in handling. In BJ systems researchers achieved smoother surface finish [83] and greater fired density [80] by using multimodal material. On the negative side, the fine additives increase the required pressure and time for binder infiltration into the powder-bed which can result in printing problems such as balling [84].

2.4.2 Fine Powders

Spreading problems of fine particles is a prime obstacle in layer-wise AM processes, fine powders have more surface area that makes them sensitive to environmental conditions [85] and amplifies the impact of inter-particle forces that increase cohesive strength of unpacked powder—reducing flowability during handling and feeding process [86]. This results in non-uniform powder packing and shrinkage variations that cause distortion during sintering.

Yet, smaller particles are favorable for higher resolution and thinner layers [87]. Additionally, high specific surface energy improves sintering characteristics. This is particularly valuable in fabricating materials with high melting points such as ceramics [88] or tungsten [89]. Pressureless sintering of refractive materials require very high temperature and long sintering time which leads to undesirable grain growth and weak mechanical properties [90]. These advantages of small powders has motivated exploration of new ways to tackle fine powder spreading.

Adding press-rolling to the printing sequences has been reported a successful way to improve the deposition homogeneity of fine powders [91]. Other practices to improve bed density include modification of the particles' morphology to mitigate surface roughness [92-96], adding nano-sized guest particles [94], and use of powder agglomerates [6, 97, 98].

2.4.2.1 Slurry

As particles reach approximately one micron in size, electrostatic and other forces dominate gravity and spreading an even layer of dry powder is unsuccessful [99]. To overcome the challenges the powder is dispersed in a liquid to form a slurry [100]. The slurry is sequentially deposited through nozzles on a porous medium to wick out the liquid and then stabilized by jetted binder [101, 102]. During putting down the slurry, solid, liquid and gas phases are present that may result in critical challenges such as bleeding, bubbling, cracking and segregation [103-106]. A typical slurry formulation involves plasticizer, binder, dispersant and defoamer that necessitates optimization of the constituents. Theoretical models [104, 105] as well as computer simulations [107-109] provide insights to tailor rheological characteristics of the slurry. Investigation on minimizing the crack formation is carried out by stress relaxation test in which the substituents fractions can be optimized [110-112]. But in many cases optimal amounts are found by trial and error [100, 102, 113-116].

Slurry layering is rather a slow process, however, it has some advantages mainly in terms of the print resolution, smaller feature definition and improved sinterability [117]. Further benefit is that porosity and composition can be localized in micron or submicron level by depositing different materials separately from nozzles [118, 119]. Fine alumina perhaps is the most common ceramic processed by slurry BJ. Grau et al. demonstrated that the layers of alumina can reach green densities of 60%- 67% and exceed 99% of the theoretical density after firing [119, 120]. They also mentioned that the stair stepping defect was nearly eliminated for the layer heights of 100 and 150 μm and the surface finish tremendously enhanced in comparison with dry processing [119, 120].

Several other materials have also been attempted to be used through the slurry based BJ. Wang et.al produced gradient-index lenses with Alumina-doped silica [121]. Further examples of

the processed slurries include; utilizing Nickel oxide–yttria stabilized and lanthanum strontium manganite to create porous structures for full cells [122] and tungsten carbide/cobalt oxide to create tungsten carbide cobalt [123]. Some metal oxides could be reduced to the corresponding metals through the thermal-chemical post-processing [124]. Williams utilized metal-oxide powder system containing iron oxide, nickel oxide, cobalt oxide and molybdenum which was reduced in post processing to produce Maraging steel with ~60% theoretical density [124].

2.4.2.2 Methods of Depositing a Slurry

Slurry deposition in binder jet context shares many aspects with traditional ceramic fabrication methods. The first step of creating a layer is implemented by depositing slurry evenly on a porous substrate such as plaster through slip or tape casting [117]. In the slip cast method the individual deposited lines of slurry are deposited then stitch together and slip cast while in the tape casting a thin film of the paste is levelled by doctor blade in one pass [100]. Before depositing a fresh layer, the previously deposited material has to be dried otherwise bleeding makes ragged dot edges [103].

The slip cast method is prone to forming an undulating surface where the discrete deposition paths stitch to each other. The inter-line defects compromise the strength of the printed part [115]. Bjorn used a single orifice raster system and examined three devices to mitigate the stitching defect; spinning arm, moving belt and bicycle wheel apparatus out of which the last device was able to create smooth surfaces with the barely seen ridges in a particular operating window [100]. He showed that if the time between deposition of adjacent lines was reduced sufficiently, the size of the ridges could be practically eliminated [114].

Tape casting is primarily used in manufacturing the substrates. Benefits of the tape casting approach include easy control of the sheet thickness, higher production rate, smaller device

footprints and tailoring the powder concentration for each layer [125, 126]. These advantages make it a preferable route in producing ceramic microelectronics such as RF resonators, capacitors and dielectric insulators [115, 127, 128]. By varying the powder concentration, the composition of the material can be altered which allows fabrication of gradient index (GRIN) lenses with Alumina doped silica [121].

2.5 Binder Selection

Introducing new materials to BJ systems necessitates considering requirements in binder selection. For any BJ process, the binder, in the first place must be printable. An ideal binder would have low viscosity which allows the stream of individual droplet beads to form and then break off from the nozzles rapidly [84]. Also, binder must have chemical stability against the large shear stress induced by actuators [129]. The proper interaction with the powders, burn out characteristics, shelf life, hazardousness of waste and product composition constraints are additional criteria considered in binder formulation [130, 131].

In general, for dry-based deposition two methods are used to initiate the primary bonds between the particles; In-Liquid and In-Bed binding mechanism. In the former. First; the binding agent entirely is carried by jetted liquid while in the latter a rhetorically simple liquid is printed and interact with the dry glue particles embedded in the powder bed and bonding bridges are initiated upon hydration [132, 133].

In comparison with In-Bed mechanism, the In-Liquid solutions [134-136] cause more premature failure of print-head due to drying of the glue agent in the nozzles but offer wider range of powder systems [25, 118, 137-139]. Instances of commonly used In-Liquid binders that contain organic cross-linking agent [140] are butyral resins [141], polyvenyls [142], polysiloxanes [143],

polyacrylic acids (PAA) [144] and acrysol [145] which typically thermally decompose and leave little residue [132, 146, 147].

The adhesive agents in the In-Bed binding mechanism are usually leached out in post-processing and leave voids in the structure. Therefore this binding formulation is not favorable to produce dense high strength objects [132, 148, 149]. Instead, researchers have fabricated porous structures by composition of aqueous solutions and In-Bed agents such as starch [148], dextran [148] and maltodexterins [150]. Silica colloids are another well-known exemplary of the inorganic solution that interact with an acid e.g. citric acid and undergo a pH reduction from ~ 9-9.5 to ~7.5 preventing binder from excess migration [141, 151].

In some cases, the application of the manufactured part needs to be incorporated in binder formula. For example, in sand casting applications the existing binder in the printed mold is exposed to the molten materials in high temperatures. This requires considering the burn out characteristics of the binder as it could potentially create gases that trap during the process causing defects in cast products [131]. No-bake binders such as furan meet the constraints and predominantly are used in such applications [152]. It should be noted that, the amount of binder has to be carefully determined otherwise during casting either the excessive gas would emit [153] or the mold/core structure would be prone to erosion [154]. An exhaustive review of the binding methods and formulation can be found in reference [132].

2.6 Wetting of Powder

In BJ process, the binder and powder interaction is both profoundly important and very complex. Thus far, researchers have performed many experiments and proposed multiple models to predict the binder droplet interaction with the loose powder-bed. One of the first studies on interaction of a liquid on a porous medium was conducted by Wenzel wherein the model predicts

the contact angle of a liquid resting on a surface with homogeneous chemical composition [155]. But if the air pockets trap in the surface grooves, the heterogeneity of the surface increases the hydrophobicity of the surface for which case typically Cassie-Baxter model is used to predict the contact angle [156]. The two models are applicable in many cases [157-163] yet are insufficient to explain the kinetics of the droplet sitting on the powder-bed surface.

The roughness of the powder-bed acts as a surface texture that tends to amplify the inherent tendency toward wetting or non-wetting behavior. It can turn a weakly wetting surface into a non-wetting surface [84]. However, overtime the liquid may slowly infiltrate into the powder to reach a Wenzel state due to the capillary force and to lesser degree gravity [164-168]. As a result the air pockets are no longer thermodynamically stable and liquid begins to migrate through the particles [169-171]. Less wetting powders can also form liquid marbles and hybrid structures [172, 173].

Later, models incorporated the impact of a droplet on a rigid porous substrate. The models relied on experimental works and demonstrate that the Weber and Reynolds number are the two key dimensionless numbers in droplet spreading on the substrate [174-176]. The actual powder-bed tends to have a heterogeneous bed structure with the presence of macro void spaces. Hapgood et al. defined a new parameter, effective porosity (ε_{eff}), to propose a two phase model to incorporate the large void spaces [177]. The equation can also include gravity and viscosity and then be analyzed by using some functions such as Lambert function [178].

Aside from these models, researchers have used imaging techniques to study the actual case of binder and powder-bed wetting interaction by ejecting a single droplet on surface of the powder-bed. The fluid properties, impact kinetics coupled with surface geometrical morphology and compositions have been examined for a variety of the materials and impact conditions [165, 179, 180].

In a typical binder dispensing process, the stream of 60,000 individual beads per second successively strike the surface at 9-10 m/s. The kinetic energy of the droplet is of the same order of magnitude as the energy of the surface energy of the wetted powder and interactions with adjacent droplets can have a significant impact on droplet absorption characteristics. This complexity necessitates conducting experimental investigations to fully understand the liquid/powder interaction [84]. Some of these studies are presented in Table 2.1. The impact followed by the binder infiltration could be a root cause for some printing defects. For example the droplet momentum disturbs the powder-bed and may eject the particles from their original place. This problem is often found in processing the fine particles and is referred as ballistic ejection. Efforts have been taken to tackle this issue by enhancing cohesiveness of the powder-bed. Adding moisture and/or a chemical fixative to the surface were reported effective to stabilize the powder-bed [181].

Table 2.1. Summary of the reported works on wetting of a powdery medium

Research objective	Variables	Ref.
Droplet rebound	Impact velocity	[182, 183]
	Wetting liquid	[182]
Droplet spread thickness	Impact velocity	[180, 182]
	Wetting liquid	[180]
Droplet spread diameter	Impact velocity	[182, 184]
	Humidity content	[182]
Droplet penetration time	Powder bed characteristics	[185, 186]
	Wetting liquid	[177, 182, 183, 186]
	Impact velocity	[177, 182, 183, 187]
	Humidity content	[182]
Agglomeration	Impact velocity	[188, 189]
	Wetting liquid	[188, 189]
	Powder characteristics	[190]
	Formation mechanism	[189]
	Saturation level	[191]

Another printing issues that might happen on the powder-bed surface are balling and splashing. In the former, the binder infiltrates at a slower rate rather the binder delivery. Therefore the binder droplets coalesce to each other on powder-bed surface and then form large liquid beads to reduce surface energy. To overcome this defect the wetting of the powder/binder system needs to be improved which requires altering surface tension of the binder, binder viscosity, powder size/shape, or coating the powders with hydrophilic agents [27]. Droplet infiltration rate can also be increased by using smaller droplets [192].

In splashing phenomena, the binder droplet disintegrates into smaller satellite droplets. The break ups mostly occur in the last stage of spreading [181], rebounding [174] and in rare cases at the beginning of the contact because of the perturbations [179, 181]. The weber number along with the underlying surface roughness have been studied to determine the conditions that prevent splashing [176, 193].

The powders adhere to each other when the binder starts migrating between the particles from a fully saturated zone into the pores network. As a result the air pockets are partially filled with binder-defined as saturation level [6]. As Bredt showed, the liquid permeation in loosely packed powders depends on saturation level and capillary pressure which are inversely correlated to each other [151]. However the product of the two factors does not impact the liquid wicking direction and the pore distribution in the powder compact is the key player [151, 192].

The smaller pores exert more attraction rather the large void spaces. Therefore binder is transported unevenly and a pressure gradient is created. The gradient reduces as the particles rearrange until a uniform pressure is attained through the moistened powder volume control [194]. If the equilibrium is realized rather late, two defects might appear in the print; feathering and bleeding. The undesirable migration of binder in microscale outside the intended geometry is

known as feathering which damages the feature definition sharpness. The bleeding is the severe case of the defect wherein the gravitational force overcomes the hydrostatic pressure and the liquid flows downward out of the print boundaries [151].

In order to control the excess wick of binder within the powder some strategies might be applied. On commercial BJ machines the saturation level is an adjustable variable and can be further controlled by performing a heating process –typically by crossing over a heat lamp - after binder dispensing to reduce the fluid content. Another option is using a viscous binder which may cause dispensing problems and shorten the print-head service life [26].

In addition to the methods mentioned above, in some cases a second phase of material is mixed into the bulk powder to alter the rhetorical properties of the binder as it penetrates into the powder-bed [195]. The migration control substance can either be dissolved by the binder or initiate a chemical reaction to form a gel, both of which will decrease hydraulic conductivity in the compact by increasing the binder viscosity [194]. However, this approach, up to present, is applicable for a limited material systems- as discussed in "Binder Selection" section.

2.6.1 Basic Hysteresis of Wetting That Traps Liquids in Powder

The binding agent aggregates the particles together by forming liquid bridges between them, but liquids cannot penetrate into poorly wetting or non-wetting powders. This condition generates a printing defect called "balling". These "balls" will usually cause difficulties in spreading subsequent layers. The balls can form liquid marbles consist of a liquid core with a surrounding powder shell, which can be dried to form a hollow granulate [185]. This problem is reduced by using smaller droplets, larger powders, or by improving the binder/powder wetting through powder coatings or binder additives.

2.7 Printing

The mechanical properties and aesthetic quality of the part largely depend on the binder load of printing. Insufficient binder cannot join the powders firmly and the printing process will fail [196]. By the same token excess binder may cause undesired travel of binder within the powder bed which in turn is deleterious to density and dimensional accuracy [20]. Binder load is function of multiple parameters; The droplet dispensing duration and frequency, the binder beads size, the distance between the constituent lines of 2D slices (referred as line spacing) all can effect on lateral and vertical migration of binder during feature formation [197].

On standard binder jet systems typically the saturation level and drying conditions are optimized by trial and error. The printing saturation level is defined as the percentage of the powder void space that is filled with printed binder. Typical saturation levels are around 60%. In many cases, the binder is partially dried after each printed layer. This helps to improve spreading of the next layer by removing surface moisture and can also reduce the saturation level to decrease the chance of bleeding. As saturation level depends on the void fraction of the spread layer density, an alternative printing parameter termed the "binder level" is defined that is powder bed independent. The binder level represents the fraction of the part volume that was filled with powder and is related to the saturation level and the powder bed fraction packing [6, 198].

A number of efforts have been taken to apply the optimization processes to tune the saturation level for different materials. For instance the Taguchi optimization method was utilized for stainless steel 420 [199] and 316L to identify the equilibrium saturation level and the resultant parts showed enhanced mechanical characteristics [200]. Recently Miyanaji et al. introduced a physics-based model based on the binder and powder bed interactions to precisely determine the saturation level [201]. They reported that the internal microscopic surface areas that do not

contribute to the wetting of the powder, could result in overestimation of the optimal saturation levels [201]. Aside from the models, he experimentally derived graphs, like the one shown in Figure 2.2 can correlate saturation level to hydraulic permeability, and precisely determine the saturation level as they incorporate complexity of the real cases [84, 192, 201].

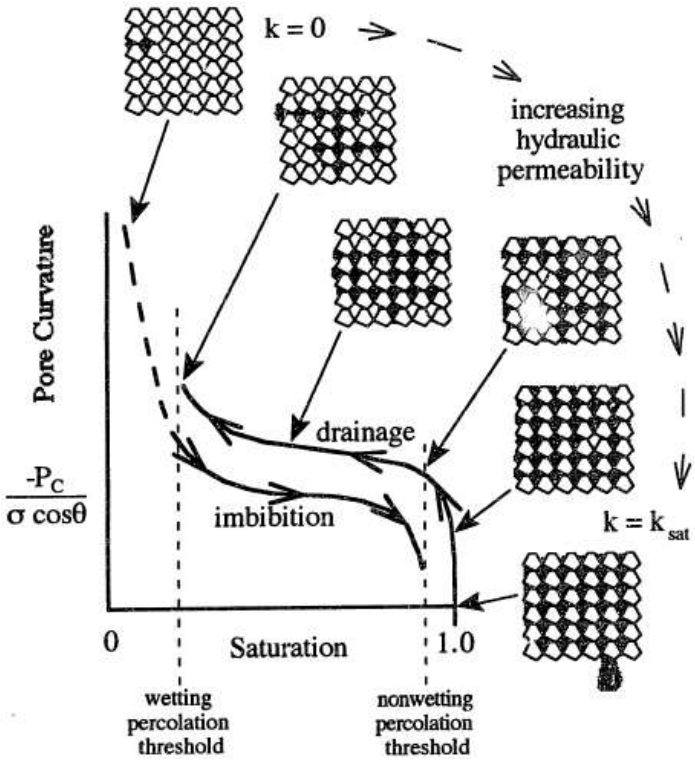

Figure 2.2. A typical capillary pressure-wetting fluid saturation curve. Reprinted with permission from [84]. Copyright permission is included in the appendix A.

In order to define sharp edges and clean geometries, the droplet generators must issue a precise amount of binder and the binder beads must be accurately steered toward the desired areas of the powder bed. The strike of binder droplets on the powder bed forms clusters of bound particles known as primitives. The primitives coalesce and create lines which ideally stay stable with two parallel sides until they coalesce and solidify. Davis suggested that the stability of the liquid rivulets depends on the contact angle of the liquid on the medium and conditions of the moving bead stream[202] which later on was confirmed for a number of inks and mediums [203-

205].Therefore the binder formation devices that reliably dispense binders are compelling to be utilized on the BJ machines.

2.7.1 Print Head Technologies

Two major technologies to generate binder beads in 3DP are continuous jet (CJ) [206] and Drop-on-Demand (DoD) [207] both of which have a few sub-categories [208].In the CJ print heads, the ink is vibrated near the Rayleigh frequency of the stream at high frequencies namely ~100 kHz to squeeze out a constant stream of the droplets [209] making it a favorable choice for high printing rate and large coverage areas. To somewhat control the continuous droplet beads, electrostatic field is utilized to deflect any unwanted droplets to a reservoir (gutter) for recycling. Also the droplets can be steered to mitigate the step stair defect at the edges of the 2D slices [49], even though in reality, surface energy minimization tends to smooth out these effects significantly anyway.

The DoD class of print heads, when needed, issue droplets at lower rate - on the order of ten kHz or less. The rather slow rate of binder bead formation enables ink composition manipulation during printing but CJ print heads necessitate supplying inks from separate reservoirs[210]. Further advantage is that in defining sharp edges where a high accelerations is induced to trace around small radii, DoD print heads are preferred [49].

Typical ways to create pressure pulses to issue droplets are piezoelectric transducers [211] and fast acting heaters [212]. The other alternatives technologies for these systems are liquid spark jetting [213, 214], electro hydrodynamic inkjet [215], electro-rheological fluid jetting [216], focused acoustic beam ejection [217]. Comprehensive information on these various methodologies can be found in references [216, 218]

2.7.2 Droplet and Line Spacing

The landing position of droplets depends on print head speed, drop-to-drop distance and line spacing. These variables can be manipulated to adapt the pattering strategies [83]. Often, the print heads are spaced farther apart than one line spacing and so they will make multiple passes. It is also possible that they would print every other droplet so that they have time to absorb before printing the droplets between them. However, this would add a second pass and reduce the production speed.

In ideal cases of BJ, the individual droplets quickly are absorbed into the powders, coalesce and leave cohesive primitives after solidification [219]. The line spacing must be sufficiently low such that the formed lines stitch to each other and create a cohesive layer [220]. Theory suggests that the diameter of a single primitive line can be estimated by multiplying the root square of the droplet spacing in a constant value-which depends on the combination of binder and powder-bed [221]. In practice, however, the mean diameter proportionally varies with droplet size, dispensing rate, binder incident velocity, powder morphology, binder dose and wetting condition [222, 223].

Small line spacing poses the risk of oversaturation and bleeding but as the spacing increases, beyond a critical point, marginal stitching appears. A study on a bimodal alumina showed that when droplets land at closer distance to each other the resultant line segment would be defined cleaner. However there is a lower bound for the droplet spacing as otherwise the high binder dose degrades the resolution of the print by forming large diameter lines[83]. So the smoothest geometry was achieved for lower drop-to-drop distance and removing excess liquid by heating the surface with a lamp after binder dispensing [27].

2.7.3 Vector, Raster, Vector with Raster Fill

In BJ technology the print head could traverse over the powder bed based off the three scanning alternatives; simple vector, raster and vector trace with raster fill style. In the vector scanning type, a stream of droplets generate the outline contour of the part geometry and moves inward to progressively trace smaller contours until entire layer is completed. Vector process is the most accurate process and produces the smoothest exterior, but is also the slowest. The layer printing time depends in particular on the complexity of the layer.

A more detailed discussion on the vector operation and assessment of resultant test geometries can be found in reference [224] for two different DoD print head types.

In raster based scans the print head moves back and forth on X direction of XY plane over the straight lines. Between the steps the print head moves one line space in Y direction and the process starts over for the new line path. As a result, a stair-stepping effect appears from line to line similar to that in the z direction [225]. The major benefit of the raster system over the vector based machines is the ability to increase speed with additional print heads. Since in raster fashion the print head moves over the entire object footprint, if the surface area to volume ratio of model is large, a major amount of time would be wasted with only little value added to the print. Some systems subdivide the fill area into smaller square regions and use switchable raster scans between the squares [10].

The third possibility of scan is vector trace with raster fill which is combination of the two basic vector and raster scanning styles. This scanning strategy has the same footprint as the vector approach but instead of using one nozzle - for the basic vector and raster style - the entire nozzles of the print head would be involved in the printing process during the raster phase of printing. This scanning style drastically increases the layers definition rate and shortens the required time to

complete the print [27]. Further, compare to the raster printing, an improved surface finish as well as cleaner edges could be attained [225].

2.7.4 Layering Conditions

Of the key variables of the print, the layer thickness is found a dominant factor on the print characteristics. It has been proved that thinner layers mitigate stepping stair defect and for most of the powders improves the mechanical properties of the print [20, 88]. Doyle et al. investigated layer thickness effect on 420 stainless steel with bronze infiltrant. They reported around 30% increment in ultimate tensile strength by reducing layer thickness from 200 μm to 50 μm due to the chemical alteration of the composition [9].

The orientation of the print can also be manipulated to accommodate the print(s) in the build envelop or to reduce the printing job time. There are inconsistent conclusions as to the print orientation role on the print characteristic. Doyle reported that the mechanical characteristics of the 420 steel powders print negligibly depends on orientation [9], whereas Farzadi et al. showed that it matters for plaster-based powder and a water based solution with 2- Pyrrolidone as a binder [226].

2.8 Post-Processing

After printing, the green body is embedded in unbound powder. To convert the part to an end-use product, a series of post processing steps must be completed based on the powder and binder used. Key steps that are part of many post processing methods are summarized below.

2.8.1 Powder Removal

The printed part must be separated from the unbound powder. However, some binders require post processing to achieve adequate strength before the parts can be extracted. Often this is a drying or thermal curing process.

The binder chemistry determines the treatment process which might be; reduction of a salt-based binder [227] and conversion of a preceramic polymer[220]. However, the most common case is heating in a furnace to remove residual solvent and possibly initiate reactions such as cross-linking in the binder. Further polymerization can be carried out by using other curing options include visible light, vacuum, heat, and pressure [228]. The key requirement in all the treatments is that the manipulation should not alter the unbound particles properties or consolidate the entire the powder-bed.

Generally for dry processed powders, after curing the binder, the "green" part must be carefully removed from the powder bed by brush or air gun in a de-powdering station. Depending on the complexity of the cured portion, depowering can be either simple or delicate work. For the slurry based BJ, part retrieval is trickier. The fine powders and organic additives typically used to stabilize the slurry, the unprinted regions are cohesive and cannot be simply brushed away. Instead, the unprinted region of the powder bed is re-dispersed by placing the powder bed in a liquid solvent or in an ultrasonic cleaning bath [229]. The unprinted powders retrieved in powder removal stage can usually be processed and re-used.

2.8.2 Sintering

The green parts made by BJ are generally complex and unique and the particles are held in place by adhesive polymer. So the green parts must undergo a high temperature heat treatment (sintering) to densify and attain the required strength for most applications. During sintering, the parts are heated and transport (predominately diffusion) reduces surface free energy, alters the geometry of the raw material to form bonds between particles. Depending on the material phase present in the process, sintering is divided into two main classes; i.e. solid state and liquid state sintering [230] which have been discussed in books [230-233] and review articles [234, 235].

Sintering is a common practice in injection molding method and shares many aspects with BJ fabricated parts. Since typically the BJ green bodies have fine features, the pressing operations- which are commonly utilized in powder metallurgy- are not a general solution. The quality of sintering process for BJ green parts, in general, depends on two class of variables; one is powder variables (size, additives, etc.) and the second is the process conditions. The powder system can be suited to promote densification. It is proven that the particle morphology influences on sinterability [236]. The smaller particles favor sinterability of the compact thanks to higher surface energy [6, 237]. Similarly the shape of powders determines how the powders pack in green state thereby influences the density of the sintered print [238].

In addition to powder morphology option, adding small amount of sintering aid to the base material can improve sintering behavior of the compact [222, 223, 239]. A well-known example of such additives for solid state sintering is adding magnesia to alumina compact [240]. In liquid phase sintering case, adding some substances may facilitate the liquid flow within the green part. For instance in a research conducted by Humenik et al. the contact angle declined from 30° to zero after addition of molybdenum to the nickel -titanium carbide [241]. Some other aid substances reduce the process temperature e.g. introducing Li_2O-B_2O_3-SiO_2 glass into Ba-Zn-Ti provides extra energy at the early stage of LPS sintering and drops the sintering temperature from 1150 °C to 875 °C [242]. Further examples of the sintering aids in powder metallurgy can be found in references [243-245] which have potential use in BJ bodies sintering.

2.8.3 Transient Liquid-Phase Infiltration (TLI)

Retaining the green object geometry is a key for successful sintering of a BJ-made part. Using fine powders, high initial packing fraction and supporting the part by packing in coarse ceramic powder, all are practices to address the deformation problem. For sintering to density

dimensional changes are 15-20%. Sometimes the printing shape can be offset to compensate, but variation in shrinkage must be minimized for good accuracy. Transient Liquid-Phase Infiltration (TLI) is an approach wherein the infiltrant melts below the sintering peak temperature allowing pore mitigation in the green body. This method especially is found useful in sintering large green bodies where differential shrinkage may lose stability of the skeleton volume. The infiltrant used in TLI is normally composed of the base powder material plus a melting point depressant in order to ease homogenization after the liquid metal fills the void space [246].

Upon melting infiltrant, the capillary force directs the filling liquid through the runners toward the sintering tabs. Experience is needed to design tap locations to deliver the liquid evenly and sintering the entire green part homogenously [247]. Once the liquid infiltrant introduces into the skeleton, two competing mechanisms start; migration of the liquid into the skeleton and diffusion of the infiltrant into the powder. The mutual solubility, infiltration time and temperature determine the winner. In case the solubility is high the liquid diffuses inside the grains, solidifies and subsequently blocks the liquid routes. This disrupts interconnectivity of the structure and voids are cut off from the pores network. This phenomenon is known as freeze-off and limits the infiltration distance and inhibits homogeneous infiltration [248, 249].

2.9 Materials

2.9.1 Ceramics

Wide applications of ceramics has been always impetus to explore new ways to process these materials. In the first attempt of using BJ of Mgo doped alumina the ~ 99.2 % final density was achieved [250]. As the ceramics generally include oxides, nitrides or carbides compounds so even the metal parts can be achieved starting with metal oxides. Tungsten carbides is an examples of the ceramics where during heat treatment the hydrogen gas reduces the oxides and leaves metal

part after sintering. For instance in one study, researchers used binder jet system to process the micron and submicron powders to fabricate complex metal cutting inserts from WC-cobalt oxide - IPA slurry and polyethylenimine as binder [123]. After sintering the part was processed by Hot Isostatic Pressing (HIP) and reached 14.2 g/cc which is comparable with 14.5 g/cc obtained by conventionally processed parts [123].

Alumina has been processed in both dry and wet states. In the recent researches by processing the alumina powder in dry state it was stated that if the powder size is sufficiently large to form defect-free layers then by altering the print parameters the fired density can be achieved to approximately 96% of the true density and 10% shrinkage in vertical direction [88]. The same sintered density was achieved for slurry deposited alumina but the samples underwent large shrinkage at around two times in all three directions compare to the dry processed parts [251]. We encourage readers to refer to [252] for summary of the researches that have been performed by binder jetting on the ceramics based off their application category.

2.9.2 Metals

The metal powders are not new to BJ, yet mitigating the voids and cracks are still subject of ongoing research. The highest density for steel powders with gas atmosphere sintering was limited in the 92% to 95% range due to the resisting pore closure on the grain boundaries [253]. Recently adding 0.5% boron additive to 420 steel was found extensively helpful to attain the final densities near full density - 99.6% - in vacuum sintering condition [254]. Subtle differences in chemistry of other ferrous alloys require different production protocols to get the desired properties of the printed parts. For example nanoparticles (~ 7-10 nm) can enhance the quality of 410 stainless steel. Moreover, the creep deflections and shrinkage were reduced up to 95% percent and 60% respectively [255]. Same approach was tested on the 316L binder jet parts by using 316L

stainless steel nanoparticles which resulted in further densification [256]. Other notable metals produced by binder jetting include, but not limited to, Inconel [257], Copper [20] and cobalt-chromium (Co-Cr) alloy [258].

2.9.3 Polymers

Local composition control (LCC) is another attractive point of BJ that allows creation of a component with tailored properties that can be function of multiple discrete segments. In this class of BJ process, different materials are supplied through different nozzles, each onto the specified place [259]. While the merits of sequential powder deposition method over to the other LCC fabrication approaches have been mentioned in reference [260], the stepped gradient was indicated as a concern which could be addressed by using a step special synchronized distributor [260]. Tailoring index of refraction, electrical conductivity, magnetic properties, hardness, etc. could be benefit from LCC [259]. The most used application of LCC is color printing for appearance. Just like inkjet printing on paper, multiple colors can be combined to produce full spectrum of color [261-263].

One interesting utilization of LLC is fabricating the gradient index (GRIN) lenses by slurry-based BJ [121]. In the study Wang et al. heat treated Aluminum nitrate to be decomposed to alumina. The resultant material was ink jetted as dopant with different concentrations into silica powder bed. Then the alumina-doped silica layers were sintered at 1650 C for 30 minutes to optical transparency. The benefits of the as-described process over the conventional methods [253, 264, 265] was not only the shortened process time from >100 hours to 70 hours but also improved compositional flexibility and increased index profile dimensionality [121].

Local composition control method is also useful to fabricate bimetallic strips where two sheets with different compositions are attached to each other and deflect dissimilarly against the

heat. In an effort NiO and Fe_2O_3 slurries were printed on Fe-30Ni base powders and reduced to Ni and Fe respectively after sintering [266]. With aid of Hot Isostatic Pressing (HIP) the density increased to as high as 93% theoretical density to achieve the bimetallic bars functionality [266]. In addition to functionally graded materials, many novel material systems such as NdFeB based magnets [267], solid oxide fuel cell (SOFC) [122] or even customized food fabrication [268], etc. have been explored in research level yet not used for mass production.

2.10 Applications

In higher volumes, mass production with BJ is expensive relative to traditional methods. However it does provide strong advantages for low volumes. The porous green parts from BJ are readily adapted for production of no-bake core and molds for use in standard investment and sand casting applications at lower cost rather the printing metal itself [269]. The geometric freedom of BJ can allow for lower cost fabrication of prototypes as well as enabling unique geometries that would be difficult to pattern by traditional methods like sand molds. Prior researches have been focused on improving the mold quality. Examples are curing heat treatment effect on permeability and compressive strength of the mold [270], the resultant cast roughness [271], gas generation off the mold and improving dimensional tolerance [272]. Cooling process of the mold significantly impact on the cycle time as well as on part warpage. Complex shapes need built-in curved cooling channels with constant distances from the edge for optimal cooling which generally cannot be created by conventional machining.

Conformal tooling inserts creation was attempted for a textured surface with hardenable stainless steel powder and a bronze (90Wt% copper, 10Wt% tin) copper infiltrant [273]. The investigation indicated predictable shrinkage within ±0.25 %. Furthermore, 15% enhancement in production rate and declining of part distortion by 9% were reported [273]. Fabrication of porous

parts is an emerging topic in BJ field. Temporarily bonding the base powders [6, 274], adding fugitive space holders [6] are the recent examined fashions to increase void fraction within the parts. Such studies provide a promising route for producing filter components, electrodes, acoustics, lightweight structures, etc.[40, 274, 275].

2.11 Summary

After over 25 years of emerging Binder Jetting, this method is rather well developed for standard commercial powders. The inherent advantage of BJ as an additive manufacturing approach and being able to process most of powdery materials makes it a potential solution where conventional methods fail. The development of the machine in order to process new material systems in more economical and faster way still is a challenge that is being studied by the experts of the field.

CHAPTER 3: BINDER-JET PRINTING OF FINE STAINLESS STEEL POWDER WITH VARIED FINAL DENSITY[1]

3.1 Abstract

While Binder jetting produces relatively weak porous parts that are strengthened through sintering and/or infiltration, this paper reports on the two different methods of preparing fine 316 Stainless steel powder and the impact of each method on the final sintered density relative to direct printing into -22 micron powder. The first method uses agglomerates of fine powder. In the second, nylon 12 powders are mixed with the steel powder as a fugitive space holder to increase porosity. Sintered density and sintering shrinkage of agglomerate material is shown to vary with the density of the spread powder bed. However, with added nylon the shrinkage correlates with the shrinkage of the base steel powder while the density depends on the quantity of the nylon. Thus, it is possible to create varied sintered density with compatible shrinkage levels—a key step towards creating binder-jetting systems with spatially controlled porosity.

3.2 Introduction

Additive manufacturing (AM) is a very flexible technology that is used to synthesize 3D objects in layers by directly from a digital definition [146]. Each AM technique has strengths and limitations. Most of the manufacturing processes require the use of support structure to support overhangs or to reduce deformation due to shrinkage during processing. Yet, in powder bed AM

[1] This chapter was published in JOM (Ziaee, M., Tridas , E.M., Crane, N.B., Binder-Jet Printing of Fine Stainless Steel Powder with Varied Final Density, JOM, Vol. 69, No. 3, 2017). Permission is included in the appendix A

methods the unbound powder temporarily supports unconnected portions of the component that allows internal volumes to be formed without additional support structures so that waste of materials is reduced [24].

Many powder bed AM methods utilize an energy source to fuse raw materials together. In the powder bed fusion AM processes 316L stainless steel is broadly used as the carbon content lower than 0.03% wt., confers a suitable weldability to this powder material [276]. Bandar Al Mangour investigated the influence of the addition of TiB_2 and TiC reinforcement particles to manufacture 316L stainless steel based nanocomposites by laser melting. It was observed that the controlled density was achieved by both the starting reinforcement content and the particle size [277]. Electron beam melting of stainless steel powder has also been demonstrated successfully [278, 279]. The results show that acting time, the electron beam current, and beam focus profoundly affect the interlayer bonding quality. Moreover, it was shown that for the fabrication process of 316L stainless steel the ratio of the electron beam power to the scanning velocity is the key factor affecting the top surface topography [280].

In contrast to powder bed fusion processes, binder jetting (BJ) utilizes inkjet printing technologies to bond the particles layer by layer so that no heat is required during fabrication [277]. It can work with a wide range of powdered materials including stainless steels. Since the powder does not melt during BJ, the density after printing is about 50% - 60% of the theoretical density and further processing is required to achieve desired properties [281]. Even where porosity is desirable in the final part, additional processing is typically required in order to increase the strength of the interparticle bonds. One option that minimizes shrinkage is to infiltrate the part with a lower melting point material [276, 282, 283], but this typically creates a composite material with poor mechanical properties compare to the base material. While techniques for homogenous

infiltration have been demonstrated, they are not feasible for all material systems [248, 284]. Alternatively, parts can be densified by sintering to density if they are printed with sufficiently fine powders though this leads to significant processing shrinkage (15-20%). In order to mitigate the voids and cracks problem in BJ parts, studies have been done on the influence of the print parameters and consolidation processes such as sintering (heat treatment profile and sintering aid additives) [223, 239, 285].

Since most BJ work has focused on achieving full density parts, the control of porosity and density in BJ processes has not been extensively explored. [121]. While, Verlee et al. investigated how the sintering profile and particle geometry affect the final density and permeability of the parts made by sintering of the 316L stainless steel with no infiltrant [163], they have not investigated the effect of agglomerates or porogens on the process.

The ability of fabricating porous parts with complicated geometries could have broad applications in energy management, acoustic, lightweight structures etc.[14, 286]. This would be particularly valuable if the density of the parts could be readily varied spatially with pores below the printing resolution limits. This requires the ability to fabricate parts with varied porosity but similar processing shrinkage. As a first step towards this goal, this paper compares the density and shrinkage of 316L stainless steel powders with different powder preparation methods but the same sintering conditions.

The quality and reliability of the powder-based AM techniques is strongly dependent on key powder properties including particle size, size distribution, and shape as well as environmental conditions such as humidity. Of these parameters, one of the most important is the particle size. Small particle sizes are favorable because they can support higher resolution printing (thinner layers, higher in-plane printing resolution) and smoother surfaces. They also have more surface

area to drive strengthening and densification by sintering [287]. However, the increased surface area and decreased particle weight makes them much more sensitive to environmental conditions [288]. Additionally, finer powders have smaller pores through which the binder must travel to penetrate the powder. This can cause printing difficulties such as balling in which the droplets stay on the surface rather than penetrating into the powder.

To address these competing challenges, this paper investigates the use of agglomerates of fine powders. The processed powder will behave more like a coarse powder during spreading, and printing. However, they act as a fine powder during sintering. If the agglomerates binder is soluble in the printed binder, the particles may also reorient and densify during the printing/drying process. Williams et al. utilized agglomerates of mixed metals and oxides previously in binder jetting [289]. They successfully reduced the oxides and sintered the final samples. However, they did not report the densities of the samples during the processing. This paper addresses direct printing of cured metal powder and nylon/316L stainless steel mixtures and compares the density and the dimensional variation of the fabricated parts during each stage of the processing. By using metal powders, the total system shrinkage should be reduced compared to printing of oxide powders. A second set of specimens were produced from a mixture of stainless steel powder and a fugitive powder that decomposes during sintering to leave pores. The resulting density and shrinkage are compared to the fine stainless steel powder with and without agglomerates.

3.3 Experimental

3.3.1 Materials Preparation

All powder preparations began with raw 316L stainless steel powder with D90<22 μm size obtained from Carpenter Powder Products. The procedure for making agglomerates of the fine powder is illustrated in Figure 3.1. Blocks of bound powder were made by tapping the base powder

until no further volume change was observed. ExOne M-Flex solvent-based binder was added to the powder at a volume equal to that of 90% of the void volume of the powder. The powder/binder mixture was heated in an oven at 50 °C for 24 hours in order to evaporate the solvent from the binder.

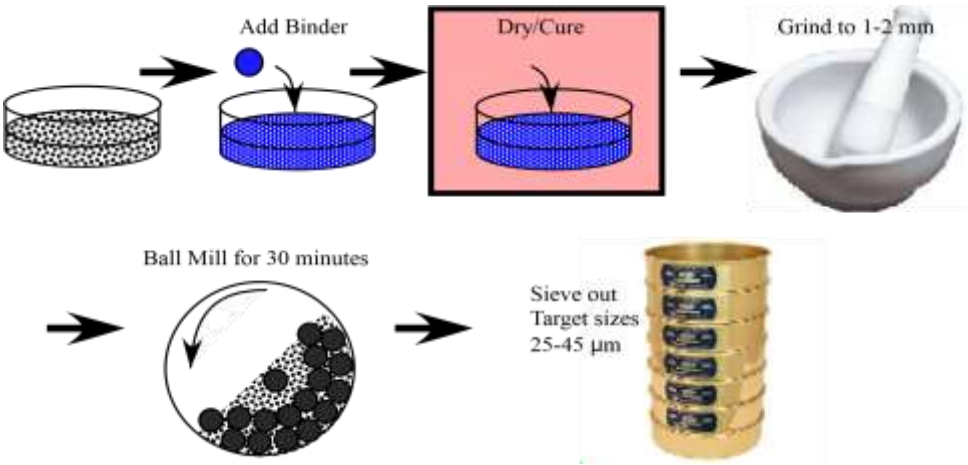

Figure 3.1. Making agglomerates procedure using 316L< 22 µm stainless steel raw powder.

Afterwards, the second heating step was performed separately for the obtained mixtures at 100°C or 185°C for 4 hours. The loose powders were dried to two different temperatures, 100°C and 185°C, to permit different levels of rearrangement after printing. The lower temperature cured particles are expected to dissolve more fully during printing to permit reorientation. In both cases, the result was a puck of brittle, bound powder. Using a mortar and pestle, the puck was ground to a size of approximately 1–2 mm. These granules were placed into a ball mill with equal volume ¼" 316L stainless steel ball bearings and ground for 30 minute intervals. After each interval, the agglomerate powder was fractioned using a series of sieves and the individual size fractions collected. For this study the fraction of cured size from 25 to 45 µm were used. Material above the target size was returned for further ball-milling.

SEM image of the agglomerates (see Figure 3.2) shows that the agglomerates are irregular in shape with a significant volume of the constituent particles below 10 μm. After preparation, all materials were stored at room temperature in sealed containers in order to reduce moisture absorption. The low temperature cured materials seemed particularly sensitive to moisture absorption and stored with desiccant in the container. If stored without a moisture absorber, the powder would quickly begin to clump together.

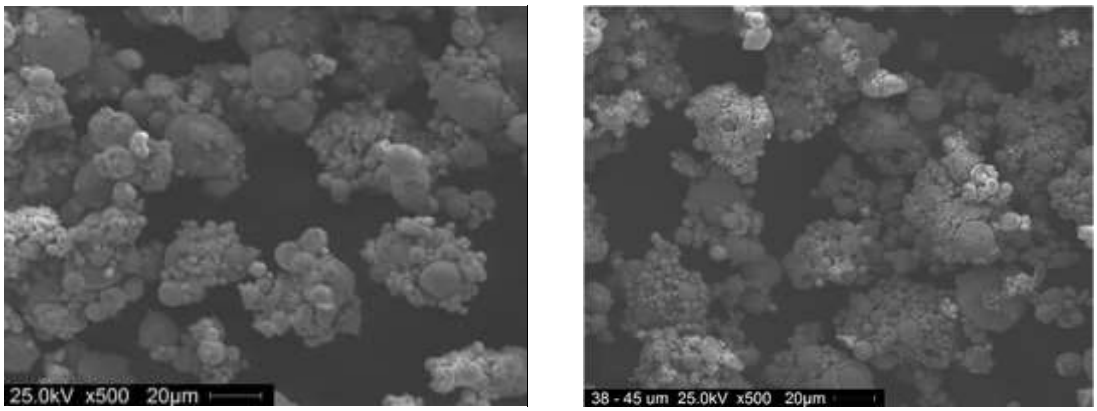

Figure 3.2. Powder agglomerates cured at 100°C produced using As-described procedure. Left: At 25 -38 μm range, Right: At 38-45 μm size range.

Another approach to creating porosity is the introduction of a fugitive material that decomposes during post processing. This approach was tested using EOS polyamide 12 powder with an average particle size of 55 μm. Two different volume ratios of the PA 2202 powder to the raw 316 powder were prepared containing 25% and 33% nylon by volume. Each batch was prepared by measuring the components and mixing until a visibly homogeneous mixture was produced. A 50% mixture of nylon/stainless steel powder was also attempted. However, when a test coupon of this powder mixture was sintered, the resulting part was inhomogeneous with a large pore indicating likely separation of the nylon and stainless steel powder.

Comparison of the density of the processed powder with the raw powder was done through each processing step. These included measuring the bulk, tapped, spread, and sintered densities

of the powders. The shrinkage of the printing components was also measured. The sintered samples were further sectioned for examination of the pore structure of the different components.

3.3.2 Fabrication of the Porous Parts

In this study all printing was completed using an ExOne Innovent printing system. This system has a powder supply mechanism that deposits powder on a 160 mm×65 mm×65 mm build volume. However, the mixed and cured powders were manually deposited in front of the re-coater to reduce the required material for printing. A small amount of powder was placed on the edge of the print bed where the parts were located. The counter-rotating roller of the ExOne Innovent would spread the powder in a uniform layer over the build area.

The binder is selectively deposited on the powder bed in layer by layer fashion and the parts are printed on the build platform which travels in the Z-direction. The print head scans along the Y-direction and the linear array of jets that deposit binder are parallel to the X-direction.

Cubes (5 mm ×5 mm ×5 mm) were printed for each powder type. After printing, the samples were placed in a curing oven for 4 hours at 185°C. The nylon mixes were cured at 140°C to avoid bonding of the unprinted powder due to melting/sintering of the nylon. After curing, the green parts were removed from the powder bed and the dimensions were measured by digital calipers in X, Y and Z directions. All dimensional changes were calculated relative to the nominal dimensions of the STL file (5 mm).

3.3.3 Sintering

Sintering of the green parts was accomplished according to the sintering schedules shown in Figure 3.3. All sintering was performed under a reducing environment using an Argon/Hydrogen mixture (95% Ar, 5% H_2), which was flowed at a rate of 10 SCFH. The internal volume of the furnace was 0.186 m^3. Samples were packed into a graphite crucible and supported

using a coarse grain alumina powder. Heating rates were chosen based on the capability of the furnace. The hold at 800°C provides time for the binder to fully decompose before further heating. The peak sintering temperature is based on literature observations [290].

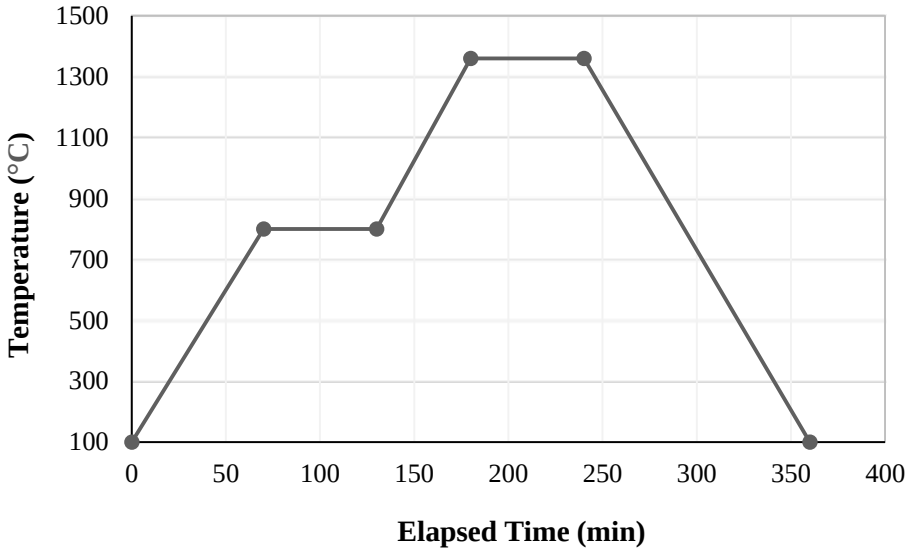

Figure 3.3. Sintering schedule for the samples. Between the starting temperature and 800°C the ramp rate was 7°C/min. The temperature was held constant at 800°C for one hour. From 800°C to 1360°C the ramp rate was 10°C/min and the hold time at maximum temperature was one hour. The cooling rate was 10°C/min.

3.3.4 Density Measurements

For each feedstock bulk, tapped and spread density of the material were quantified with three repetitions of each measurement. The agglomerates and mixtures are compared to the as received 316L powders as a reference to see how each procedure affected the densities of the powders. In order to determine bulk density, the material was sifted by a sieve with 0.5 mm aperture. Afterwards the powder was poured gently into the 25ml graduate cylinder with 0.2 ml precision to measure the volume and mass. The tapped volume of the powders the cylinder was measured in accordance with ASTM B527-15 [291] using a custom-built apparatus.

To measure the spread densities of the powder beds produced from each powder an 80 μm thick plastic sheet was placed on the build platform after spreading several foundation layers. Twenty-four layers of powder of 100 μm thickness each were spread on top of this sheet. A sharp-edged steel punch tool with an internal diameter of 19.05 mm was inserted into the spread bed until it contacted the plastic sheet. The remaining powder around the tool was brushed away and the mass of the powder inside the tool was measured. Powder height was assumed to be equal to be 2.4 mm. The process is schematically shown in Figure 3.4.

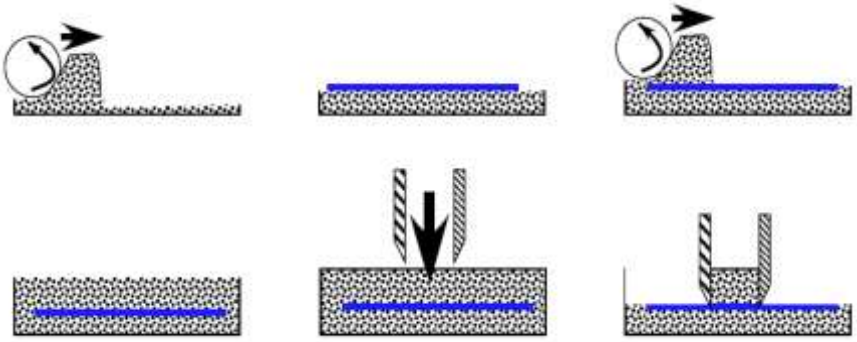

Figure 3.4. Spread density measurement.

The sintered density for each part was measured using Archimedes method from six printed samples. First the dried sample weighed. Then, the weight of the submerged sample was measured and the volume calculated assuming a water density of 999 kg/m^3. The sample was dried with a soft tissue and then reweighed to measure water absorbed by any open pores. Relative density was calculated using (7.99 g/cm^3) as the true density of 316L stainless steel.

3.4 Results and Discussion

3.4.1 Printability

Because of the interparticle forces and humidity, fine powders tend to clump together and have poor flowability characteristics. This typically corresponds to poor layer spreading

characteristics. This issue was more severe as for 316L<22 μm. To approach this problem the powder was sieved and heated up to 50°C for 4 hours to reduce the moisture in the aggregated particles before printing. However for the cured agglomerate powders as well as nylon/316L mixes this process was not necessary.

The key printing parameters are the layer thickness, printing saturation level, and drying conditions. Printing saturation level is defined as the percentage of the powder void space that is filled with printed binder. Typical saturation levels are around 60%. Since saturation levels are a function of the spread layer density, an alternative printing parameter termed "binder level" is defined that is powder bed independent. The binder level (β) is defined as the fraction of the part volume that was filled with binder and is related to the saturation (S) by

$$\beta = S(1 - f) \qquad \text{Equation 3.1}$$

where f is the powder bed packing fraction. On the Innovent, the drying is controlled by setting the drying time and lamp intensity. Lamp intensity was maintained at 100% for all powders.

As the size and spread density of the powders were different, some adjustments were required in the print parameters. For 316L<22 μm and nylon/316L mixtures the same values were set on ExOne machine to fabricate the samples because both have fine < 10 μm powder particles. However, for the agglomerated powders larger pores are expected in the powder bed which results in weak binding and subsequently weak interlayer bonds.

To decrease the void spaces and increase re-arrangement of the powders each layer was printed twice. This was accomplished by setting the machine layer thickness to 50 μm but only depositing powder every other layer. The resulting binder loading would be equivalent to printing 100 μm layer at 120% but in two steps with a drying cycle between—allowing more time for dissolving the bonds within the agglomerates and permitting rearrangement of particles. While the

extra binder should increase the strength of the green parts, the green part strength was not measured. To compensate for the higher binder loading, the drying time was also increased to avoid oversaturation and bleeding. Table 3.1 summarizes the parameters used to fabricate the test samples.

Table 3.1. Summary of key printing parameters used for each powder on ExOne Innovent printer.

	Binder Level	Drying Time (S)	Layer Thickness Setting (µm)
316L<22 µm	24 %	12	100
25% Nylon+316L			
33% Nylon+316L			
Agglomerates(Cured at 100°C)	48 %	20	50
Agglomerates(Cured at 185°C)			

3.4.2 Density Measurement Results

The density measurements are summarized in Figure 3.5. These results demonstrate notable variation with powder feed stock, suggesting that the interparticle forces differ significantly between the various powder preparations. All of the tested powders flowed relatively well and produced smooth layers during spreading with the counter rotating levelling roller. In all cases, the measured bed density exceeded the density of tapped powder suggesting that the roller was able to re-arrange the particles due to the small thin layers or due to fraction of the agglomerates, consequently led to the higher bed density. Among the tested samples 316L< 22 µm reached the highest packing after layer deposition reaching 56.5 % of the theoretical density.

The agglomerated powder shows lower densities when cured at 100°C. In addition, the agglomerated powders at 100°C appears to absorb moisture from the air and clump together unless it is stored with desiccant. Thus it is possible that the moisture form additional bonds to create very irregular powder particles with high level of friction that reduces the compaction quantity.

This is consistent with the observation that this powder readily clumped together and did not flow easily.

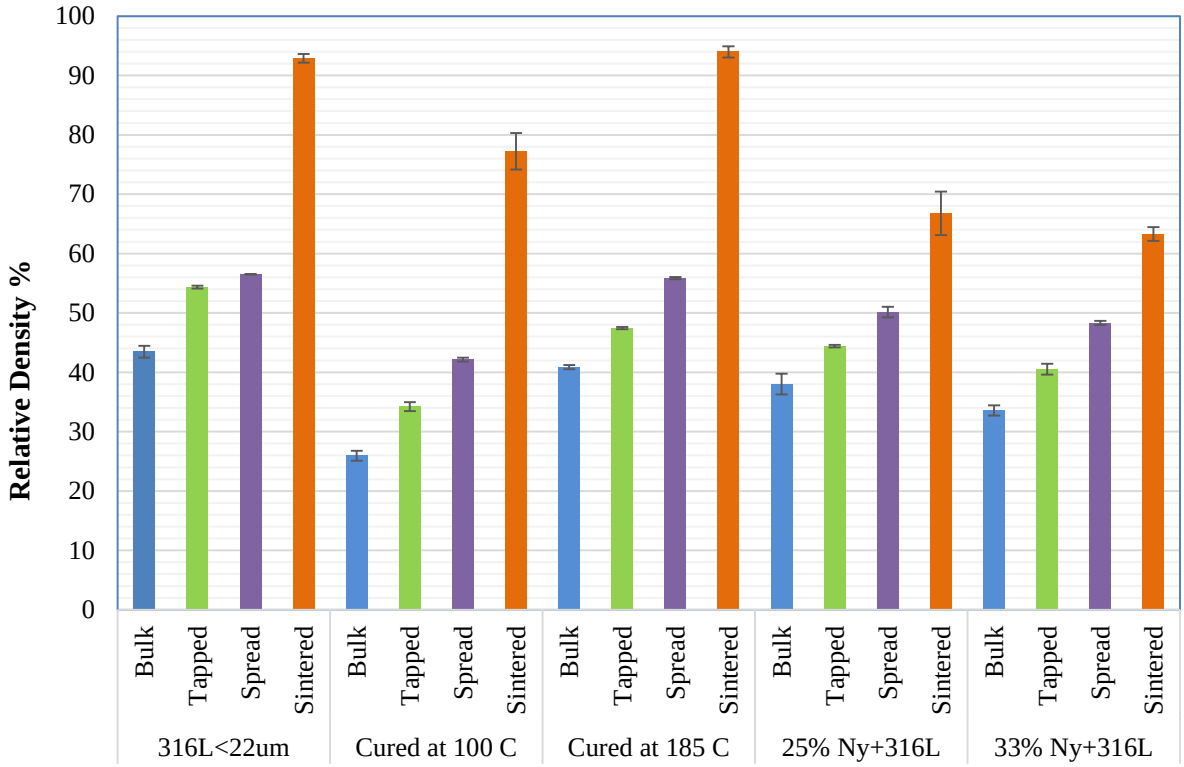

Figure 3.5. Relative bulk, tapped and spread density for the raw 316 and processed powders. To determine relative density percentage each of the obtained densities was divided over true density of 316L, 7.99 g/cm^3. Error bars represent one standard

The binding of the low-temperature cured agglomerates should dissolve when wet by fresh binder-permitting particle rearrangements and possibly densification. However, no evidence was seen for this in the density of the printed parts. In contrast, if the binder is cured at 185°C it will not tend to re-dissolve when exposed to fresh binder—suggesting that it underwent a chemical reaction such as cross-linking that has left it less sensitive to moisture. These powder agglomerates were more flowable.

The agglomerates cured at 185°C showed lower bulk and tapped density than the raw powder, but the spread density is comparable to the untreated powder. It is unusual that the spreading would achieve significantly higher densities than the tapped density as seen in this material but this was seen in all the special sample preparations. It is possible that the roller is fracturing the agglomerates so that it behaves more like the untreated powder.

In general, air pockets and nylon inclusions in the powder feed stocks reduce the packing level by reducing the contact areas between the steel particles which is evidence of the fundamental occurrences during sintering. It is noticeable that for the tested materials with no nylon addition, the spread density strongly influences the final sintered density. Thus samples with similar spread density (-22 µm raw powder and the agglomerates cured at 185°C) have very similar sintered densities (with 92.9% and 93.9% respectively) whereas this number is 77 % for the agglomerates treated at 100°C.

The nylon inclusions cause a very different response. The mixture spreads to a high packing density (relative to a volume weighted density of the material). When the printed parts are sintered, these particles would be expected to decompose above 300°C leave voids behind comparable in size to the particles (55 µm mean particle size). These voids are much larger than the voids between steel particles so that they are unlikely to densify through sintering. After sintering, the density is calculated relative to bulk steel density.

The nylon/316L mixtures had much lower final density as would be expected. The results indicate that the final density is not very sensitive to nylon concentration over the range studied with final sintered densities of 66.8% and 63.3% for the powder mixtures with 25% and 33% nylon respectively. The resulting parts have sufficient porosity to be useful for filter, heat exchanger, and other energy applications, but still exhibit good strength. However, many applications would

benefit from still higher porosity levels. If coarse or multiscale porosity is desired, this could be achieved by defining the large porosity in the printed model while the fine porosity is created by the fugitive powder. However, it may be difficult to achieve substantially higher porosities (relative density <40%) by adding a fugitive space filler alone as the remaining structure may not have sufficient strength before and during sintering to maintain the geometry.

3.4.3 Dimensional Error

The size of the printed parts was measured for each set of conditions and compared to the STL file dimensions (5 mm ×5 mm × 5 mm) as presented in Figure 3.6. This data represent dimensional error rather than shrinkage which in practice, the CAD model could be scaled to compensate for the average dimensional errors.

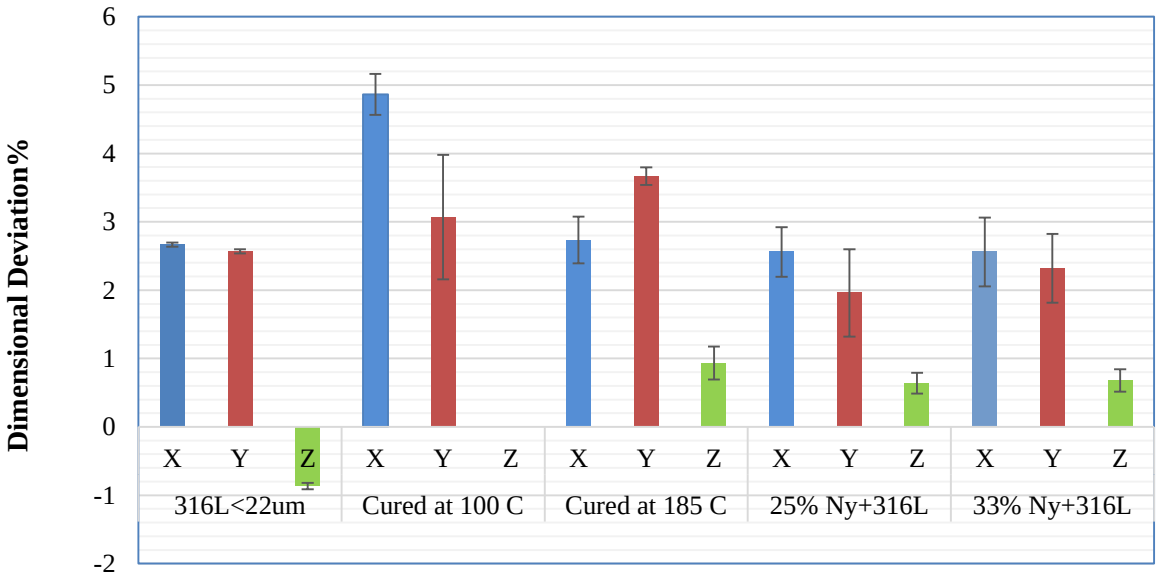

Figure 3.6. Dimensional deviations for X,Y and Z directions for the fabricated green samples. Error bars represent one standard deviation of the measured value.

Binder jetting uses precisely controlled printed droplets to create each layer of the green part. Because of the different processing on the raw 316L stainless steel powder the density,

structure and wettability of the loose powders varied which resulted in different dimensional variations for each set of the samples (see Figure 3.6).

The X-Y dimensional variation is on the order of the printing resolution (~75-100 μm) for these small parts and was relatively consistent between samples. The Z-part errors were relatively consistent except for the agglomerates with 100°C cure. These showed a significant anomalously large shrinkage in both the green and sintered state. This is due to a printing error in which the binder did not migrate in Z direction and several layers were separated from the green bodies.

Figure 3.7 summarizes the dimensional change after the 1360°C sintering treatment. It can be seen that all samples experienced significant shrinkage in all three axes. It is also noteworthy that the dimensional change in Z direction is highest in every powder type. This suggests that there may be more porosity between layers than within layers.

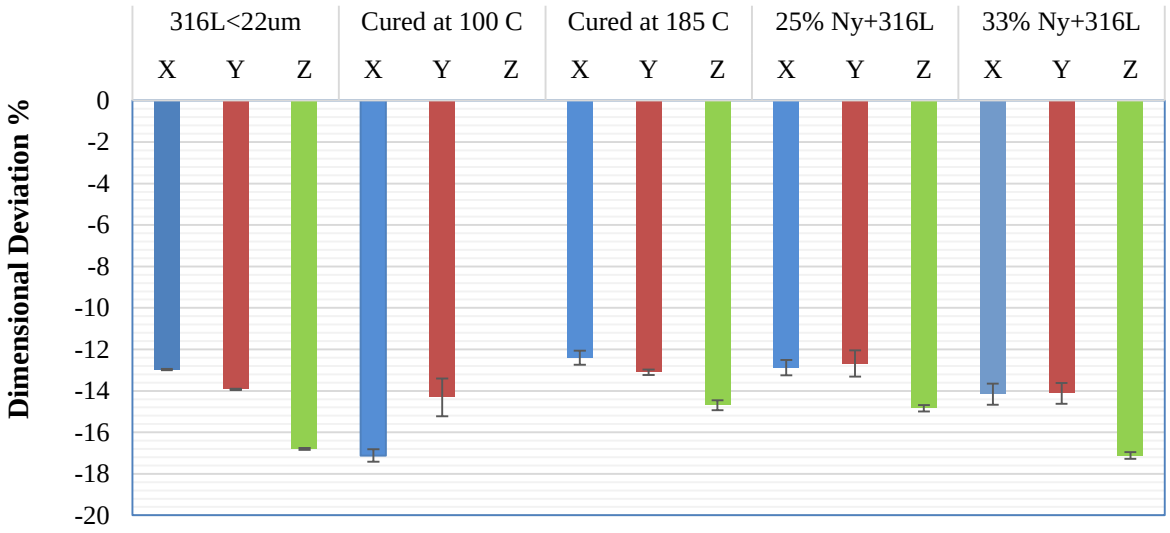

Figure 3.7. Dimensional deviation for X, Y and Z directions for the sintered samples. Error bars represent one standard deviation of the measured values.

The lowest shrinkage is obtained using the samples with highest spread density except when the fugitive nylon powder is added. The 25% nylon mixture and 185°C cured agglomerates

are very closely matched in shrinkage in all three axes despite very different final sintered density (66.8% vs 93.9%). The shrinkage values of these materials may also be compatible with the untreated powder in the X-Y dimensions.

Similarly, the as-received <22 μm powder has very similar shrinkage in Y and Z axes to the 33% nylon mixture but with final sintered density of 92.9% and 63.2% respectively. This decoupling of shrinkage from final density is critical to enabling manufacturing processes that permit controlled spatial variation in density within the same part.

The Cross section images of the samples, as seen in Figure 3.8, show that powder processing significantly changes the pore structure. Studies have shown that austenitic stainless steels experience densification via lattice diffusion during the intermediate stage sintering [292, 293]. During this regime, surface diffusion is also active therefore combination of lattice and surface diffusion contribute in pore migration. From the microstructure images, it can be seen that most of the pores are attached to the grain boundaries suggesting that grain boundary diffusion is the main bulk transport mechanism driving part densification during sintering [294]. The images also reveal that the samples made with raw 316L powder show small isolated pores formed during the intermediate stage of sintering while for the agglomerates the number of pores declines and the size of the pores become significantly larger—even when achieving a high final density as in the 185°C cured agglomerates.

The nylon mixes show much larger, clearly interconnected porosity. No clear spatial orientation of the pores can be seen. It appears as though the steel regions have densified almost completely (> 90%) while the remaining pores arising from the fugitive nylon powder. Because

the steel powder is the same in all the samples, the steel sintering should be unchanged—explaining the similar shrinkage levels observed (see Figure 3.8) despite very different final densities.

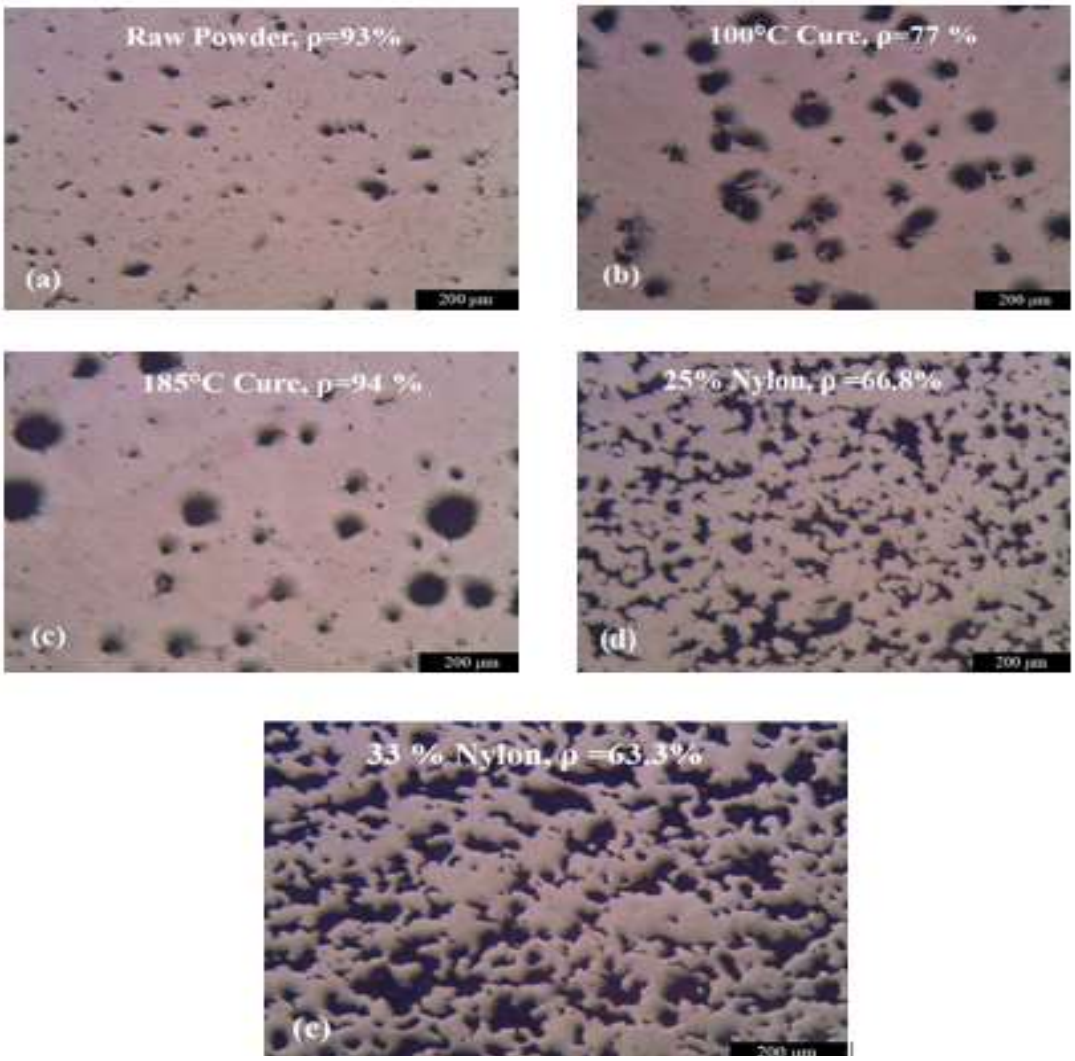

Figure 3.8. The porosity on the cross-section of the samples made by feedstock materials. a) Raw 316L<22μm, b) Agglomerates cured at 100°C, c) Agglomerates cured at 185°C, d) 25% Nylon+316L, e) 33% Nylon+316L. Scale bar represents 200 μm.

Most variables that change the final density also change the shrinkage levels. If a part is produced with spatially varying shrinkage levels the part will be distorted during sintering. Since the fugitive nylon mixtures achieve different final densities but with similar processing shrinkage, this process could enable a printing process that can vary density spatially. Such variation could

be used to create enhanced heat transfer surfaces if exposed to air or other exchange medium. Alternatively, they could be used internally to reduce heat transfer in undesirable directions. This approach is promising for porosity variation between printed layers. However, it would be difficult to vary the concentration of pore generating particles within the printing plane using most printing processes.

While new approaches would be needed to get full spatial porosity control, these results suggest a criteria for creating a range of porous structures with similar sintering shrinkage levels. The key criteria is to start with the same base powder, but selectively introduce pores that densify much more slowly than the pores between the finer powder particles. Such a pore structure could be implemented using other mechanisms besides nylon pore generators. If this can be implemented with spatial control, it could be of great use in tuning the properties of printed structures. The resulting voids can also be filled with other materials to introduce new functionalities. Further work is needed to test this hypothesis and to explore the range of porosity values that can be obtained.

3.5 Conclusion

This study has assessed the density and shrinkage impact of printing with agglomerates of fine 316 stainless steel and mixtures of steel with nylon powder to results with the base material. These results show that sintered density can be reduced both with agglomerates that spread to a low density and by adding fugitive nylon powders to raw steel powder. Agglomerates that spread well can achieve the same sintered density as the raw powder (>93%). Changes to the sintering process will likely increase the density of both the raw and agglomerate powder closer to full density.

These results also show that fugitive agents can be used to reduce the sintered density below 70% while maintaining compatible shrinkage with high density (>90%) materials. If the shrinkage is the same for different porosity levels, then varied porosity can be created in a single part without deformation due to differential shrinkage rates. This could provide a way to spatially vary critical material properties such as stiffness and thermal conductivity at smaller scales than can be achieved with printed features.

CHAPTER 4: A REVIEW OF ADDITIVE MANUFCTURING APPLICATION IN SCAFFOLD ENGINEERING

4.1 Introduction

Bone is a dynamic tissue and can repair itself after most injuries. However, in severe cases, where the injury results in large void, the fracture might be treated by supplying a porous scaffold to guide the cell and help tissue to grow back in its original shape.

Thus far, many researches have reported successful creation of porous structures with synthetic materials as a substitute for spongy architecture of the bone. Exemplary of such efforts include emulsion freezing/freeze-drying [295], solvent-casting/particulate leaching [296], gas foaming [297] and fiber bonding [298]. However the challenge of the synthetic materials has been to avoid stimulating the immune system of the recipient's body and implant rejection [299].

Another traditional solution to treat orthopedic defects is machining bone allografts into standard clinical shapes from donated cadaveric bone. This approach is advantageous over the synthetic materials since it simulates internal architecture and mechanical properties, plus it has excellent osseointegration [300]. However, the allografts are available in only a limited range of geometries and must fit the envelope of a donated bone. For example, a small quantity of standard bone blocks might be cut from a single long bone. All these methods share the weaknesses of insufficient ability to produce complex geometries [301].

The technology challenge of bone scaffold implant is being able to replace a failed biological tissue with a guest material and have no negative effect on the recipient's body. This imposes three key requirements as following for a bone replacement;

- Biologically safe
- Mechanical match
- Anatomical match

Biological and mechanical properties of the implant are primarily determined by the materials. However, in some cases these properties and also anatomical match extensively are inked to the fabrication approach flexibility. That said, additive manufacturing as the most versatile method seems to be the best candidate to produce customized medical scaffolds.

4.2 AM for Orthopedic Implants

Additive manufacturing can implement individually every element of the medical scaffold and incorporate the specifications into the part precisely. So by AM there should be virtually no technological challenge to create any sort of patient specific implant. The process of fabricating patient's orthopedics by AM starts from medical scanning or imaging which are to be processed to get the patient's own CAD model. The next step includes producing the physical model, post processing and pre-surgery sterilization [302].

Researchers of the field have explored different classes of the AM techniques to advance tissue engineering. Various AM techniques including selective laser sintering [303, 304], stereolithography [305, 306], ink-jet printing [307-309], fused deposition modeling (FDM) [310-312], etc. have been tried to fabricate scaffolds as skeleton for cell in-growth. In some cases to improve mechanical and biological properties of scaffolds, reinforcing [311, 313] or bioactive agents [314-316] are added into the base material. Some of such works have been reviewed in references [317-321] and in the book [319].

4.2.1 Large Area Projection Sintering Potentials in Tissue Engineering

The Large Area Projection Sintering (LAPS), utilizes visible light energy to selectively pattern the image onto the powder bed to build a 3D geometry. Up to date there is no work reported on fabrication of 3D structures for tissue engineering by using LAPS [322]. The LAPS can project the images of the slice with locally varying power. This could be a promising route to mimic the natural bone structure - in particular long bones which are denser in the outer shell than the interior part [323]. However, the uneven level of shrinkage is expected issue that needs to be addressed.

4.2.2 Selective Laser Sintering (SLS) Application in Tissue Engineering

The Selective Laser Sintering (SLS) uses a CO_2 or Nd: YAG laser to deliver energy to the powder bed [324]. The laser energy density can be varied by adjusting power, beam diameter, hatch distance (distance between adjacent tracks of the laser) and scan speed [325]. The high energy density could lead to warpage and dimensional inaccuracy [326].

In order to tune porosity in an object the process variables can be adjusted to vary sintering level between the particles [327]. For a certain beam diameter, the energy delivery to a spot can be reduced by increasing scanning speed and/or lowering laser power. The hatch spacing alters the pore channels formed through the SLS process. The greater line spacing descends the amount of energy delivered to the powder bed and potentially lesser extent of sintering within the layers. The weak layers result in poor mechanical properties of the part right off the machine and necessitates a secondary sintering in furnace to get the desired mechanical properties [328]. Different types of material i.e. polymers, composites, metals and ceramics have been successfully processed by SLS [329].

Fredric et al. created a composite scaffold of polyamide (PA2200) filled with hydroxyapatite for bone reconstruction with the porosity ranged between 41%-51% [327]. They

demonstrated that the laser energy and particle content are key players on the mechanical properties and the density of the HA-reinforced PA components. Eosoly et al. used hydroxyapatite and poly-ε-caprolactone material with 30:70 weight ratio. The quality of the print was concluded to be strongly dependent on laser filling power, outline laser power, scanning overstepping and part orientation [330]. Further instances of the recent SLS works in medical applications can be found in this publications [26, 331].

4.3 Biomaterials

Biomaterials are naturally derived or synthetic materials which are compatible with body environment. The biomaterial selection is extremely site dependent as they are intended to have similar physical and biochemical properties to the replaced tissue. The four main categories of biomimetic materials are ceramics, metal, polymers and composites [332]. Ceramics and metals have higher mechanical properties than the natural tissue, so they are suited to be used as hard tissue implants or as the reinforcement agent [333-335]. The brittleness of ceramics make them susceptible in load bearing applications [336]. But as bio-ceramics enhance the bonding between bone and the scaffold they are preferred option to be used as coating for the implants or fill in the defects [337, 338]. Important examples of ceramics are bio-active glasses, calcium phosphate and bone graft [339, 340].

Metals properties can be controlled somewhat in processing. Ease of manufacturing and availability are the advantages of bio-metals. The key metals used in musculoskeletal implants include stainless steel 316L, Cobalt base alloys and Titanium alloys [341-343]. Corrosion and mechanical mismatch are the two biggest risks of using metal implants [344-346].

Polymers are corrosion resistant, tough and ductile. The most important plus point of the bio-polymers is that when degraded, they produce glycol and lactic acid which are harmless to

human body. Among the synthetic polymers, polylactic acid (PLA), polymethyl metacrylate (PMMA) and polycaprolactone (PCL) have been widely used in constructing scaffolds [339, 340, 347]. Insufficient wearing resistance and fatigue are deficits of polymers [348]. The purpose of using composite biomaterial is to improve physical or biological characteristic of the implants to emulate the natural tissue bio-functionality [349]. The ceramic film on metal and combination of polymers with ceramic or metal particles have been used in tissue engineering [332].

4.3.1 Bio-absorbable Scaffolds

Bio-absorbable scaffold is an extremely active area of biomaterials and tissue engineering research. Conceptually, the tissue forms as the scaffold electrochemically breaks down to harmless substances and eventually the new tissue replaces to the external material overtime. The degradable ceramics and metallic implants typically are intended to eliminate the implant removal surgery that is associated with the risk of damaging the tissue that just grew back [350]. But the polymeric scaffolds can be suited for guided cell-ingrowth and regenerate the injured graft and eliminate the concern of implant movement in long-term.

However, the polymeric materials lack the mechanical properties for load bearing uses so typically reinforcement phase is needed to provide suitable mechanical and biological function [351]. The additives of bioactive glasses [352, 353] graphene [354], carbon nanotube [355], calcium phosphate [353] and natural bone [356, 357] have been focus of a number of studies.

One of the most common used biodegradable polymer material is Polycaprolactone (PCL). PCL is a semi-crystalline polymer with good biocompatibility and bioresorbability. The rather low melting point of 65℃ adds the popularity of it for scaffold fabrication [250, 358]. The hydrolysis mechanism of PCL can be altered by molecular weight to change the degradation time in span of

4 years in body environment [359, 360]. Additionally, incorporation of other polymers or reinforcement phase influences the degradation rate [361, 362].

Williams et al. used SLS to process polycaprolactone. They demonstrated that even though the porosity of the CAD model of the scaffold was in the range of 63%-79%, the final part turned out to have 17% to 55% porosity[363]. These scaffolds showed similar mechanical properties to cancellous (trabecular) bone which is sufficient to bear early functional loading [363]. The in-vivo investigations confirmed the hypothesis of bone in-growth capability of the PCL-based scaffolds. Chen modified the surface of the PCL based scaffolds with collagen or gelatin and enhanced the mechanical and biological properties after production by SLS [364].

4.3.2 Bone Matrix Mixtures

The use of bone particles in AM is still in development stage. The bone source could be the patient's own body or donated bone-typically from cadavers. Each has some pros and cons reviewed in [365]. Bone granules whether with human or animal source has some advantages over the synthetic materials thanks to being non-toxic and biological cues that expedite the healing process. Hung et al. utilized extrusion based additive manufacturing to fabricate pure PCL and demineralized bone/PCL hybrid scaffolds. They demonstrated that the hybrid scaffolds enhanced the healing process within 1 to 3 months after transplantation [314].

4.4 Approaches to Creating Porosity

An ideal implant should mimic the natural host tissue. The mechanical mismatch between tissue and the implant could even degrade the mechanical properties of the adjacent natural bones [366]. The rigid implant incurs bigger portion of the load and over time the adjacent tissue gets weaker and susceptible to fracture–referred as stress-shielding [367]. This can result in implants loosening or bone re-fraction after implant removal. In addition to mechanical properties, in order

to improve cell in-growth and attachment, the implant should have both macro and micro –sized inter-connected pores [366].

The AM enables designing the pore structure in the computer model and realize it in the physical model. A number of studies optimized the pore configurations to have the maximum stiffness and area to volume ratio enhancing efficiency of the nutrient transform and metabolites from the scaffold [368-371]. The methods for porosity assessment techniques have been summarized here [4].

As a fact of practice, in some lattice configurations, the processability limits the design of the pore network structure. For example Xu-bin processed a femur artificial bone with laser AM and observed that the orthogonal periodic in the digital model turned out circular after printing leading to a serious deviation from the intended geometry [372]. So the processability of the material and creation of the voids below the printing resolution demand alternative methods.

Typical methods to tailor porosity in powder-based AM includes using powder of different morphology and adjusting heat treatment variables [4, 276]. Verlee et al. reported around 35% increase in open porosity by sintering steel compact in a lower temperature heat treatment cycle. They pointed out ~ 25% increase in porosity by switching from powder size of 20-53 μm to 45-90 μm [276]. Utilizing temporary space holder is another way that has been practiced in many AM studies and conventional methods. The fugitive material can be burned out [6] or leached out [148] in post processing and leave void spaces behind. However the meager control on the pore formation is the major drawback of this approach.

4.5 Contribution of Current Work

The Demineralized Bone Matrix (DBM) and Polycaprolactone (PCL) composite is an excellent material for making temporary implants. The concern of retaining biological benefits of

DBM extensively limits the processing options. Thus far, fused deposition modeling (FDM) has been attempted to process actual human bone particles which inherently has many deficiencies for DBM/PCL scaffolding.

The filament of bone/polymer has to be void-free to fulfil printing job, therefore the pore formation is dictated by printing resolution unless the temporary progens are added. The removal operations of the space holders raise biological concerns. Further, the bone particles may readily clog the extruder unless the nozzle is designed fairly large which in turn reduces the minimum feature size of the print. Additionally, during extruding the filament, the key components of the system come in contact with the material, so in order to minimize the risk of disease transmission, before switching to new source of bone, a vigorous cleaning process or part replacement is required which add on to the cost and the lead time of the process.

This work employs layer-wise processing of DBM/PCL with considering temperature limit of material (65℃). The layer-wise nature of the methods (LAPS and SLS), allow stochastic formation of pores below AM system printing resolution which otherwise could be possible by adding space holder fillers. In addition, heat source in LAPS and SLS has no contact with material and minimizes the disease transmission risk.

The results of the second part of this dissertation opens up a new route for manufacturing scaffolds with superb biocompatibility with a wide range of mechanical properties by changing bone to PCL fraction and post processing conditions.

CHAPTER 5: FABRICATION OF DEMINERALIZED BONE/POLYCAPROLACTONE COMPOSITES USING LARGE AREA PROJECTION SINTERING (LAPS)

5.1 Abstract

Cadaveric decellularized bone tissue is utilized in many musculoskeletal surgical procedures. Typically the allograft acts as a scaffold to guide tissue regeneration with superior biocompatibility relative to synthetic scaffolds. This work focuses on the development of porous structures composed of granulated cortical bone and polycaprolactone. In this study, the Large Area Projection Sintering (LAPS) method is evaluated as a fabrication method. This method selectively heats the deposited material layer-by-layer to create 3D geometry. We evaluated the composite materials in terms of spreading behavior, and the mechanical properties of LAPS fabricated samples in lyophilized and hydrated states. The results indicate that the LAPS-manufactured composites of 45-55% bone particulates produced strength comparable to processed and demineralized cancellous bone.

5.2 Introduction

Treatment of the bone failure caused by trauma, aging or disease resulting in large voids is a challenge. Three dimensional constructs are needed to incorporate the macroscale interconnected pores and micro features for nutrient transport and cellular modulation [373] so that voids can heal effectively. Thus far, many researches have reported successful creation of porous structures with synthetic materials as a substitute for spongy architecture of the bone. Instances of such efforts include: emulsion freezing/freeze-drying [295], solvent-casting/particulate leaching [296], gas

foaming [297] and fiber bonding [298]. Another traditional solution to treat orthopedic defects is machining bone allografts into standard clinical shapes from donated cadaveric bone. This approach is advantageous over the synthetic materials since it matches internal architecture, mechanical properties and has excellent osseointegration [300]. However, the allografts are available in only a limited range of geometries and must fit the envelope of a donated bone. For example, a small quantity of standard bone blocks might be cut from a single long bone. All these methods share the weaknesses of insufficient ability to produce complex geometries [301].

With additive manufacturing (AM) technologies, forming complex features is not a challenge. Various AM techniques including, selective laser sintering [303, 304], stereolithography [305, 306], ink-jet printing [307-309], fused deposition modeling (FDM) [310-312], etc. have been tried to fabricate scaffolds for bone ingrowth .In some cases, reinforcing [311, 313] or bioactive agents [314-316] are added into the base material to improve mechanical and biological properties of scaffolds.

Hung et al. utilized extrusion based additive manufacturing to fabricate pure PCL and DBM/PCL hybrid scaffolds. They demonstrated that the hybrid scaffolds enhanced the healing process within 1 to 3 months after transplantation [314].

Although extrusion based method showed good capability to create complex geometries, the contamination of the DBM scaffold is still a problem which necessitates a vigorous cleaning process or components replacement before using different source of the donated bone particles. Further, the filament must be void-free to allow smooth printing. Thus pores must be designed into the CAD model which limits the minimum void size to the minimum printed feature or are introduced by adding temporary space holders that are removed in a secondary process which is associated with biocompatibility concerns. Such deficiencies created an impetus to explore new

layer-wise AM methods to process DBM/PCL hybrid powders with no guest substance to form the pores.

This study evaluates a novel layer-by-layer additive manufacturing technique i.e. Large Area Projection Sintering (LAPS) [374] to identify the challenges and potentials of this new method in fabrication scaffolds composed of demineralized bone and polycaprolactone (PCL) powder mixture. The LAPS, utilizes visible light energy to selectively pattern the image onto the powder bed to build the 3D geometry. The light heats the powder to melt the embedded PCL in the exposed areas and created the 2D slices layer by layer. This work explores the ability of cadaveric bone and polymer (polycraprolactone) composites to replicate the mechanical properties of demineralized bone allografts. It is expected that the inherent porosity of the fabricated composite will allow formation of pores below the printing resolution itself and expedite the bone regeneration process thanks to the biological cues to the recipients' cells from the bone tissue [314].

5.3 Experimental Procedure

5.3.1 Materials

Donated cadaveric bone was processed at LifeLink Tissue Bank, where a proprietary clinical cleaning process was used to remove the blood, lipids, viable cells, and micro-organisms. The cortical bone was further processed by grinding to create a coarse powder. The PCL was purchased from Polyscience Inc. with average particle size of approximately 600$\boldsymbol{\mu m}$ and molecular weight of 50,000 with the melting point of ~ 60℃ . In order to improve the printing resolution and decrease the minimum layer thickness, both as-received materials were sieved to eliminate particles larger than 300μm.

5.3.2 DBM/PCL Ratio Selection

Effective scaffolds require a combination of mechanical strength and bio-functionality. Increasing PCL favors the mechanical properties, but reduces the bone content and consequently the bioactivity of the structure. To find the minimal PCL content required for adequate mechanical strength, the bone particulates were mixed with PCL in different ratios to form a homogeneous mixture. The bone content was varied from 35Wt% to 75Wt% in 5% increments. Rectangular molds were filled with the resultant mixtures and heated to 65°C (above melting point of the PCL) for three hours to initiate bonding throughout the samples. Afterwards, the mechanical integrity of each sample was evaluated by checking how readily samples break in handling. The 45Wt% and 55Wt% bone mixtures with PCL demonstrated good strength while maximizing bone mass fraction. These compositions were utilized for all subsequent testing.

5.4 Steps Towards Additively Manufacturing

5.4.1 Powder-Bed Formation

The powder bed density and structure plays a key role in final part properties in many powder-based AM processes [375]. Higher spread density results in more inter-particle bonding sites for increased strength and reduced shrinkage in many processes [376]. Although theory provides insight on the optimal powder packing configurations [28-30], when spread, the powders usually pack randomly. So a comprehensive spread behavior of bone and PCL particles was studied for the two most commonly used spreading methods: scraper and roller.

A CNC table with mobility in Z-direction and XY-plane was modified to distribute the powder mixture across the build platform. A small amount of powder was manually deposited on one edge of the powder bed. A traverse speed of 19 mm/s was used with two different leveling methods to spread the powder across the bed. These were forward rotating roller (press-rolling)

and scraper. The rotational speed of the roller was set on ~80 rpm. After each layer, the height of the tool was incremented by the target layer height and the process was repeated. After depositing six layers, a metal cylinder of known cross-sectional area and a sharp edge was used to isolate a small amount of powder as shown in Figure 5.1. The mass of the powder was measured. The spread volume was calculated from the cross sectional area of the cylinder with the height assumed to be 6X layer height. The experiment was repeated three times for each deposition condition.

To assess the layer thickness effect on the powder bed density, the materials were first deposited as thick as 1250 μm where the spreading tools leveled the layers uniformly. Then the experiment was repeated for thinner layers - to find the lower bound of thickness for which the roller and scraper could form uniform layers.

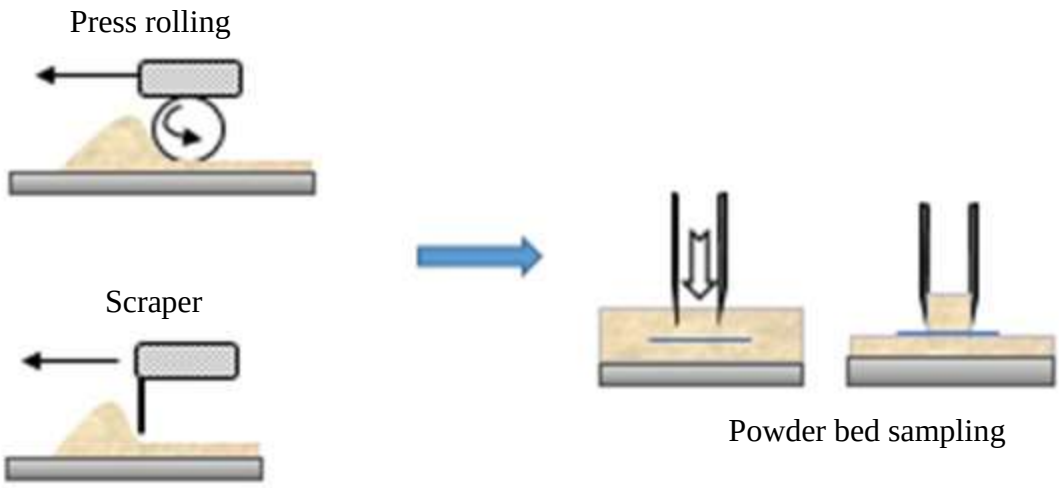

Figure 5.1. Formation of layer by roller and scraper spreading tools and sampling powder bed to measure spread density.

5.4.2 Sample Creation by LAPS Method

Two groups of samples were created by LAPS additive manufacturing method for each of the selected powder mixtures - 45 Wt% and 55 Wt% bone. One series was processed with the

lowest possible thickness of the layers identified in layer formation experiments and the second set was fabricated with 1000 μm layer thickness to see how the layer thickness influences mechanical properties of the samples.

The source to provide the required energy to cure the PCL was a conventional projector modified to boost the optical intensity to ~ 1.28 W/cm^2. The 2D image of the tensile bar was projected onto the powder bed and an Infra-Red camera was used to monitor the curing temperature through the process. The image was sustained until the temperature reached 65 °C where the PCL is molten and bonds the bone particles. This temperature limit was selected to avoid altering the favorable biological features of the bone. Then the cured layer was allowed to cool down to 30 °C to ensure that the PCL does not bond to the loose powder when depositing the next layer. Six layers were cured for completion of the samples. The schematic layout of the manufacturing set up and projected image are shown in Figure 5.2.

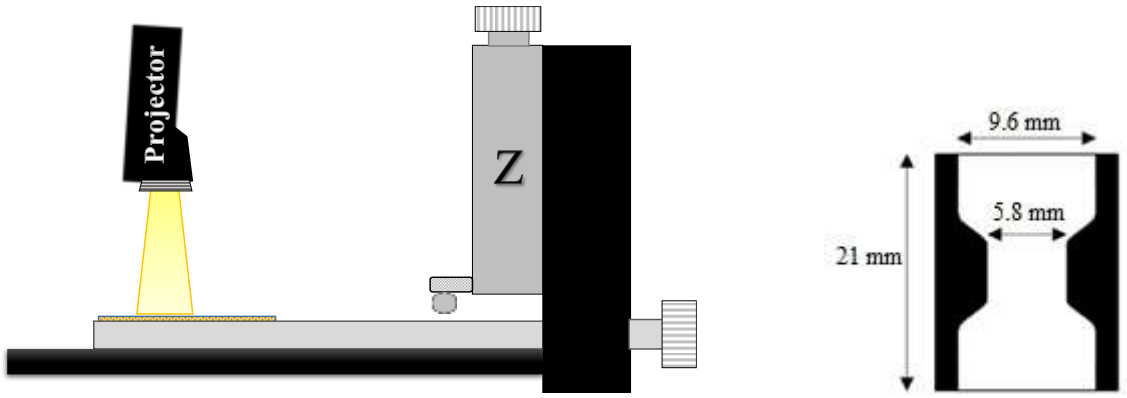

Figure 5.2. The 3D tensile bars creation. Left: The LAPS additive manufacturing set up the image projected onto the powder mixture to fabricate each sample. Right: Representative sample dimension.

5.5 Reference Controls

The porous structures made by LAPS are envisioned to be used as replacement for conventionally fabricated scaffolds. So two different traditional methods were used to create

reference samples. As the first reference, the demineralized cancellous bone strips with around 6 mm in thickness, 13 mm width of the narrow section and 21 mm of the gauge length were machined into tensile bar shape as shown in Figure 5.3.

Figure 5.3. The machined demineralized bone graft prepared for tensile test.

To prepare the second group of reference samples, a mold was printed by using extrusion based additive manufacturing method such that the virtual dimensions of the resultant samples comply with the ASTM D638-10 standard with 13 mm gauge width and 3.6 mm thickness.

5.5.1 Sample Preparation for Tensile Test

Scaffolds must be sufficiently sturdy to survive pre-surgery handling and to realize the biological tasks after implantation. Therefore strength of the samples were quantified by using a universal hydraulic testing set-up. To prevent excessive deformation of samples in gripping, a low viscosity epoxy was infiltrated into the pores in the grip sections of the tensile bars. Each end was dipped in the epoxy resin and then was left at room temperature overnight to be cured. Three to five specimens were prepared for each batch. The induced tensile forces were measured with a 100 lbf load-cell capacity at grip displacement rate of 1.5 mm/min. Tensile properties were measured rather than compression as the tensile properties are more readily measured for thin samples.

To mimic in vivo conditions, the mold samples and the machined demineralized bone tissue were tested in dry and hydrated states. In order to mimic the body environment, the hydrated

samples were immersed for 30 minutes in a solution of 8% by weight NaCl in deionized water [377]. The tensile strength was measured immediately after removal. In addition to the hybrid samples, pure PCL samples were prepared using the molds and then tested to determine the upper bound of the mechanical strength.

5.6 Results and Discussion

5.6.1 Optimal Conditions for Bed Formation

The results of the material layering experiments (see Figure 5.4) indicate that, regardless of the bone fraction in composites, the packing level of the layers are correlated to the spreading tool and the layer thickness.

It also can be seen that the roller spreads denser layers than scraper methodology. In addition, it is able to create thinner layers (300 μm) when compared against the scraper (500 μm) as the lower bound of layer formation. These differences can be attributed to the contact dynamic of spreader tools with material [378].

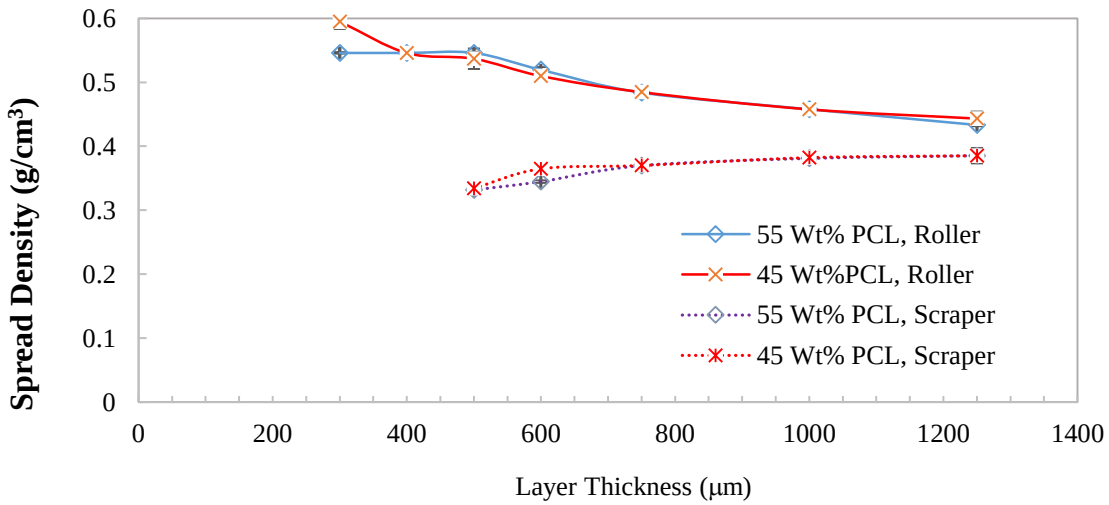

Figure 5.4. The variation of the powder bed density for using two spreading tools; roller and scraper

The rotational movement of roller induces friction between roller and powders and aligns the asymmetric powder particles in the plane. Increasing layers thickness reduces powder bed density suggesting that the alignment is less effective in thicker layers. Further, it was observed that the powder bed had some springback after the roller passed over. This resulted in an overestimate of the powder bed density since the height was assumed to be the layer thickness times the number of layers.

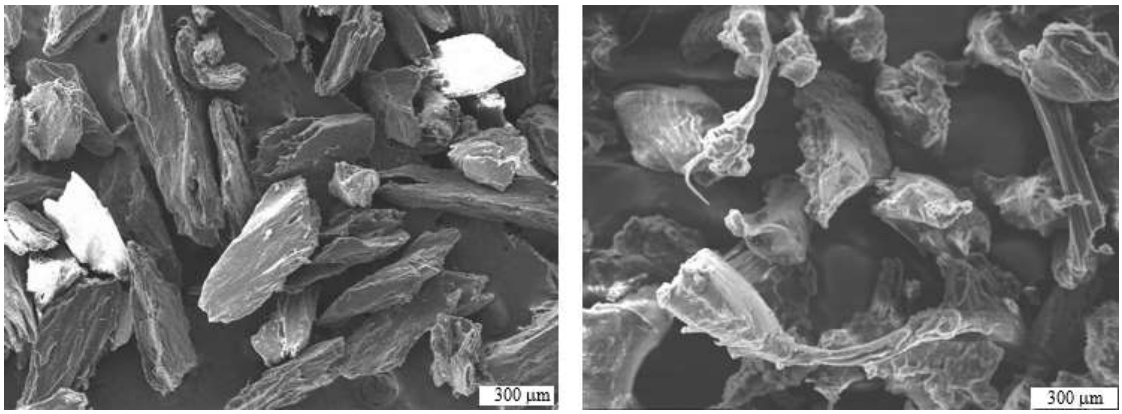

Figure 5.5. The SEM image of the powders sieved down to < 300 µm.
Left: Bone particulates, Right: Pure PCL powders. Scale bars represent 300 µm.

On the other hand, the scraper has short acting time on the materials and induces less shear stress making this device less effective to re-align the particles. The microscopic images of the materials, shown in Figure 5.5 indicates that the sieved particles have irregular rod shape with less than 300 µm in one direction but approaching 1 mm in length. Thus, it is expected that in forming thin layers, a larger fraction of the particles get displaced by the scraper and the spread density is reduced and the minimum layer thickness increased compared to the roller case. This is consistent with the observation that the material could not be processed at layers thinner than 500 µm. At thicker layers, the density from the two methods seem to be approaching the same value with decreasing differences.

5.6.2 Mechanical Characterization

As shown in Figure 5.6, the ultimate tensile strength (UTS) varies significantly based on the fabrication method and composition. It is evident that the PCL fraction is a key factor in mechanical strength in both LAPS and mold method.

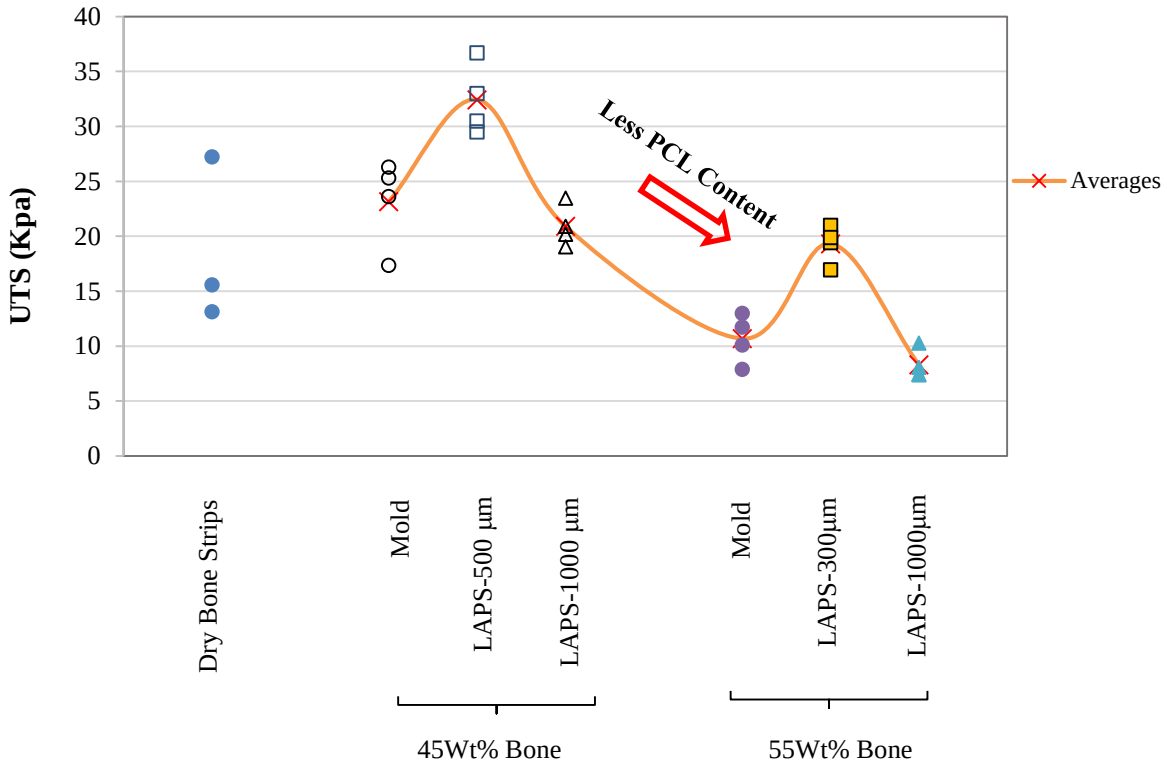

Figure 5.6. Comparison of the ultimate tensile strengths for natural cancellous bone and PCL/bone composites fabricated by heating in a mold and LAPS with varied layer thickness. All testing was done in the dry state.

Micro-image of the fracture surface indicates a significant deformation in PCL fibers before specimen failure and suggests that the PCL bears most of the load in tensile testing (see Figure 5.7). The hybrid bone/PCL samples made by LAPS show comparable mechanical strength with the demineralized cancellous bone and mold samples. Considering the results for each set of additively fabricated samples, it is clear that the layer thickness plays an important role on the ultimate tensile strength (UTS).

For both powder mixtures the UTS magnitude increases by nearly double when the layers' thickness reduces from 1000 μm to the least thickness of each compound i.e. 300 μm and 500 μm for 55Wt% and 45Wt% bone compounds respectively. This is consistent with the expectation that closely packed powder bed would create a sample with improved mechanical properties.

Further, comparing the results for LAPS-fabricated to the molded samples reveals that for each bone/PCL powder stock, if the samples are made layer-wise with the identified thin layer, they show better mechanical characteristics than the molded samples.

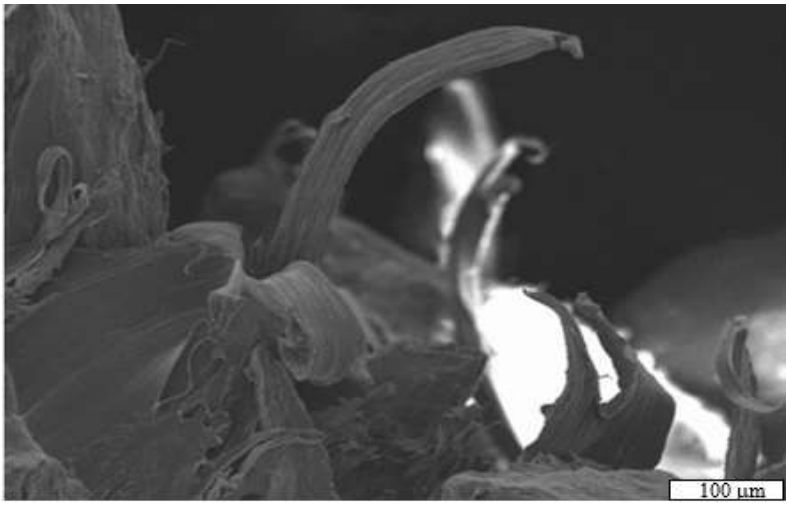

Figure 5.7. SEM image of the PCL fibers at the fracture face of tensile test of a 45Wt% PCL/Bone mold sample. The view direction is perpendicular to X-Y plane, scale bar represents 100 μm.

In addition, the LAPS additive manufacturing method can be potentially manipulated to form scaffolds with fairly complex geometries and features. The strength and the resolution in Z-direction from one side and fabrication rate from the other side are the tradeoffs that need to be determined according to the needs.

The mechanical characteristics of the hydrated samples is compared to that of the dry state as shown in Figure 5.8. In general, all sample groups weaken significantly weaken after hydration. For the machined demineralized bone strips, the UTS drops down by ~30 times, consistent with prior observations [379]. For bone/PCL hybrids, however, the hydration impact is reduced and there is an inverse relation between the PCL content of the samples and the relative reduction of UTS. Based on the increased strength of LAPS samples compared to molded samples, it is reasonable to expect that both 45% and 55% bone samples will be able to produce adequate hydrated strength to replicate the bone strips.

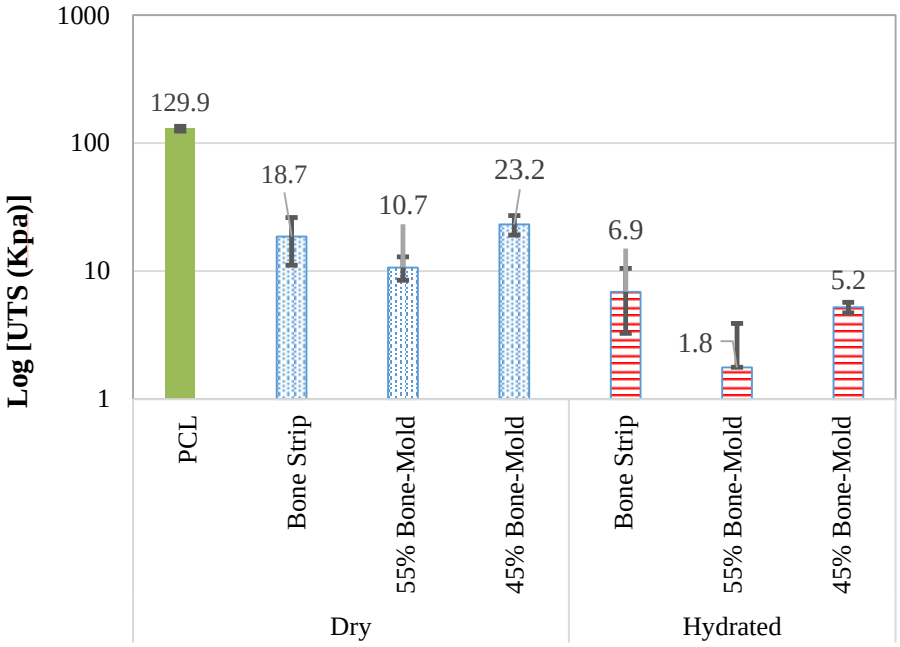

Figure 5.8. Summary of hydration impact on ultimate tensile strength.

5.7 Conclusion

Composites of PCL and cortical bone particulate can create highly porous scaffolds for orthopedic applications. The study illustrated the two promising mixture ratios for creating scaffolds for both mechanical and clinical needs. Demineralized bone fraction between 45Wt% -

55Wt % was identified as the mixture ratio that result in sufficient mechanical properties for handling while containing significant bone particles to aid bio-integration. Mechanical testing of the samples made with these two ratios demonstrate that increased PCL content improves the mechanical properties. The UTS of specimens produced by LAPS largely depends on the layer thickness.

The samples composed of 1000 μm thick layers show comparable strength to the molded specimens with the identical materials. The UTS improves when processing in thinner layers. This is possibly due to the increase in spread density. Hydration reduces the UTS of the composite specimens less than the demineralized cancellous bone. Overall, the results demonstrate that bone/PCL composites produced with the LAPS additive manufacturing methodology have suitable mechanical properties to create patient-specific implants. Future work will address the biological performance of these composites and methods of controlling the resulting pore structures.

CHAPTER 6: FABRICATION OF DEMINERALIZED BONE/POLYCAPROLACTONE COMPOSITES USING SELECTIVE LASER SINTERING (SLS)

6.1 Abstract

Selective Laser Sintering (SLS) is a popular manufacturing method. It utilizes a collimated laser beam to selectively melt the surface and define fine features. However, the proper adherence of particles to each other narrows the material range suitable for SLS. The purpose of this chapter is to identify preliminary challenges of utilizing selective laser sintering in processing Demineralized Bone Matrix (DBM) and Polycaprolactone (PCL) composites. The interaction of CO_2 laser with DBM/PCL was studied by creating single square layers for different key procedure variables. The results identified the sets of variables that should be harmless to DBM biological features and allow stacking up the printed layers to produce three dimensional geometry. After printing, the mechanical properties of the parts were enhanced through isothermal heat-treatments. The maximum tensile strength of samples for each batch of samples was found strongly dependent to shrinkage level. The results open up a new route to construct complex patient-specific scaffolds with potential for enhanced biological excellence thanks to the presences of DBM particles.

6.2 Introduction

Selective laser sintering (SLS) is an additive manufacturing (AM) technique that uses laser as the power source to sinter the particles to each other based on the 2D slices of the CAD model. The 2D layers are processed sequentially and build up a 3D physical object. The ability of SLS to define fine features has made it a broadly used manufacturing method in industry. The

precise and high speed control of the laser beam allows accurate steering of laser beam to the selectively coalesce the powders. Further development of SLS is tied to the range of materials that can be sintered. In this regard, one of the most promising directions in its ongoing growth is creating products that are based on composite materials.

Efforts to apply the SLS process for tissue engineering includes designing the geometry or altering material system (by inclusion of guest material). For example, Loh et al. reviewed the researches that controlled the pore size with SLS to produce varying properties of scaffolds [5]. As an instance of such works, calcium phosphate was processed by an intermediate polymer which was thermally removed during post processing [380]. Tan et al. conducted a study on producing polyetheretherketone (PEEK) and hydroxyapatite (HA) biocomposite. The Single layers were fabricated first with bed temperature of 110 °C and then140 °C with laser of 12 watts in both cases. The bed temperature increase, resolved a delamination problem and enhanced the layer integrity [381]. They produced different level of inter-particle boding in scaffolds by adjusting SLS process parameters [381].

In spite of the significant efforts to expand SLS application to process new materials, the DBM particulates have never been part of the material system. However, Hung et al. reported that DBM/PCL composite scaffolds fabricated by extrusion based AM, have improved cell proliferation compare to control samples with pure PCL [314].

This research primarily focuses on assessing SLS capability to process DBM/PCL hybrid scaffolds for tissue engineering. In spite of the fact that DBM has superior bio-compatibility, in manufacturing regard, DBM particles impose a strict limitation on the process conditions and has not been reported previously. We conducted an optimization process by investigating single layer quality and determined the suitable set of variables that enables using SLS for making DBM/PCL

constructs- a big step toward expanding choice of material to manufacture temporary scaffolds with fine porosity.

6.3 Experimental

In this study, different combinations of SLS variables were utilized to process single layers of DBM/PCL mixture to identify which power settings could reliably form 2D slices with no visible damage to DBM particles. In order to create 3D construct, a customized layer forming machine was designed to spread layers of material and was placed in a commercial laser cutting system. Between the layers, the laser scanned the previously spread layer until the entire 3D print is complete. To further strengthening the green samples, a heat treatment process with different lengths was performed which caused anisotropic shrinkage. Then the dimensional change as well as mechanical properties of the samples were evaluated as a function of the heat treatment time.

6.3.1 Materials

Scaffolds require to meet combination of mechanical and bio-functionality. The PCL content promotes mechanical properties but reduces the bio-agents fraction in the composites. As demonstrated in section 5.3.2, the 45Wt% DBM and 55Wt% PCL mixture results in good handling properties while maximizing DBM content. This mixture was used to perform optimization process and fabricating tensile bars. The DBM and PCL powders were smaller than < 250 μm and < 300 μm respectively.

6.3.2 Laser Parameters Identification

There are over 50 variables that play a role in laser-based additive manufacturing which fall under four major groups [382]. The first category of variables is laser characteristic and scanning strategies that are subject to adjust in this dissertation. The other three categories include; powder properties, spread layer quality and processing environment conditions [383, 384].

In SLS, the key variables that govern energy density of a laser include: laser power, scan spacing and scanning speed. The energy per unit area (or Andrew's number [385]) is calculated by following equation:

$$An = \frac{P}{d \times V} \qquad \text{Equation 6.1}$$

in which the laser power (P) is the amount of energy transferred to material and presumably is equal to the laser input wattage. The line spacing (d) is the gap between two neighboring scan vectors and scanning speed (V) refers to tracing velocity of laser beam across the powder bed. The beam spot size is the area of the point when the lens is in focal length.

6.3.2.1 Laser Specifications and Scanning Strategy

Processing of the powder was implemented by a conventional laser cut/engraving machine. To provide the required energy for fusing the materials, Rabbit HX-SE-1290 system with a CO_2 laser tube that operates at 80 watts nominal power was employed.

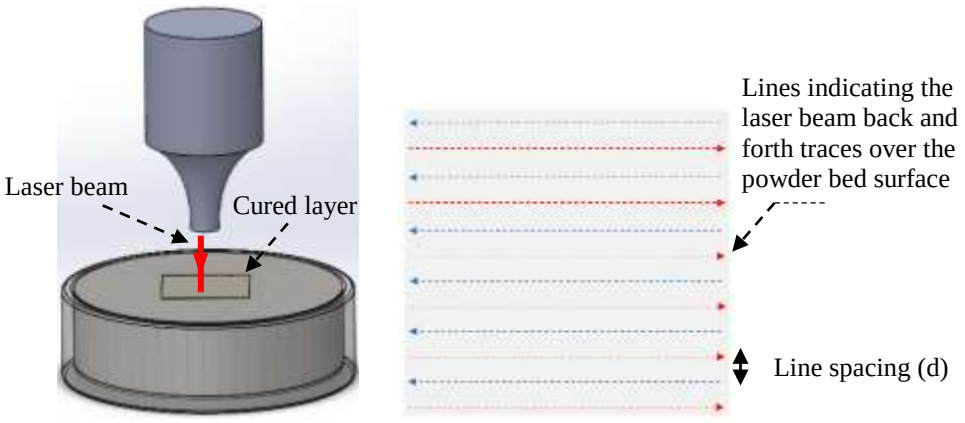

Figure 6.1. The schematic of the bidirectional raster laser scanning.

The focal distance of the lens was 2 inches and the machine was able to create feature size as small as 1 mm×1 mm. The beam spot size was estimated 200 μm at the focal point. For consistency, all experiments were performed by bidirectional rastering pattern (see Figure 6.1) at room temperature (no bed preheat).

6.3.2.2 Layer Primitives

Using primitive shapes is a common way in AM studies to find the best set of procedure variables. Depending on the goal of optimization, the primitive could be opted to have different geometries such as line, square, cube, etc. [381]. The outcome of primitive studies helps to understand the challenges and paves the way to manufacture the actual 3D objects. In this study, retaining the biological feature of the DBM particulates is extremely critical and in order to determine the suitable process setting, a single layer primitive of 1 cm was selected to be studied first.

6.3.2.3 Printing Requirements

The key process variables, as described in section 6.3.2, were varied to see how they would influence the laser interaction with the material. The laser parameter setting started with a low laser power at which no bonding initiated. Then for each set of scanning conditions, the laser power was gradually raised until inter-particle bonding emerged, marking the lower bound of processing power. Then incrementing continued by 0.008 or 0.08 watts until the color change of DBM material occurred - identifying an upper bound of the processing power range.

In order to improve cohesiveness of the layers, two different methods were examined: smaller line spacing and increasing the distance between the bed surface and the laser exit aperture to enlarge the laser spot size. The optimization process was repeated for each set of parameters.

The second criteria was related to processability of the primitive layers and is crucial for successful layer-wise AM printing. Processability in this context includes combination of layer upward curling and integrity of the layer. The curling could be a source of part shifting during the spreading of the next layer and may cause printing failure. The layer integrity refers to the strength of the layer cohesion which must be at least sufficient to handle the final part.

The curling and integrity were found to be interrelated. To illustrate that how power setting affects the layer distortion level, either power or speed was varied separately with the constant line spacing of 100 μm. The curling was assessed by qualitative inspection of the layers and the weight of the primitive layers was considered as an indicative of thickness and integrity of the layer.

In the first group of experiments, the scanning was performed with 150 mm/s speed and four different powers were attempted. To fabricate the second group of primitive layers, power was set at 5.36 W and the scanning speed was varied between 50 mm/s-200 mm/s. The optimization process was carried out by inspecting layer primitive quality and will be discussed in section 6.4.2.

6.3.3 Sample Preparation

The function of a selective laser sintering (SLS) system was simulated by adding a layer forming set-up into a commercial laser cutting system. A layering set-up was designed and built considering the space limitations inside the laser cut work envelope. The samples were fabricated by the optimum lasing parameters (identified in primitive layers' study) and further post-processed through an isothermal heat treatment to increase part strength.

The confined work-piece size of the laser cut machine dictates some requirement on layering set up design. As seen in Figure 6.2, a limited clearance over the powder bed is allowed to avoid the risk of strike between the laser exit and the set-up. A pulley-belt mechanism driven

by a stepper motor was designed to move the spreading tool back and forth to meet the small clearance requirement over the powder bed. The roller was selected to implement powder deposition because it offers more flexibility in layering material by switching rotation direction and speed. The roller spins by means of a DC motor at 120 rpm and moves back and forth with the linear speed of 5 cm/s.

In order to minimize the vertical size of the entire set up, two pistons were designed side by side, one serves as a feed piston and the other as the build platform. These pistons were motorized by two stepper motors. This design saves some vertical space rather than the typical deposition systems wherein a hopper crosses over the powder bed to deliver the material.

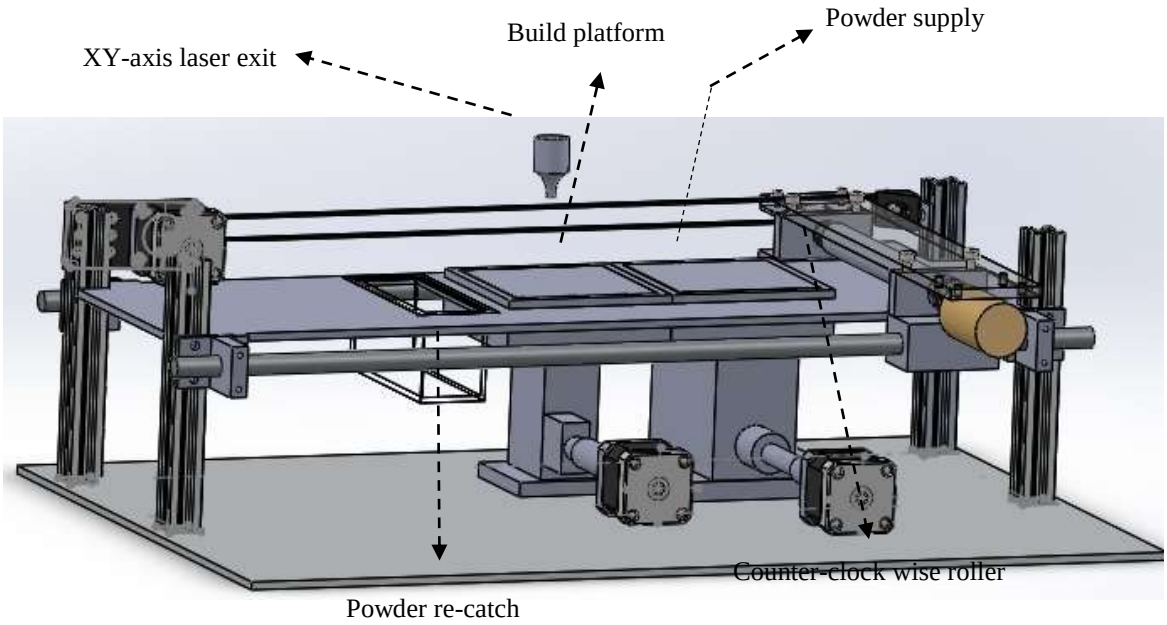

Figure 6.2. The schematic of the powder deposition system designed to deliver the composite material through a layer-wise additive manufacturing process.

To form a layer, the powder supply piston (see Figure 6.2) raises the material, at the same time the build piston goes down to accommodate one new layer. Then the counter rotating roller

recoats the material over the build platform, deposits the extra material into the powder re-catch box (to be retrieved) and retracts to its initial place. The laser is triggered manually and implements one 2D layer based on the CAD model. By repeating this process and putting down the successive layers, the 3D geometry is created.

The current build platform enables fabrication of the samples as big as 8 cm by 8 cm planar dimension and 2 cm height. The motion sequence of the components of the entire unit is controlled by an electronic board (Arduino) and Marlin firmware.

6.3.3.1 Tensile Bar Geometry

In total 9 tensile bars composed of 45 Wt% DBM and 55 Wt% PCL with 500 μm layer thickness were created. The CAD dimensions of the gauge section was in accordance with ASTM D638-10 standard with 13 mm width and 6 mm thickness. The overall length of the samples was 64 mm.

6.3.3.2 Post-Processing Heat Treatment

It was observed that the green samples have insufficient mechanical properties for handling and need to be strengthened. Three groups of samples (each of which had three tensile bars) were heat treated separately to assess the resultant shrinkage and mechanical properties improvement. All the isothermal heat treatments carried out in a curing oven at melting point of PCL (65℃) in which PCL turns to liquid phase but has low viscosity to flow and misshape the part. The examined curing times were 3 hours, 5 hours and 7 hours.

6.3.4 Shrinkage and Mechanical Testing

The different length of the heat treatment caused non-uniform shrinkage in different levels which is expected to influence the mechanical properties of the cured samples. To evaluate the

shrinkage, the sample height, gauge section and the overall length were measured for each batch of the cured tensile bars and were compared to the design values from the CAD model.

The tensile strength of the samples was studied by using universal hydraulic testing set-up. In order to acquire accurate data, the grip section of the samples must not deform during testing. Thus, a low viscosity epoxy was infiltrated into the pores in the grip sections of the tensile bars and hardened overnight at room temperature. The induced tensile forces were measured with a 200 lbf load-cell capacity at grip displacement rate of 1.5 mm/min.

6.4 Results and Discussion

6.4.1 Proof of Concept

The interaction of polymer with the laser depends on its thermal, optical and rheological properties. These intrinsic properties are dictated by molecular structure of the polymer and are difficult to manipulate [386]. To see how readily the CO_2 laser is absorbed by PCL, a PCL powder (< 300 μm) was filled in a pitcher dish with 10 mm depth and scraped to make it flat and then was scanned by a laser beam for patterning a square of 1 cm.

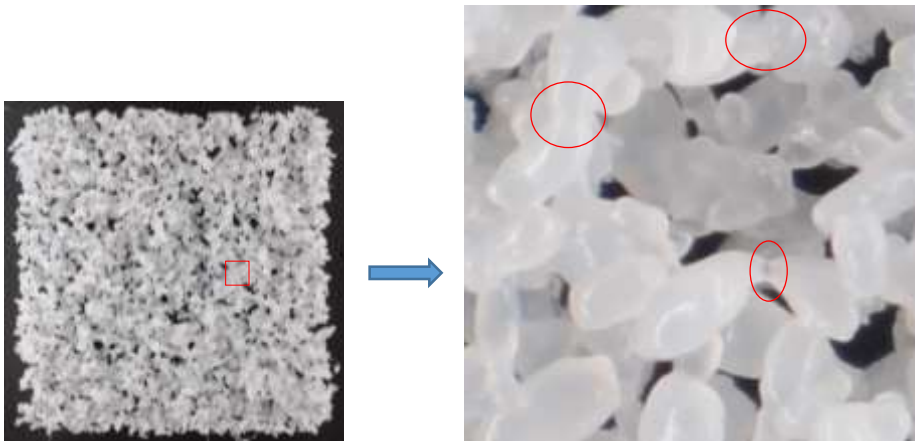

Figure 6.3. A primitive layer of 1 cm scanned by CO_2 laser. Left: The clean definition of the edges, Right: The neck formation between the particles in 50X magnified photograph.

Taking a close look into the resultant layer (shown in Figure 6.3) reveals that as laser beam traces the surface, local bonds form between PCL particles. The edge roughness of the scanned square is on the order of the particle size indicating that SLS of DBM/PCL composite might be able to fabricate features similar to the particle size.

6.4.2 Laser Sintering Process Window

This section is devoted to evaluate the primitive layers quality that were produced by varying laser power setting. The purpose is to identify an operation window over which the DBM's color does not alter and the layer is flat and sufficiently cohesive to form effective geometries.

6.4.2.1 DBM Discoloration

The figures of this section show that how processing conditions affect the safe operation window. For the data in Figure 6.4, beam spot size was estimated 0.2 mm and the line spacing was reduced from 100 μm to 50 μm. But in Figure 6.5, the line spacing was constant at 100 μm and the laser-powder bed distance was increased from 2" to 2 ¼" resulting in expanded beam spot size of 0.8 mm. The beam spot size was estimated by scanning a 1cm× 1 cm square pattern on a chipboard with stepover of 1mm to form separate traces. The widths of the lines were averaged out and estimated as the beam spot size (0.2 mm and 0.8 mm for 2" and 2 ¼" processing distance respectively). The experiments were conducted for four different speeds. The power varied from no inter-particle bonding condition and increased to identify bonding and DBM discoloration threshold between which would be desirable area that meets bone discoloration criteria.

Figure 6.4 summarizes the line spacing effect on the DBM discoloration. It is expected that by reducing stepover distance by half, the cured lines stitch to each other more effectively but this strategy has its own drawbacks as well. It is evident that the variation of stepover changes the operation window by increased required beam speed. The 100 μm line spacing expands for higher

vector speeds while layers made with line spacing of 50 μm show much less sensitivity to scan speed.

On the downside, delivering excessive energy into material may burn the DBM in the powder bed. This is more critical at the end of laser vector where the beam turns back to trace a fresh line in which case the previously delivered energy has not sufficiently been dissipated and overheating is more likely to happen. That said, running the process with small line gaps would necessitate using a tightly controlled laser power with minimal fluctuation.

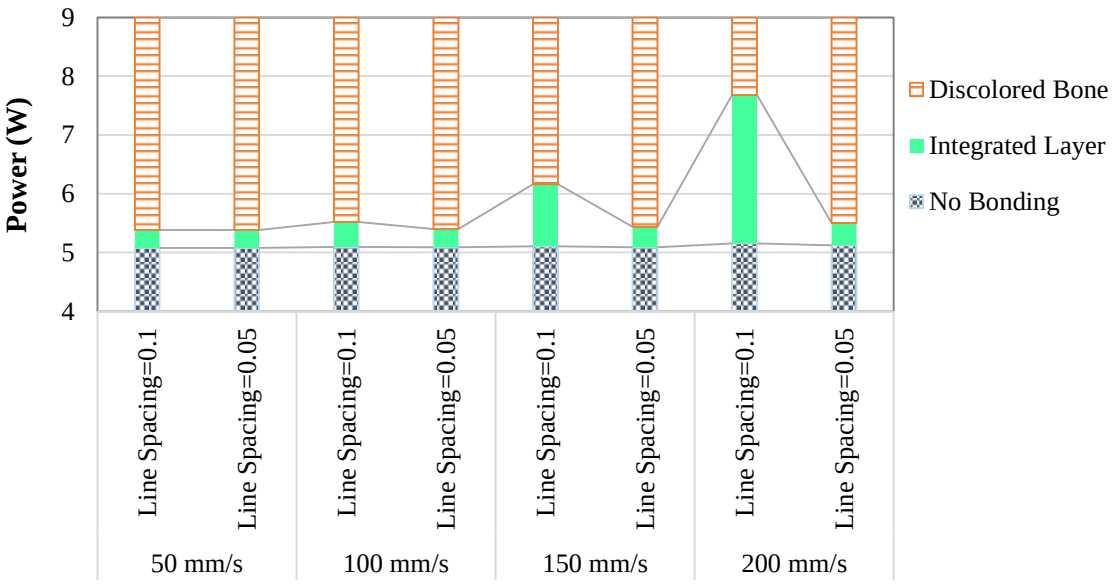

Figure 6.4. The assessment of the line spacing effect on the DBM/PCL color change to identify safe operational window for combination of scan speed and power. The powder bed distance from the lens is 2”
with the spot size of 0.2 mm

The effects of scanning with enlarged exposure area are summarized in Figure 6.5. The expanded beam spot delivers energy into a wider trace of material and keeps the PCL softened for longer period of time yielding better cohesion in the layer. The attenuation of the energy intensity

can be compensated by operating at higher laser power. Lowering the energy density allows operating the laser power at wider range but the print feature size is limited to beam size (0.8 mm).

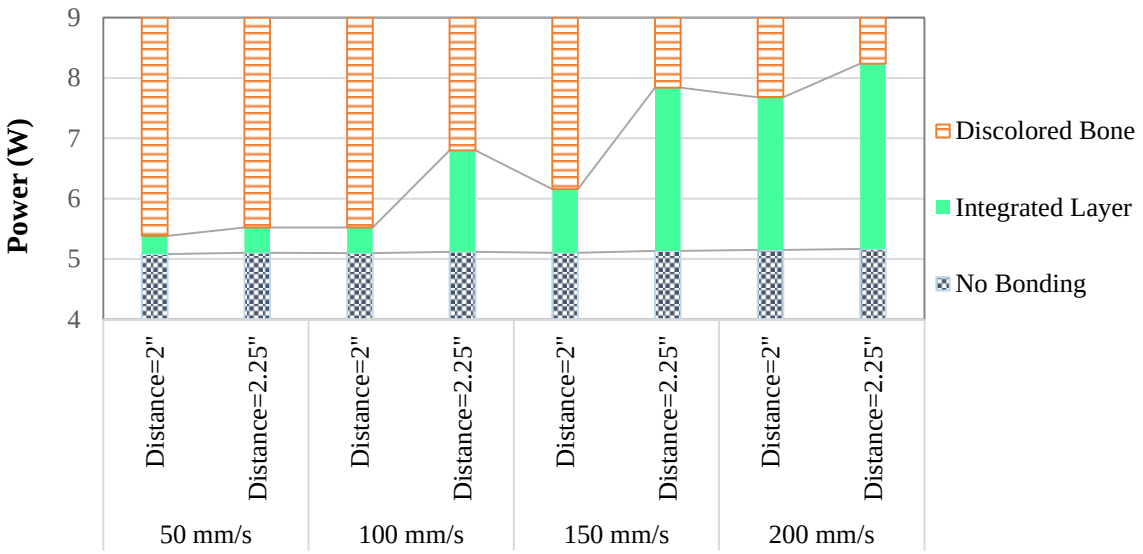

Figure 6.5. The comparison of safe operational range for processing DBM/PCL as a function of the laser-powder distance and scan speed. The spot size for 2" and 2 ¼" processing distance are 0.2 mm and 0.8 mm respectively

6.4.2.2 Laser Fluctuation

When the laser operates below 10% of the nominal power, the output power cannot precisely adjust itself with the input wattage and laser power fluctuates during operation. This makes it critical to operate in regions with wider processing windows, when the power gets closer to the lower bound, the power spike cures some lines and randomly skips others. The resultant layer is formed incompletely which is a critical problem for layer integrity printing defect.

Similarly, when the power is set close to the upper bound, still within the safe zone though, the sudden increase of the power would burn the DBM particles. These defects emerged at slower scan speeds; 50 mm/s and 100 mm/s suggesting that in such conditions the power variation is dramatically detrimental to the DBM content (see Figure 6.6). So to minimize the risk of bone

discoloration, higher speed of scan (here 150 mm/s or 200 mm/s) and operating power with some margins from the bonding and burning thresholds are preferred for SLS of DBM/PCL material.

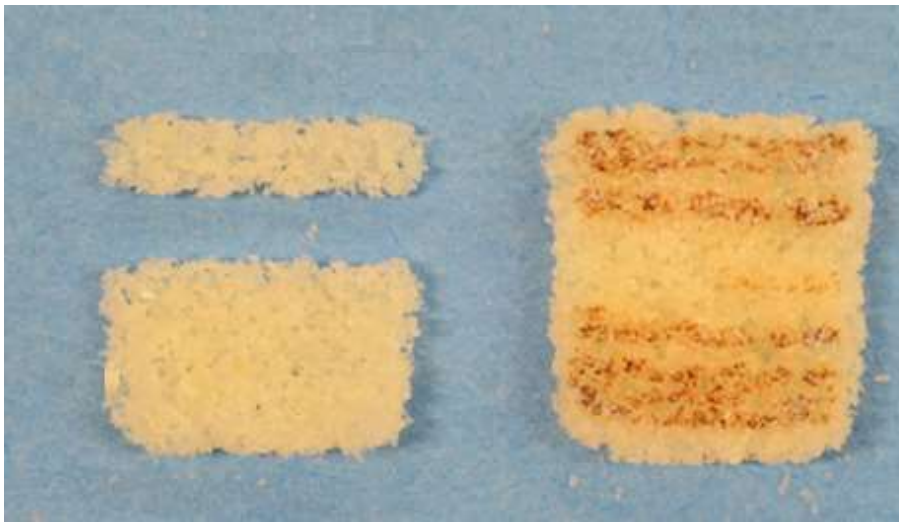

Figure 6.6. An example of laser fluctuation effect at scanning speed of 50 mm/s or 100 mm/s. Left: incomplete layer at lower bound, Right: Discolored bone traces at upper bound.

6.4.2.3 Layer Distortion

Figure 6.7 shows the power effect on amount of curling. It can be seen that even though the layer gets stronger by power increase, the curling issue is more severe. This caps the energy density option to improve layer integrity. Reduction of speed has a similar impact on the layer aesthetic feature (Figure 6.9) since it is inversely related to energy density. Looking at both figures reveals that boosting energy density increases the transferred energy to the bulk material and cures more material in depth of powder bed-as the primary reason for stronger layer formation.

The dramatic mass growth of the layers is reflected in Figure 6.8 and Figure 6.10 for constant speed and power respectively. However, the decision cannot be made solely upon samples' weight (thickness) as the severe curling occurs for excessively cohesive layers. The process setting has to meet combination of DBM discoloration requirement with minimal curling and acceptable cohesion.

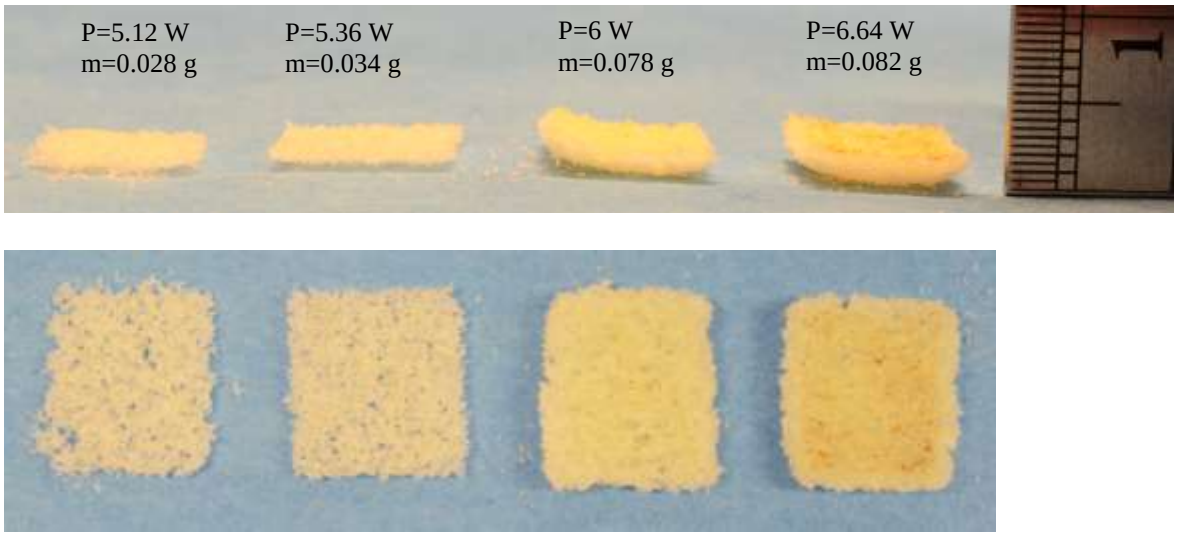

Figure 6.7. The distortion of layers caused by different laser powers for processing at focal distance of 2 inches. Laser scan speed=150 mm/s, line spacing =100 μm
The images on top show side view of the samples shown in bottom.

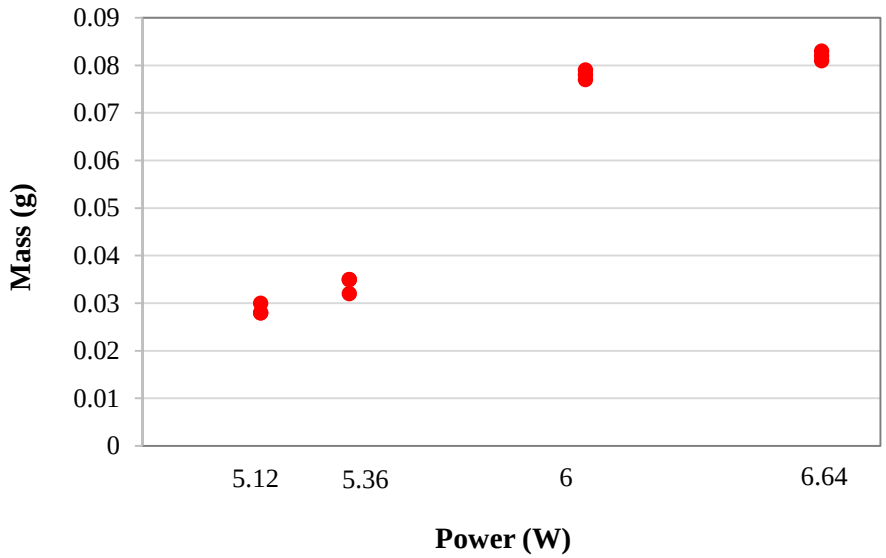

Figure 6.8. The amount of cured mass for square layers of 1 cm produced by different power percentages with fixed beam speed of 150 mm/s.

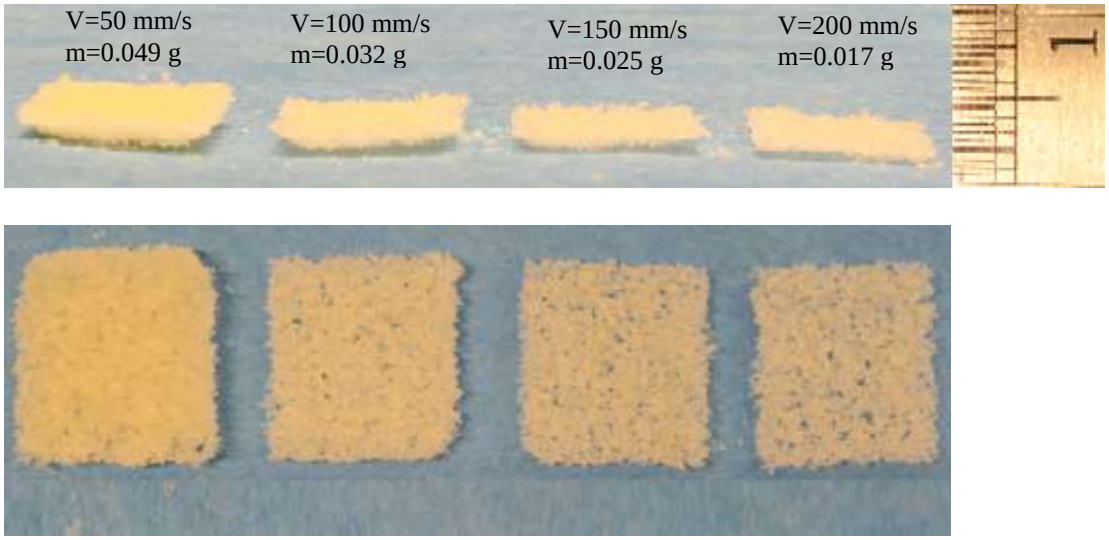

Figure 6.9. Scanning speed effect on layer integrity and curling at power of 5.36 W. Focal distance=2 inches, line spacing =100 μm. The images on top show side view of the samples shown in bottom.

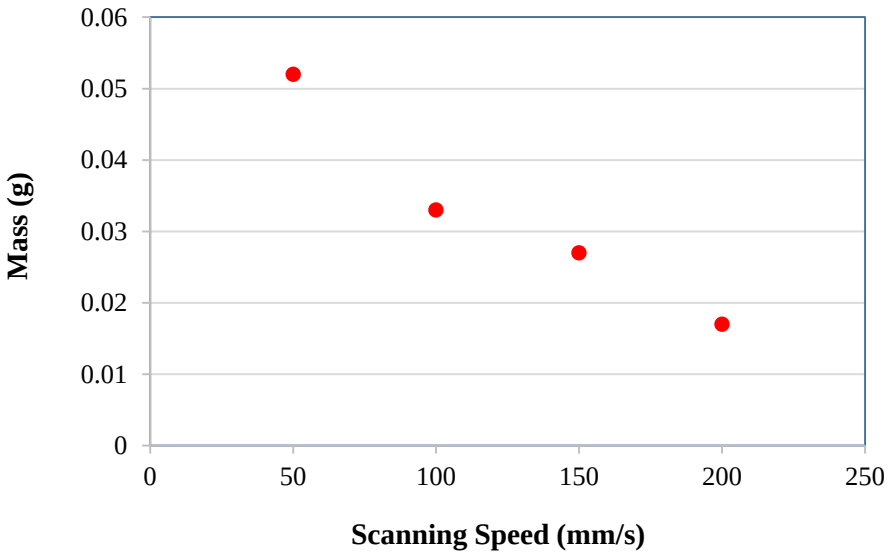

Figure 6.10. The scanning speed impact on the cured mass of square layers of 1 cm.

6.4.2.4 Optimized Processing Variables

By incorporating the observations of the single layer primitive study, it is concluded that for processing at room temperature, improving cohesion of the layers sacrifices the layer flatness and layer distortion would become a serious challenge for layer-wise processing. Among the processed layers the following set of variables created the best quality of the layer primitive; power=5.36 W, line spacing=100 μm and scan speed= 150 mm/s. This set of variables falls in safe operational window discussed in section 6.4.2.1 and were utilized to manufacture all the tensile bars.

6.4.3 Dimensional Accuracy

The shrinkage of the 9 tensile bars that printed was assessed in green state as illustrated in Figure 6.11. The overall length of tensile bar was very close to the target 64 mm. Scanning was performed lengthwise along the tensile bar for scanning layers. The lateral heat conduction causes some material to stick to the edges of the print and make planar green dimensions turn out slightly greater than CAD model.

It should be noted that since the beam width is constant during printing the amount of the neighboring material that sticks to the layer width and length is expected to be approximately similar. This dimensional increment results in greater ratio of shrinkage in the narrower part (gauge) of the sample.

In addition, the beam movement inaccuracy, optical aberration and beam scattering in the powder bed could be other sources of error [387]. The Z-shrinkage is highest as the material settles down after curing each layer and gravity promotes the rearrangements in this direction as well [388].

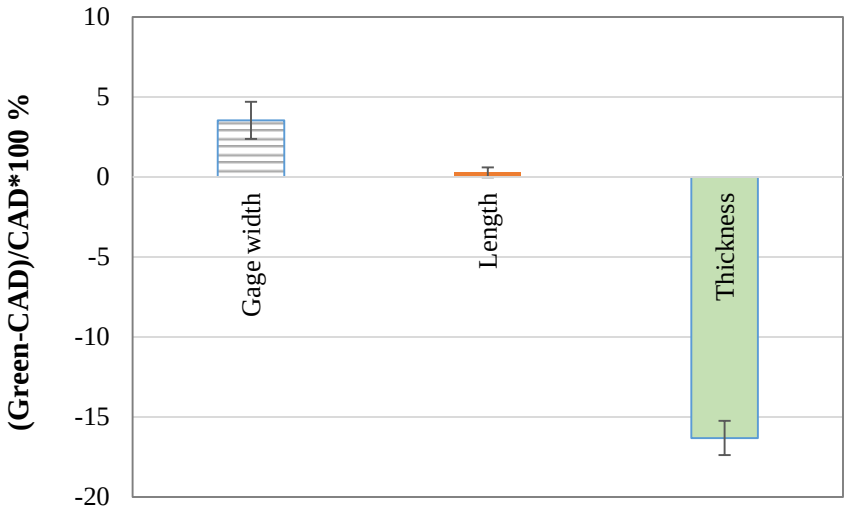

Figure 6.11. The dimensional deviation of the green samples.
P= 5.36 W, spot size=0.2 mm, line spacing =100 μm.

Each group of three samples was heat treated in an oven separately for 3, 5 and 7 hours. An example of the heat treated sample is shown in Figure 6.12. The dimensional change of the samples is presented in Figure 6.13 which indicates that the 3 hour heat treatment slightly shrinks the sample. But samples cured for 5 hours experienced significant shrinkage. Comparing the values for 5 and 7 hours shows that after major shrinkage occurrence, the molten PCL would not have as much tendency to move and the compact gets closer to metastable condition. This is desirable because the initial model can be compensated to offset for the mean shrinkage, however the variation becomes the error.

Looking at Figure 6.13 illustrates that the shrinkage in Z is slightly greater than the other studied dimensions. The continuous scan of laser along the sample length compare to the perpendicular direction (samples gauge) - which has been scanned by line gap of 100 μm - causes more shrinkage in the green state. Therefore after curing in oven less dimensional change occurs in samples length.

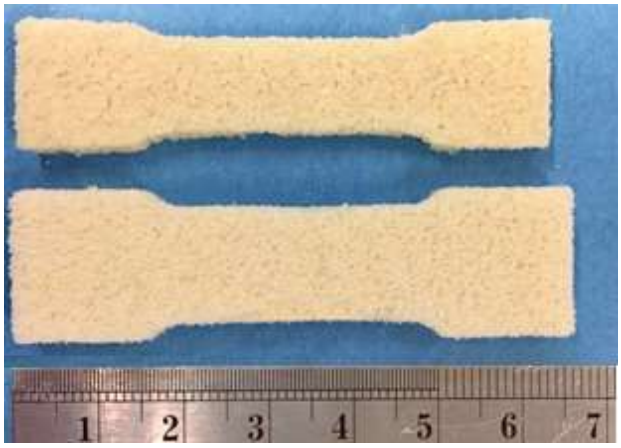

Figure 6.12. Example of tensile bars built by SLS. Bottom; green body. Top: cured at 65℃ for 5 hours.

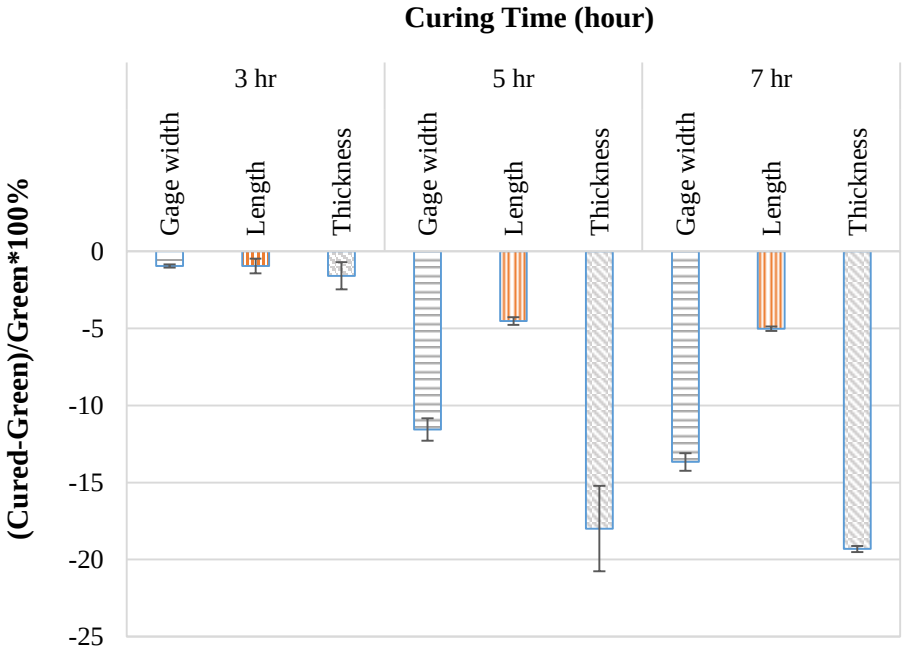

Figure 6.13.The breakdown of shrinkage in different directions caused by various curing times.

6.4.4 Tensile Strength Assessment

Figure 6.14 states that the maximum tensile strength is linked to the theoretical gauge cross sectional area. The samples cured for 3 hours, have the least dimensional change and retain their weak mechanical property. The tensile strength experiences a significant raise for 5 hour heat treated test coupons which indicates that the longer time of heat treatments promotes the ultimate tensile strength (UTS). It can be deduced that, the molten PCL has more time to migrate into the DBM particles and adhesion of the bonding promotes thereby.

The heat treatment for longer time (7 hours) makes a slight improvement in mechanical properties and particles rearrangement which suggests that maximum tensile strength reaches a plateau when further heating does not increase shrinkage. The tensile strength of the cancellous bone strips (prepared as discussed in section 5.5.1) falls within that of the manufactured sample which suggests that the fabrication process can be tailored to match up with the mechanical properties of the natural neighboring tissue.

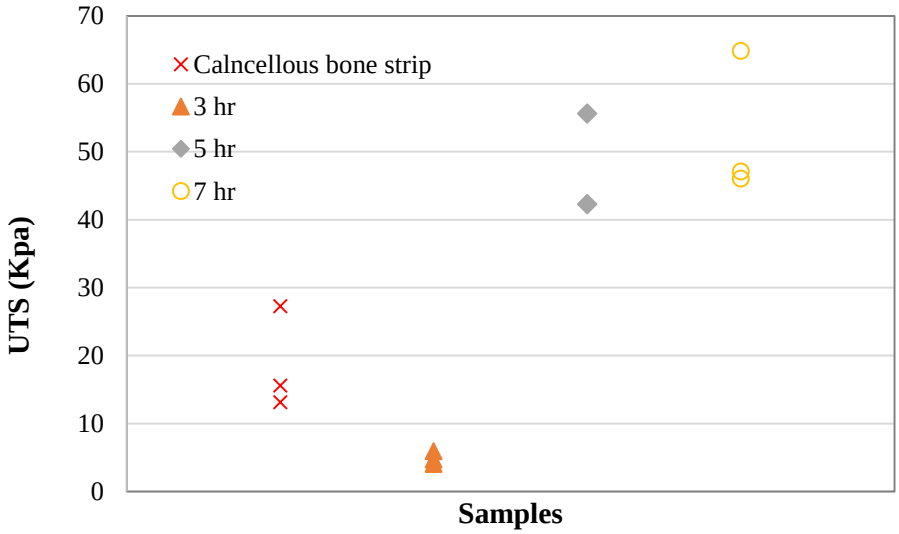

Figure 6.14. The comparison of the maximum tensile strength of the heat treated samples to the natural cancellous bone strips.

6.5 Conclusion

This work employed SLS capability to process DBM/PCL mixture. It was shown that the energy density, solely, is not a good metric for the processing conditions for these samples. Thus the flatness of the layer also was taken into consideration to ultimately find the best set of variables. The post processing strengthened the samples and the shrinkage level was identified for different curing conditions. At the end it was proven that the tensile strength tightly depends on the curing times. The results of the work indicate that SLS has a great potential to fabricate temporary scaffolds of bio composites containing natural bone particles.

CHAPTER 7: CONCLUSION AND FUTURE WORK

This study's objective is to employ Additive Manufacturing (AM) free form advantage to produce porous constructs. In order to achieve this goal the material properties coupled with processing variables of fabrication methods were adjusted to perform a successful printing.

The first part of the work employs Binder Jet (BJ) printing to process different powder feedstock of stainless steel 316L fine powders -potentially for engineering applications.

The second part is devoted to creating porous structures for tissue engineering applications. The material system contains Demineralized Bone Matrix (DBM) and is expected to have superior capability to resemble bio-functionality of the natural tissue. The two powder-fusion AM methods examined in the study were Large Area Projection Sintering (LAPS) and Selective Laser Sintering (SLS) both of which utilize non-ionizing range of electromagnetic wave to preserve favorable biological features of the material.

7.1 Key Contributions

7.1.1 Tuning Shrinkage and Density Independently

Many traditional methods have shortcomings to tune porosity level through a part, for example, these methods cannot create complex geometries. Additionally, the layers of different porosity level sinter inconsistently, thus, cause warpage in the final object. In the first part of this dissertation, the fine (< 22 μm) stainless steel particles were used as a raw material due to their favorable capability to get high densities. However, since the inter-particle forces are dominant, such powders are difficult to spread and print with.

So, a variety of treatments on the raw powder were performed to find the procedures that resolves the flowability challenge. The identified treatments can be used in any powder-based AM method. The resultant powder feedstock were further processed by a BJ system to create 3D test samples. After sintering, the dimensional deviation of the printed samples were studied and out of which the ones with consistent shrinkage level in all three dimensions were determined. The preparation process of these powder feedstock can be a key to create geometrically complex shapes with porosity gradient in a single part without final part distortion.

7.1.2 Creating DBM/PCL Scaffolds by Photonic Energy

One of the common ways to treat fractured bone is supplying a porous scaffold structure into the broken tissue to facilitate the cell culture and helping tissue to regain its original shape. Conventional methods to fabricate scaffolds have insufficient ability to replicate the complex geometry of the pre-injured bone. In addition, these methods utilize synthetic materials and implanting and have been always concerning due to lack of integrity with the surrounding bone tissue.

As an alternative to utilizing synthetic materials, cadaveric decellularized bone tissue is utilized in many musculoskeletal surgical procedures. The limited source of the donated bone graft as well as the geometrical constraints of the donated allografts have been the critical obstacles to best use of the donated human bone. The traditional way i.e. machining the donated cadaveric tissue into the standard forms, wastes a fraction of this material and consequently leads to serving less patients bone grafts. In an effort to overcome this deficits, we screened prime AM candidates and found LAPS and SLS suitable to process powder composite and adaptable to the clinical constraints. The results of the study could be a key step to fabricate implants that matches to the

recipient's body anatomy with cell-ingrowth excellence thanks to the bone powder existence in the structure.

First, we attempted LAPS as a novel additive manufacturing method. LAPS uses visible light to selectively heat the deposited material through a layer-to-layer process. Specific behavior of bone and polycaprolactone (PCL) mix necessitated investigation of the DBM/PCL compound spreading behavior which led to identifying the required conditions to spread uniform and at the same time compact layers. These results were used to implement a layer spreading system for fabrication of tensile testing specimen. The mechanical properties of the samples showed that the LAPS-fabricated composites of 45-55% bone particulates produced strength comparable to cast DBM/PCL composites and conventionally fabricated demineralized cancellous bone.

The definition of finer geometries motivated us to utilize a focused beam of energy with a wavelength that is readily absorbed by PCL. Therefore, Selective Laser Sintering (SLS) method was examined. The optimization process was carried out by varying key laser parameters. The results identified the operation windows that do not damage the DBM content. Out of the determined power settings, the one that created flat layer and allowed layer-wise processing was identified. The inspection of the fabricated parts indicated an improved print resolution by SLS. After printing, the green tensile bars were isothermally heat treatment in different curing times. Then the dimensional change and the tensile strength of the resultant samples were evaluated. The results could be a basis to implement a customized scaffold with fine features and superb biofunctionality.

7.2 Future Directions

7.2.1 Tailoring Material System in Binder Jetting

Our experiments in the first part of dissertation indicates that powder morphology has a strong impact on the porosity level and pore structure in the sintered compact. In this regard, future work should focus on tailoring the powder rearrangement during printing. The agglomerates could be spread and selectively heat treated by means of a heat source to tune the inter-particle bonding strength before depositing binder droplets. It is expected that upon binder strike on powder bed, the agglomerates rearrange in different levels and enable tailoring porosity in a single layer- which is critical to precisely tune the porosity in a functionally graded structures.

Adding fine powders to agglomerates could be another subject to look into. As far as flowability characteristic permits, different fractions of fine material can be added to agglomerates to fill in the voids and promote the green density as a paramount factor on final density and controlling shrinkage. The advantage of agglomerate flowability is combined with favorable sintering of fine powders and could create denser parts.

The byproducts of binder and Nylon PA 2202 powder may introduce impurities into the metallic materials in sintering. The carbon residue can change solid state or liquid sintering thermodynamic and also reduce mechanical properties of the part. Thus studying the binder and fugitive material burnout characteristics and examining alternative material that leave minimal residue could be another subject to explore. Layer-wise Manufacturing of DBM/PCL Scaffolds

7.2.2 Powder-Based Additive Manufacturing of DBM/PCL Scaffolds

Part shifting is a challenge in layer-wise AM. The problem gets severe when the 2D area is small and cured material has light weight. It was noted that during fabrication of CAD models with fairly small cross-section, the layers shifted along the linear movement of roller. The results

of a primary study indicates that combination of aspect ratio (see Figure 7.1) and the cured mass seem to be effective factors. Further testing seems necessary to fully understand the correlation of these factors on part shifting defect.

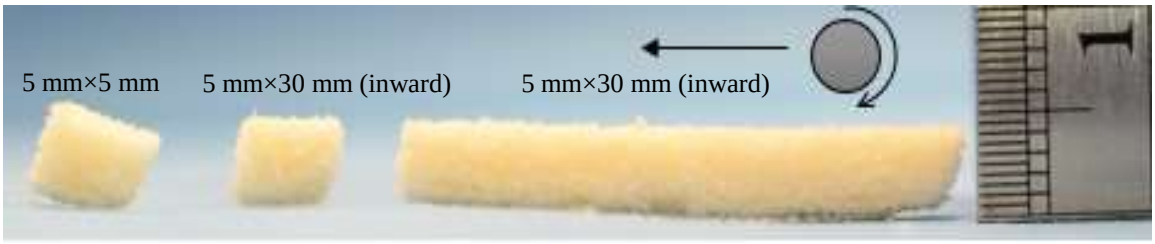

Figure 7.1. Aspect ratio effect on part shifting. Left: Cube of 5 mm, Middle: 30 mm into the paper, Right: 30 mm along the roller movement. Layer thickness=0.5 mm, P=5.36 W, f=2" and scanning speed=150 mm/s.

In addition to the open questions mentioned above, efforts to tackle the problem may include using particles with more controlled morphology. In this regard, both PCL and DBM particulates used here did not have spherical shape. It is expected that if the spherical PCL is used instead, the shear stress between the roller and the treated material would reduce and shifting problem would be alleviated to some degree.

Other possible experiments could be reduction of roller surface friction (by coating with Teflon for instance), attempting increased layer thickness to lower the shear stress and anchoring the first few layers of the 3D object by printing peripheral layers to hold the layers in place.

The material system could be adjusted to minimize the shrinkage level or increase the remaining pores in the final structure. Biocompatible space holders (such as cornstarch and Glucose) could be mixed in the DBM/PCL mixture and leached out at the end of the process. The shrinkage and pore structure variation is another interesting topic to investigate.

At the end, the medical application is the ultimate target of DBM/PCL scaffold, therefore the in-vitro and in-vivo testing are extremely important to fulfil the main goal of this project.

REFERENCES

[1] B. Vayre, Vignat, F., & Villeneuve,, "Metallic additive manufacturing: State-of-the-art review and prospects," Mechanics & Industry, vol. 13, pp. 89-96, 2012 2012.

[2] L. Salari-Sharif, T. A. Schaedler, and L. Valdevit, "Hybrid Hollow Microlattices With Unique Combination of Stiffness and Damping," Journal of Engineering Materials and Technology, vol. 140, pp. 031003-031003-14, 2018.

[3] H. J. Fraser, "Experimental Study of the Porosity and Permeability of Clastic Sediments," The Journal of Geology, vol. 43, pp. 910-1010, 1935.

[4] P. Freni, P. Tecchio, S. Rollino, and B. De Benedetti, "Porosity characterization of biomedical magnesium foams produced by Spark Plasma Sintering," in 2014 IEEE International Symposium on Medical Measurements and Applications (MeMeA), 11-12 June 2014, Piscataway, NJ, USA, 2014, p. 6 pp.

[5] Q. L. Loh and C. Choong, "Three-Dimensional Scaffolds for Tissue Engineering Applications: Role of Porosity and Pore Size," Tissue Engineering. Part B, Reviews, vol. 19, pp. 485-502, 2013.

[6] M. Ziaee, E. M. Tridas, and N. B. Crane, "Binder-Jet Printing of Fine Stainless Steel Powder with Varied Final Density," pp. 1-5, 2016.

[7] T. W. a. T. Gornet, "History of additive manufacturing " 2012.

[8] T. T. Wohlers, "Additive Manufacturing and 3D Printing State of the Industry : Annual Worldwide Progress Report," Wohlers Associates, US2013.

[9] M. Doyle, K. Agarwal, W. Sealy, and K. Schull, "Effect of Layer Thickness and Orientation on Mechanical Behavior of Binder Jet Stainless Steel 420 + Bronze Parts," Procedia Manufacturing, vol. 1, pp. 251-262, 2015.

[10] I. Gibson, Rosen, David, Stucker, Brent, "Additive Manufacturing Technologies," 2015.

[11] Additive Manufacturing: Materials, Processes, Quantifications and Applications, 1 ed. US: Butterworth-Heinemann, 2018.

[12] Additive manufacturing : innovations, advances, and applications US: Taylor & Francis, 2016.

[13] P. S. Liu and G. F. Chen, "Chapter One - General Introduction to Porous Materials," in Porous Materials, P. S. Liu and G. F. Chen, Eds., ed Boston: Butterworth-Heinemann, 2014, pp. 1-20.

[14] P. S. Liu and G. F. Chen, "Chapter Three - Application of Porous Metals," in Porous Materials, P. S. Liu and G. F. Chen, Eds., ed Boston: Butterworth-Heinemann, 2014, pp. 113-188.

[15] S. Honda, S. Hashimoto, S. Yase, Y. Daiko, and Y. Iwamoto, "Fabrication and thermal conductivity of highly porous alumina body from platelets with yeast fungi as a pore forming agent," Ceramics International, vol. 42, pp. 13882-13887, 2016.

[16] E. Sachs, M. Cima, P. Williams, D. Brancazio, and J. Cornie, "Three Dimensional Printing: Rapid Tooling and Prototypes Directly from a CAD Model," Journal of Engineering for Industry, vol. 114, pp. 481-488, 1992.

[17] Available: https://en.wikipedia.org/wiki/Powder_bed_and_inkjet_head_3D_printing

[18] T. Caffrey and T. Wohlers, "Additive manufacturing state of the industry," Manufacturing Engineering, vol. 154, pp. 67-78, 2015.

[19] https://www.desktopmetal.com/products/production/.

[20] B. Yun and C. B. Williams, "An exploration of binder jetting of copper," Rapid Prototyping Journal, vol. 21, pp. 177-85, 2015.

[21] Exone Systems, https://www.exone.com/.

[22] Voxeljet Company. Available: http://www.voxeljet.de/en/systems/vx4000/

[23] J. W. Halloran, "Freeform fabrication of ceramics," British Ceramic Transactions, vol. 98, pp. 299-303, 1999/06/01 1999.

[24] M. S.-H. Arghavan Farzadi , Mitra Asadi-Eydivand, Noor Azuan Abu Osman, "Effect of Layer Thickness and Printing Orientation on Mechanical Properties and Dimensional Accuracy of 3D Printed Porous Samples for Bone Tissue Engineering," PLOS ONE, September 18, 2014.

[25] S. M. Gaytan, M. A. Cadena, H. Karim, D. Delfin, Y. Lin, D. Espalin, et al., "Fabrication of barium titanate by binder jetting additive manufacturing technology," Ceramics International, vol. 41, pp. 6610-6619, 2015.

[26] S. Seyed Farid Seyed, G. Samira, M. Mehdi, Y. Hooman, M. Hendrik Simon Cornelis, K. Nahrizul Adib, et al., "A review on powder-based additive manufacturing for tissue engineering: selective laser sintering and inkjet 3D printing," Science and Technology of Advanced Materials, vol. 16, p. 033502, 2015.

[27] J. Peter R. Baker, "Three Dimensional Printing With Fine Metal Powders," M.S, Mechanical Engineering, Massachusetts Institue of Technology, 1997.

[28] M. R. Schure and R. S. Maier, "How does column packing microstructure affect column efficiency in liquid chromatography?," Journal of Chromatography A, vol. 1126, pp. 58-69, 2006.

[29] A. Daneyko, A. Höltzel, S. Khirevich, and U. Tallarek, "Influence of the particle size distribution on hydraulic permeability and eddy dispersion in bulk packings," Analytical Chemistry, vol. 83, pp. 3903-3910, 2011.

[30] A. Daneyko, S. Khirevich, A. Höltzel, A. Seidel-Morgenstern, and U. Tallarek, "From random sphere packings to regular pillar arrays: Effect of the macroscopic confinement on hydrodynamic dispersion," Journal of Chromatography A, vol. 1218, pp. 8231-8248, 2011.

[31] Y. S. Lee, P. Nandwana, and W. Zhang, "Dynamic simulation of powder packing structure for powder bed additive manufacturing," pp. 1-14, 2018.

[32] Z. Jianhua, Z. Yuwen, and J. K. Chen, "Numerical simulation of random packing of spherical particles for powder-based additive manufacturing," Journal of Manufacturing Science and Engineering, vol. 131, p. 031004 (8 pp.), 06/ 2009.

[33] O. B. Kovalev, A. V. Gusarov, and V. V. Belyaev, "Numerical study of the random packings structure of solid metal powder particles," in XXV Conference on High-Energy Processes in Condensed Matter (HEPCM 2017), 5-9 June 2017, USA, 2017, p. 030055 (8 pp.).

[34] T. Kinoshita and S. Shima, "Quasi-static simulation of powder packing behavior by particulate modeling (2nd report, three-dimensional calculation)," Nippon Kikai Gakkai Ronbunshu, A Hen/Transactions of the Japan Society of Mechanical Engineers, Part A, vol. 61, pp. 2253-2258, 1995.

[35] S. Zhao, N. Zhang, X. Zhou, and L. Zhang, "Particle shape effects on fabric of granular random packing," Powder Technology, vol. 310, pp. 175-186, 2017.

[36] X. Xie and V. M. Puri, "Powder deposition in three parallel-oriented dies of cylindrical and E shapes," Advanced Powder Technology, vol. 23, pp. 1-7, 1/2012.

[37] D. J. Craik and B. F. Miller, "THE FLOW PROPERTIES OF POWDERS UNDER HUMID CONDITIONS," Journal of Pharmacy and Pharmacology, vol. 10, pp. 136T-144T, 1958.

[38] R. A. B. J.K. Prescott, Pharmaceut Technol, pp. 60-84, 2000.

[39] M. Romagnoli and F. Bondioli, "Powder flowability characterizing techniques," American Ceramic Society Bulletin, vol. 83, 2004.

[40] T. O. Althaus and E. J. Windhab, "Characterization of wet powder flowability by shear cell measurements and compaction curves," Powder Technology, vol. 215-216, pp. 59-65, 2012.

[41] M. I. Zainuddin, M. Yasuda, L. Yi-Hung, H. Maruyama, and S. Matsusaka, "Development of vibration shear tube method for powder flowability evaluation," Powder Technology, vol. 217, pp. 548-53, 02/ 2012.

[42] A. Butscher, M. Bohner, C. Roth, A. Ernstberger, R. Heuberger, N. Doebelin, et al., "Printability of calcium phosphate powders for three-dimensional printing of tissue engineering scaffolds," Acta Biomaterialia, vol. 8, pp. 373-385, 1/ 2012.

[43] R. Ehlert, "The design of a volumetric dispensing system for free-flowing powder used in three dimensional printing," Bachelor of Science, Mechanical Engineering, MIT, 1995.

[44] B. L. Pruitt, "The design of an automated powder deposition system for a three-dimensional printing machine," Bachelor of Science, Mechanical Engineering, MIT, US, 1991.

[45] B. Heywood, "Design and manufacture of a powder deposition system for a powder bed on a three dimensional printer," Bachelor of Science, Mechanical Engineering, MIT, US, 1993.

[46] P. E. Rogren, "Multi-Material Three Dimensional Printer ", 2017.

[47] C. G. T. Mühler, M.E. Ascheri, D. Nicolaides, J.G. Heinrich, J. Günster, "Slurry-Based Powder Beds for the Selective Laser Sintering of Silicate Ceramics," T. Mühler1, C. Gomes2, M.E. Ascheri2, D. Nicolaides2, J.G. Heinrich1, J. Günster2,1, vol. 6, pp. 113-118, 2015.

[48] E. M. Sachs, "Powder dispensing apparatus using vibration," ed: Google Patents, 2000.

[49] K. J. Seluga, "Three Dimensional Printing by Vector Printing of Fine Metal Powders," Department of Mechanical Engineering, Massachusetts Institute Of Technology, US, 2001.

[50] C. Shu, Q. Yang, W. Xing-Fang, and Z. Hong-Hai, "Experimental and theoretical investigation on ultra-thin powder layering in three dimensional printing (3DP) by a novel double-smoothing mechanism," Journal of Materials Processing Technology, vol. 220, pp. 231-42, 06/ 2015.

[51] N. Emanuel M. Sachs, Mass, "Powder Dispensing Appartus Using Vibration," US Patent, 2000.

[52] C. C. Furnas, " Report of Investigation," Bureau of Mines1929.

[53] C. C. Furans, Ind. Eng. Che,. vol. 23, 1931.

[54] S. J. Gregorski, "High Green Density Metal Parts by Vibrationl Compaction of Dry Powder in the Three Dimensional Printing Process," PhD, Mechanical Engineering, MIT, US, 1996.

[55] G. T. Nolan and P. E. Kavanagh, "Computer simulation of particle packing in acrylic latex paints," Journal of Coatings Technology, vol. 67, pp. 37-43, 1995.

[56] G. T. Nolan and P. E. Kavanagh, "Computer simulation of random packing of hard spheres," Powder Technology, vol. 72, pp. 149-155, 1992.

[57] G. T. Nolan and P. E. Kavanagh, "Computer simulation of random packings of spheres with log-normal distributions," Powder Technology, vol. 76, pp. 309-316, 1993.

[58] G. T. Nolan and P. E. Kavanagh, "Size distribution of interstices in random packings of spheres," Powder Technology, vol. 78, pp. 231-238, 1994.

[59] S. Yerazunis, S. W. Cornell, and B. Wintner, "Dense Random Packing of Binary Mixtures of Spheres," Nature, vol. 207, pp. 835-837, 1965.

[60] A. Marmur, "A thermodynamic approach to the packing of particle mixtures," Powder Technology, vol. 44, pp. 249-253, 1985.

[61] S. M. K. Rassouly, "The packing density of `perfect' binary mixtures," Powder Technology, vol. 103, pp. 145-150, 7/1999.

[62] N. Standish and A. B. Yu, "Porosity calculations of ternary mixtures of particles," Powder Technology, vol. 49, pp. 249-253, 1987.

[63] J. G. Berryman, Phys. Rev. A, vol. 27, 1983.

[64] L. A. P. Philipse, vol. 12, 1996.

[65] M. T. S. W. Man. A. Donev. F. H. Stillinger, W. B. Russel, D. Heeger, S. Torquatto and P. M. Chaikin, Phys. Rev. Lett, vol. 94, 2005.

[66] J. Cesarano Iii, M. J. McEuen, and T. Swiler, "Computer simulations of particle packing," International SAMPE Technical Conference, vol. 27, pp. 658-665, 1995.

[67] S. Zhao, T. M. Evans, and X. Zhou, "Random packing of tetrahedral particles using the polyhedral and multi-sphere discrete element method," in 7th International Conference on Discrete Element Methods, DEM7 2016, August 1, 2016 - August 4, 2016, Dalian, China, 2017, pp. 91-99.

[68] J. Tao and G. Di, "Simulation of granular packing of frictional cohesive particles with Gaussian size distribution," Applied Physics A. Materials Science & Processing, vol. 122, p. 803 (7 pp.), 2016.

[69] J. Q. Gan, A. B. Yu, and Z. Y. Zhou, "DEM simulation on the packing of fine ellipsoids," Chemical Engineering Science, vol. 156, pp. 64-76, 2016.

[70] L. Burtseva, B. Valdez Salas, R. Romero, and F. Werner, "Recent advances on modelling of structures of multi-component mixtures using a sphere packing approach," International Journal of Nanotechnology, vol. 13, pp. 44-59, 2016.

[71] D. C. C. Lam, "Packing model for bimodal particle packing with aligned fibers," Journal of Materials Processing Technology, vol. 79, pp. 170-6, 07/01 1998.

[72] M. D. Webb and I. L. Davis, "Random particle packing with large particle size variations using reduced-dimension algorithms," Powder Technology, vol. 167, pp. 10-19, 2006.

[73] Y. Kallus, "The random packing density of nearly spherical particles," Soft Matter, vol. 12, pp. 4123-4128, 2016.

[74] J. E. Ayer and F. E. Soppet, "Vibratory Compaction: I, Compaction of Spherical Shapes," Journal of the American Ceramic Society, vol. 48, pp. 180-183, 1965.

[75] A. E. R. Westman and H. R. Hugill, "The Packing Of Particles1," Journal of the American Ceramic Society, vol. 13, pp. 767-779, 1930.

[76] E. K. H. Li and P. D. Funkenbusch, "Experimental size ratio and compositional effects on the packing and hot isostatic pressing of spherical powders," Materials Science and Engineering A, vol. 157, pp. 217-224, 1992.

[77] N. Epstein and M. J. Young, "Random Loose Packing of Binary Mixtures of Spheres," Nature, vol. 196, pp. 885-886, 1962.

[78] W. M. Visscher and M. Bolsterli, "Random Packing of Equal and Unequal Spheres in Two and Three Dimensions," Nature, vol. 239, pp. 504-507, 1972.

[79] J. Zheng, W. B. Carlson, and J. S. Reed, "The packing density of binary powder mixtures," Journal of the European Ceramic Society, vol. 15, pp. 479-483, 1995.

[80] G. W. Yun Bai, Christopher B. Williams, "Effect of Bimodal Powder Mixture on Powder Packing Density and Sintered Density in. Binder Jetting of Metals," in Annual International Solid Freeform Fabrication Symposium, Austin, TX, 2015.

[81] R. K. McGeary, "Mechanical Packing of Spherical Particles," Journal of the American Ceramic Society, vol. 44, pp. 513-522, 1961.

[82] H. Y. Sohn and C. Moreland, "The effect of particle size distribution on packing density," The Canadian Journal of Chemical Engineering, vol. 46, pp. 162-167, 1968.

[83] M. Lanzetta and E. Sachs, "Improved surface finish in 3D printing using bimodal powder distribution," Rapid Prototyping Journal, vol. 9, pp. 157-66, 2003.

[84] J. F. Bredt, "Binder Stability and Powder/Binder Interaction in Three dimensional Printing," Ph.D, MIT, US.

[85] S. Wang, L.-M. Luo, J. Shi, X. Zan, X.-Y. Zhu, G.-N. Luo, et al., "Effect of mechanical alloying on the microstructure and properties of W–Ti alloys fabricated by spark plasma sintering," Powder Technology, vol. 302, pp. 1-7, 2016.

[86] V. Esnault, A. Michrafy, D. Heitzmann, M. Michrafy, and D. Oulahna, "Processing fine powders by roll press," Powder Technology, vol. 270, Part B, pp. 484-489, 2015.

[87] E. J. R. Parteli and T. Pöschel, "Particle-based simulation of powder application in additive manufacturing," Powder Technology, vol. 288, pp. 96-102, 2016.

[88] J. A. Gonzalez, J. Mireles, Y. Lin, and R. B. Wicker, "Characterization of ceramic components fabricated using binder jetting additive manufacturing technology," Ceramics International, vol. 42, pp. 10559-10564, 2016.

[89] Z. Zhou, Y. Ma, J. Du, and J. Linke, "Fabrication and characterization of ultra-fine grained tungsten by resistance sintering under ultra-high pressure," Materials Science and Engineering: A, vol. 505, pp. 131-135, 2009.

[90] L. Ding, D. P. Xiang, Y. Y. Li, C. Li, and J. B. Li, "Effects of sintering temperature on fine-grained tungsten heavy alloy produced by high-energy ball milling assisted spark plasma sintering," International Journal of Refractory Metals & Hard Materials, vol. 33, pp. 65-9, 2012.

[91] J. Yoo, M. Cima, S. Khanuja, and E. Sachs, "Structural ceramic components by 3D printing," in Solid Freeform Fabrication Symposium, 1993, pp. 40-50.

[92] C. C. Xu, H. Zhang, and J. Zhu, "Improving flowability of cohesive particles by partial coating on the surfaces," The Canadian Journal of Chemical Engineering, vol. 87, pp. 403-414, 2009.

[93] M. P. Mullarney, L. E. Beach, R. N. Davé, B. A. Langdon, M. Polizzi, and D. O. Blackwood, "Applying dry powder coatings to pharmaceutical powders using a comil for improving powder flow and bulk density," Powder Technology, vol. 212, pp. 397-402, 2011.

[94] J. Yang, A. Sliva, A. Banerjee, R. N. Dave, and R. Pfeffer, "Dry particle coating for improving the flowability of cohesive powders," Powder Technology, vol. 158, pp. 21-33, 2005.

[95] L. J. Jallo, C. Ghoroi, L. Gurumurthy, U. Patel, and R. N. Davé, "Improvement of flow and bulk density of pharmaceutical powders using surface modification," International Journal of Pharmaceutics, vol. 423, pp. 213-225, 2012.

[96] M. Sachs, M. Friedle, J. Schmidt, W. Peukert, and K.-E. Wirth, "Characterization of a downer reactor for particle rounding," 2017.

[97] J. Ma and L. C. Lim, "Effect of particle size distribution on sintering of agglomerate-free submicron alumina powder compacts," Journal of the European Ceramic Society, vol. 22, pp. 2197-208, 2002.

[98] K. A. Lewandowski and S. K. Kawatra, "Binders for heap leaching agglomeration," Minerals and Metallurgical Processing, vol. 26, pp. 1-24, 2009.

[99] K. J. Seluga, "Layer to Layer Registration of a Slurry Based 3D Printing Machine", Science Bachelor, Mechanical Engineering, MIT, Massachusetts, 2000.

[100] M. O. M.J. Cima, H.R. Wang, E. Sachs, and R. Holman, "Slurry-Based 3DP and Fine Ceramic Components".

[101] Y. Huang and J. Yang, "Gel-Tape-Casting of Ceramic Substrates," in Novel Colloidal Forming of Ceramics, ed Berlin, Heidelberg: Springer Berlin Heidelberg, 2010, pp. 16-73.

[102] D. Hotza and P. Greil, "Review: aqueous tape casting of ceramic powders," Materials Science and Engineering: A, vol. 202, pp. 206-217, 1995.

[103] R. K. Holman, S. A. Uhland, M. J. Cima, and E. Sachs, "Surface Adsorption Effects in the Inkjet Printing of an Aqueous Polymer Solution on a Porous Oxide Ceramic Substrate," Journal of Colloid and Interface Science, vol. 247, pp. 266-274, 2002.

[104] I. Aksay and C. Schilling, "Forming of ceramics," by JA Mangels and GL Messing, Am. Ceram. Soc., Columbus, OH, pp. 85-93, 1984.

[105] K. L. Petri and A. E. Smith, "Hierarchical fuzzy model for predicting casting time in a slip-casting process," in Proceedings of the 1996 5th Industrial Engineering Research Conference, May 18, 1996 - May 20, Minneapolis, MN, USA, 1996, pp. 217-222, 1996.

[106] L. A. Salam, R. D. Matthews, and H. Robertson, "Optimisation of thermoelectric green tape characteristics made by the tape casting method," Materials chemistry and physics, vol. 62, pp. 263-272, 2000.

[107] P. J. Witt, J. H. Perry, and M. P. Schwarz, "A numerical model for predicting bubble formation in a 3D fluidized bed," Applied Mathematical Modelling, vol. 22, pp. 1071-1080, 1998.

[108] J. Kant Pandit, X. S. Wang, and M. J. Rhodes, "A DEM study of bubble formation in Group B fluidized beds with and without cohesive inter-particle forces," Chemical Engineering Science, vol. 62, pp. 159-166, 2007.

[109] T. Mori, T. Yamada, T. Tanaka, and J. Tsubaki, "Slurry characterization by stress relaxation test for tape casting process," in 31st International Conference on Advanced Ceramics and Composites, January 21, 2007 - January 26, 2007, Daytona Beach, FL, United states, pp. 1-10, 2008.

[110] A. Kristoffersson, E. Roncari, and C. Galassi, "Comparison of different binders for water-based tape casting of alumina," Journal of the European Ceramic Society, vol. 18, pp. 2123-2131, 1998.

[111] W. Lan and P. Xiao, "Drying stress of yttria-stabilized-zirconia slurry on a metal substrate," Journal of the European Ceramic Society, vol. 27, pp. 3117-3125, 2007.

[112] T. Mori, T. Yamada, T. Tanaka, A. Katagiri, and J. Tsubaki, "Effects of slurry properties on the crack formation in ceramic green sheets during drying," Journal of the Ceramic Society of Japan, vol. 114, pp. 823-8, 2006.

[113] M. P. Albano and L. B. Garrido, "Aqueous tape casting of yttria stabilized zirconia," Materials Science and Engineering: A, vol. 420, pp. 171-178, 2006.

[114] P. C. Saxton, "Reducing powder bed layer defects in slurry-based three dimensional printing," M.Sc, Mechanical Engineering, MIT, US, 1999.

[115] B. N. DeBear, "Slurry deposition of high quality layers for 3DP printing," M.Sc, Mechanical Engineering, MIT, US, 1999.

[116] http://www.polymerinnovations.com/ThickTapeCastingDemo.pdf.

[117] E. M. Sachs, M. J. Cima, M. A. Caradonna, J. Grau, J. G. Serdy, P. C. Saxton, et al., "Jetting layers of powder and the formation of fine powder beds thereby," ed: Google Patents, 2003.

[118] G. Manogharan, M. Kioko, and C. Linkous, "Binder Jetting: A Novel Solid Oxide Fuel-Cell Fabrication Process and Evaluation," JOM, vol. 67, pp. 660-7, 2015.

[119] J. M. Jason Grau, Scott Uhland, Michael Cima, Emanuel Sachs, "High green density ceramic components fabricated by the slurry-based 3DP process," in Solid Freeform, 1997.

[120] P. L. A. Zocca, J. Günster, "LSD-based 3D printing of alumina ceramics " Journal of Ceramic Science and Technology, vol. 8, pp. 141-148, 2016.

[121] H. R. Wang, M. J. Cima, B. D. Kernan, and E. M. Sachs, "Alumina-doped silica gradient-index (GRIN) lenses by slurry-based three-dimensional printing (S-3DP™)," Journal of Non-Crystalline Solids, vol. 349, pp. 360-367, 2004.

[122] G. Manogharan, M. Kioko, and C. Linkous, "Binder Jetting: A Novel Solid Oxide Fuel-Cell Fabrication Process and Evaluation," JOM, vol. 67, pp. 660-667, 2015.

[123] B. D. Kernan, E. M. Sachs, M. A. Oliveira, and M. J. Cima, "Three Dimensional Printing of Tungsten Carbide-Cobalt Using a Cobalt Oxide Precursor," in Solid Freeform Fabrication Symposium, 2003, pp. 616-631.

[124] C. Williams, "Design and development of a layer-based additive manufacturing process for the realization of metal parts of designed mesostructure," PhD, Mechanical Engineering Georgia Institute of Technology, 2008.

[125] Y. T. Chou, Y. T. Ko, and M. F. Yan, "Fluid flow model for ceramic tape casting," Journal of the American Ceramic Society, vol. 70, 1987.

[126] E. R. T. Richard E. Mistler, Tape Casting: Theory and Practice: Wiley, 2000.

[127] J. J. Thompson, "Forming thin ceramics," Am. Ceram. Soc. Bull., pp. 480-481, 1963.

[128] R. E. Mistler, "The principles of tape casting and tape casting applications," in Ceramic Processing, R. A. Terpstra, P. P. A. C. Pex, and A. H. de Vries, Eds., ed Dordrecht: Springer Netherlands, pp. 147-173, 1995.

[129] S. Seto, T. Yagi, M. Okuda, S. Umehara, and M. Kataoka, "Lifetime improvement for full-width-array piezo ink jet print head using matrix nozzle arrangement," Journal of Imaging Science and Technology, vol. 53, p. 050305 (7 pp.), 2009.

[130] J. Liu and M. Rynerson, "Method for article fabrication using carbohydrate binder," ed: Google Patents, 2003.

[131] N. A. Meisel, Williams, C. B., and Druschitz, A., "Lightweight Metal Cellular Structures via Indirect 3D Printing and Casting," SFF Symposium, 2012.

[132] B. Utela, D. Storti, R. Anderson, and M. Ganter, "A review of process development steps for new material systems in three dimensional printing (3DP)," Journal of Manufacturing Processes, vol. 10, pp. 96-104, 2008.

[133] T. C. A. a. R. James F. Bredt, "Three Dimensional Printing Materials System" USA Patent, 2002.

[134] H. Karimian and A. A. Babaluo, "Effect of polymeric binder and dispersant on the stability of colloidal alumina suspensions," Iranian Polymer Journal (English Edition), vol. 15, pp. 879-889, 2006.

[135] K. Lee, S. Lim, A. Tron, J. Mun, Y.-J. Kim, T. Yim, et al., "Polymeric binder based on PAA and conductive PANI for high performance silicon-based anodes," RSC Advances, vol. 6, pp. 101622-101625, 2016.

[136] E. N. Kani and A. Allahverdi, "Effects of curing time and temperature on strength development of inorganic polymeric binder based on natural pozzolan," Journal of Materials Science, vol. 44, pp. 3088-3097, 2009.

[137] S. Nachum, J. Vogt, and F. Raether, "Additive Manufacturing of Ceramics: Stereolithography versus Binder Jetting," CFI - Ceramic Forum International - Berichte der Deutschen Keramischen Gesellschaft, pp. 27-33, 2016.

[138] L. Won-Hee, K. Dong-Soo, K. Jung-Su, and L. Min-Cheol, "A study on reduction of processing time and improvement of strength by using photopolymer resin in the 3DP process," Key Engineering Materials, vol. 326-328, pp. 151-4, 2006.

[139] B. J. de Gans, P. C. Duineveld, and U. S. Schubert, "Inkjet printing of polymers: state of the art and future developments," Advanced materials, vol. 16, pp. 203-213, 2004.

[140] R. Patterson, D. H. Hollenberg, R. C. Desjarlais, and G. E. Alderfer, "Ink jet printable coatings," ed: Google Patents, 1988.

[141] M. Cima, E. Sachs, T. Fan, J. F. Bredt, S. P. Michaels, S. Khanuja, et al., "Three-dimensional printing techniques," ed: Google Patents, 1995.

[142] F. K. Feenstra, "Method for making a dental element," ed: Google Patents, 2005.

[143] N. Reis, C. Ainsley, and B. Derby, "Viscosity and Acoustic Behavior of Ceramic Suspensions Optimized for Phase-Change Ink-Jet Printing," Journal of the American Ceramic Society, vol. 88, pp. 802-808, 2005.

[144] J. Moon, J. E. Grau, V. Knezevic, M. J. Cima, and E. M. Sachs, "Ink-Jet Printing of Binders for Ceramic Components," Journal of the American Ceramic Society, vol. 85, pp. 755-762, 2002.

[145] S. S. Khanuja, "origin and control of anisotropy in three dimensional printing of structural ceramics," Doctor of Philosophy, Materials science and engineering department, MIT, Massachussets, 1996.

[146] J. Yoo, M. Cima, E. Sachs, and S. Suresh, "Fabrication and microstructural control of advanced ceramic components by three dimensional printing," Ceramic Engineering and Science Proceedings, vol. 16, pp. 755-762, 1995.

[147] H. C. Sachs EM, Allen S, et al. , "Metal and ceramic containing parts produced from powder using binders derived from salt," US Patent, 2003.

[148] C. X. F. Lam, X. M. Mo, S. H. Teoh, and D. W. Hutmacher, "Scaffold development using 3D printing with a starch-based polymer," Materials Science and Engineering: C, vol. 20, pp. 49-56, 2002.

[149] H. U. S.S. Kim, J.A. Koski, B.M. Wu, M.J. Cima, J. Sohn, and L. G. G. K. Mukai, J.P. Vacanti, Ann. Surg., vol. 228, pp. 8-12, 1998.

[150] J. Suwanprateeb and R. Chumnanklang, "Three-dimensional printing of porous polyethylene structure using water-based binders," Journal of Biomedical Materials Research Part B: Applied Biomaterials, vol. 78B, pp. 138-145, 2006.

[151] J. F. Bredt, "Binder composition for use in three dimensional printing," ed: Google Patents, 1995.

[152] P. R. Carey and M. Lott, "Sand binder systems part V - furan no-bake," Foundry Management and Technology, vol. 123, pp. 26-30, 1995.

[153] D. Snelling, C. Williams, and A. Druschitz, "A comparison of binder burnout and mechanical characteristics of printed and chemically bonded sand molds," in SFF Symposium, Austin, TX, 2014.

[154] S. Meteyer, X. Xu, N. Perry, and Y. F. Zhao, "Energy and Material Flow Analysis of Binder-jetting Additive Manufacturing Processes," Procedia CIRP, vol. 15, pp. 19-25, 2014.

[155] R. N. Wenzel, Industrial and Engineering Chemistry, vol. 28, 1936.

[156] A. B. D. C. a. S. Baxter, Transactions of the Faraday Society, vol. 40, 1944.

[157] U. Cengiz and C. Elif Cansoy, "Applicability of Cassie-Baxter equation for superhydrophobic fluoropolymer-silica composite films," Applied Surface Science, vol. 335, pp. 99-106, 2015.

[158] C. E. Cansoy, H. Y. Erbil, O. Akar, and T. Akin, "Effect of pattern size and geometry on the use of Cassie-Baxter equation for superhydrophobic surfaces," Colloids and Surfaces A: Physicochemical and Engineering Aspects, vol. 386, pp. 116-24, 2011.

[159] A.-J. Hu, B.-Z. Lv, and X.-S. Wang, "Generalized cassie-baxter equation for nanodroplet on heterogeneous and spherical solid substrates," Journal of Computational and Theoretical Nanoscience, vol. 12, pp. 5144-5148, 2015.

[160] X.-S. Wang, K. Lv, J. Chen, K.-H. Zhao, and X.-B. Fan, "A generalized cassie-baxter equation for wetting phenomena of cylindrical nano-droplets on heterogeneous substrates," Journal of Computational and Theoretical Nanoscience, vol. 13, pp. 574-578, 2016.

[161] J.-J. Zhao, Y.-Y. Duan, X.-D. Wang, and B.-X. Wang, "Effect of nanostructured roughness on evaporating thin films in microchannels for wenzel and cassie-baxter states," Journal of Heat Transfer, vol. 135, 2013.

[162] S. Das, S. K. Mitra, and S. Chakraborty, "Wenzel and Cassie-Baxter states of an electrolytic drop on charged surfaces," Physical Review E (Statistical, Nonlinear, and Soft Matter Physics), vol. 86, p. 011603 (9 pp.), 2012.

[163] C. Dorrer and J. Ruhe, "Drops on microstructured surfaces coated with hydrophilic polymers: Wenzel's model and beyond," Langmuir, vol. 24, pp. 1959-1964, 2008.

[164] F. Bottiglione, R. Di Mundo, L. Soria, and G. Carbone, "Wenzel to cassie transition in superhydrophobic randomly rough surfaces," Nanoscience and Nanotechnology Letters, vol. 7, pp. 74-78, 2015.

[165] T.-Q. Liu, Y.-J. Li, X.-Q. Li, and W. Sun, "Theoretical analysis of droplet transition from Cassie to Wenzel state," Chinese Physics B, vol. 24, p. 116801 (12 pp.), 11/ 2015.

[166] T. Sui, J. Wang, and D. Chen, "Energy analysis for transition from Cassie state to Wenzel state," Huagong Xuebao/CIESC Journal, vol. 62, pp. 1352-1357, 2011.

[167] T. Koishi, K. Yasuoka, S. Fujikawa, T. Ebisuzaki, and Z. Xiao Cheng, "Coexistence and transition between Cassie and Wenzel state on pillared hydrophobic surface," Proceedings of the National Academy of Sciences of the United States of America, vol. 106, pp. 8435-40, 2009.

[168] X. Xianmin, "Modified Wenzel and Cassie equations for wetting on rough surfaces," SIAM Journal on Applied Mathematics, vol. 76, pp. 2353-74, 2016.

[169] N. K. Palakurthi, S. Konangi, U. Ghia, and K. Comer, "Micro-scale simulation of unidirectional capillary transport of wetting liquid through 3D fibrous porous media: Estimation of effective pore radii," International Journal of Multiphase Flow, vol. 77, pp. 48-57, 2015.

[170] Z. Afrassiabian, M. Leturia, M. Benali, M. Guessasma, and K. Saleh, "An overview of the role of capillary condensation in wet caking of powders," Chemical Engineering Research and Design, vol. 110, pp. 245-254, 2016.

[171] V. M. Starov, S. A. Zhdanov, and M. G. Velarde, "Capillary imbibition of surfactant solutions in porous media and thin capillaries: partial wetting case," Journal of Colloid and Interface Science, vol. 273, pp. 589-595, 2004.

[172] A. L. Mundozah, J. J. Cartwright, C. C. Tridon, M. J. Hounslow, and A. D. Salman, "Hydrophobic/hydrophilic static powder beds: Competing horizontal spreading and vertical imbibition mechanisms of a single droplet," Powder Technology, vol. 330, pp. 275-283, 2018.

[173] J. Kammerhofer, L. Fries, J. Dupas, L. Forny, S. Heinrich, and S. Palzer, "Impact of hydrophobic surfaces on capillary wetting," Powder Technology, vol. 328, pp. 367-374, 2018.

[174] S. Chandra and C. T. Avedisian, "Observations of droplet impingement on a ceramic porous surface," International Journal of Heat and Mass Transfer, vol. 35, pp. 2377-2388, 1992.

[175] A. Asai, M. Shioya, S. Hirasawa, and T. Okazaki, "Impact of an ink drop on paper," Journal of imaging science, vol. 37, pp. 205-207, 1993.

[176] M. G. H. C. D. Stow, "An experimental investigation of fluid flow resulting from the impact of a water drop with an unyielding dry surface," Proceedings of the Royal Society of London. A. Mathematical and Physical Sciences, vol. 373, p. 419, 1981.

[177] K. P. Hapgood, J. D. Litster, S. R. Biggs, and T. Howes, "Drop Penetration into Porous Powder Beds," Journal of Colloid and Interface Science, vol. 253, pp. 353-366, 2002.

[178] R. M. a. K. M. Pillai, "Wicking in Porous Materials: Traditional and Modern Modeling Approaches ", R. M. a. K. M. Pillai, Ed., ed: CRC Press, 2012, pp. 120-121.

[179] L. Jingmei, M. Nitesh, M. Sze Yi, S. Yang, and S. Ho Cheung, "Perturbation-induced droplets for manipulating droplet structure and configuration in microfluidics," Journal of Micromechanics and Microengineering, vol. 25, p. 084009, 2015.

[180] W. Yan-en, L. Xin-pei, L. Chuan-chuan, Y. Ming-ming, and W. Qing-hua, "Binder droplet impact mechanism on a hydroxyapatite microsphere surface in 3D printing of bone scaffolds," Journal of Materials Science, vol. 50, pp. 5014-23, 2015.

[181] T. Fan, "Droplet-powder impact interaction in three dimensional printing," Ph.D., Mechanical Engineering, Massachusetts Institute of Technology, Massachusetts Institute of Technology, 1996.

[182] J. O. Marston, J. E. Sprittles, Y. Zhu, E. Q. Li, I. U. Vakarelski, and S. T. Thoroddsen, "Drop spreading and penetration into pre-wetted powders," Powder Technology, vol. 239, pp. 128-36, 2013.

[183] J. O. Marston, S. T. Thoroddsen, W. K. Ng, and R. B. H. Tan, "Experimental study of liquid drop impact onto a powder surface," Powder Technology, vol. 203, pp. 223-236, 2010.

[184] L. Forny, A. Marabi, and S. Palzer, "Wetting, disintegration and dissolution of agglomerated water soluble powders," Powder Technology, vol. 206, pp. 72-78, 1/18/ 2011.

[185] T. Nguyen, W. Shen, and K. Hapgood, "Drop penetration time in heterogeneous powder beds," Chemical Engineering Science, vol. 64, pp. 5210-5221, 2009.

[186] M. L. M. Oostveen, G. M. H. Meesters, and J. R. van Ommen, "Quantification of powder wetting by drop penetration time," Powder Technology, vol. 274, pp. 62-66, 2015.

[187] K. Ashoke Raman, R. K. Jaiman, T.-S. Lee, and H.-T. Low, "Lattice Boltzmann study on the dynamics of successive droplets impact on a solid surface," Chemical Engineering Science, vol. 145, pp. 181-195, 2016.

[188] H. N. Emady, D. Kayrak-Talay, W. C. Schwerin, and J. D. Litster, "Granule formation mechanisms and morphology from single drop impact on powder beds," Powder Technology, vol. 212, pp. 69-79, 2011.

[189] H. N. Emady, D. Kayrak-Talay, and J. D. Litster, "Modeling the granule formation mechanism from single drop impact on a powder bed," Journal of Colloid and Interface Science, vol. 393, pp. 369-376, 2013.

[190] S. Weber, C. Briens, F. Berruti, E. Chan, and M. Gray, "Agglomerate stability in fluidized beds of glass beads and silica sand," Powder Technology, vol. 165, pp. 115-127, 2006.

[191] S. H. Schaafsma, P. Vonk, P. Segers, and N. W. F. Kossen, "Description of agglomerate growth," Powder Technology, vol. 97, pp. 183-190, 1998.

[192] H. M. a. L. Yang, "Equilibrium Saturation In Binder Jetting Additive Manufacturing Processes: Theoretical Model Vs. Experimental Observeations," in Solid Freeform Fabrication 2016, The University of Texas at Austin, pp. 1945-1959, 2016.

[193] R. D. Stainer and C. D. Stow, "Direct methods for the measurement of small water drops," New Zealand Journal of Science, vol. 19, pp. 135-43, 1976.

[194] B. M. Wu, "Microstructural control during three dimensional printing of polymeric medical devices," PhD, Mechanical Engineering, MIT, US, 1998.

[195] M. J. C. Charles William Rowe, Wendy E. Pryce Lewis, Donald C. and S. K. Monkhouse, Jaedeok Yoo, "Method and materials for controlling migration of binder liquid in a powder," US Patent, 2004.

[196] H. Chen, "A Process Modelling and Parameters Optimization and Recommendation System for Binder Jetting Additive Manufacturing Process," M.Sc, Department of Mechanical Engineering, McGill University, Montreal, 2015.

[197] L. E. Murr, "Frontiers of 3D Printing/Additive Manufacturing: from Human Organs to Aircraft Fabrication," Journal of Materials Science & Technology, vol. 32, pp. 987-95, 2016.

[198] H. Miyanaji and L. Yang, "Equilibrium Saturation In Binder Jetting Additive Manufacturing Processes: Theoretical Model Vs. Experimental Observeations", 2016

[199] S. Atre, J. Porter, T. Batchelor, K. Kate, M. Bulger, and P. Gangopadhya, "Process parameter optimization for binder jetting using 420 stainless steel," in World Powder Metallurgy 2016 Congress and Exhibition, World PM 2016, October 9, 2016 - October 13, 2016, Hamburg, Germany, 2016, p. European Powder Metallurgy Association (EPMA).

[200] S. Shrestha and G. Manogharan, "Optimization of Binder Jetting Using Taguchi Method," JOM, vol. 69, pp. 491-497, 2017.

[201] H. Miyanaji, S. Zhang, and L. Yang, "A new physics-based model for equilibrium saturation determination in binder jetting additive manufacturing process," International Journal of Machine Tools and Manufacture, vol. 124, pp. 1-11, 2018.

[202] S. H. Davis, "Moving contact lines and rivulet instabilities. Part 1. The static rivulet," Journal of Fluid Mechanics, vol. 98, pp. 225-242, 2006.

[203] J. Stringer and B. Derby, "Formation and Stability of Lines Produced by Inkjet Printing," Langmuir, vol. 26, pp. 10365-10372, 2010.

[204] S. Schiaffino and A. A. Sonin, "Formation and stability of liquid and molten beads on a solid surface," Journal of fluid mechanics, vol. 343, pp. 95-110, 1997.

[205] D. Soltman and V. Subramanian, "Inkjet-Printed Line Morphologies and Temperature Control of the Coffee Ring Effect," Langmuir, vol. 24, pp. 2224-2231, 2008/03/01 2008.

[206] D. A. Herron, "Continuous ink jet printer," ed: Google Patents, 1987.

[207] E. M. Sachs, B. W. Gleason, and J. G. Serdy, "Positive pressure drop-on-demand printing," ed: Google Patents, 2004.

[208] H. P. Le, "Progress and Trends in Ink-jet Printing Technology," IS&TThe Society for Imaging Science and Technology, 1998.

[209] E. Ufkes, "Continuous ink-jet printer and method of operation," ed: Google Patents, 2001.

[210] J. H. Song, M. J. Edirisinghe, and J. R. G. Evans, "Formulation and Multilayer Jet Printing of Ceramic Inks," Journal of the American Ceramic Society, vol. 82, pp. 3374-3380, 1999.

[211] R. E. Papen, "Piezoelectric-drop-on-demand technology," ed: Google Patents, 2002.

[212] R. C. Durbeck, J. M. Eldridge, F. C. S. Lee, and G. Olive, "Thermal drop-on-demand ink jet printer print head," ed: Google Patents, 1989.

[213] B. Y. Tay, J. R. G. Evans, and M. J. Edirisinghe, "Solid freeform fabrication of ceramics," International Materials Reviews, vol. 48, pp. 341-370, 2003.

[214] H. Sirringhaus, T. Kawase, R. H. Friend, T. Shimoda, M. Inbasekaran, W. Wu, et al., "High-Resolution Inkjet Printing of All-Polymer Transistor Circuits," Science, vol. 290, pp. 2123-2126, 2000.

[215] B. W. An, K. Kim, H. Lee, S.-Y. Kim, Y. Shim, D.-Y. Lee, et al., "High-Resolution Printing of 3D Structures Using an Electrohydrodynamic Inkjet with Multiple Functional Inks," Advanced Materials, vol. 27, pp. 4322-4328, 2015.

[216] E. R. Lee, Microdrop generation vol. 5: CRC press, 2002.

[217] S. Elrod, B. Hadimioglu, B. Khuri-Yakub, E. Rawson, E. Richley, C. Quate, et al., "Nozzleless droplet formation with focused acoustic beams," Journal of Applied Physics, vol. 65, pp. 3441-3447, 1989.

[218] O. A. Basaran, "Small-scale free surface flows with breakup: Drop formation and emerging applications," AIChE Journal, vol. 48, pp. 1842-1848, 2002.

[219] J. Yamauchi, K. Terada, T. Sato, and T. Okaya, "Application of poly(vinyl alcohol) with an alkyl end group containing anionic groups to coal-water slurry as a dispersant," Journal of Applied Polymer Science, vol. 55, pp. 1553-1561, 1995.

[220] J. F. Bredt, S. Clark, and G. Gilchrist, "Three dimensional printing material system and method," ed: Google Patents, 2006.

[221] R. B. a. H. K. Bowen, American Ceramic Society Bulletin, vol. 56, p. 732, 1977.

[222] I. Ganesh, S. Bhattacharjee, B. P. Saha, R. Johnson, and Y. R. Mahajan, "A new sintering aid for magnesium aluminate spinel," Ceramics International, vol. 27, pp. 773-9, 2001.

[223] R. W. Trice and J. W. Halloran, "Effect of sintering aid composition on the processing of Si3N4/BN fibrous monolithic ceramics," Journal of the American Ceramic Society, vol. 82, pp. 2943-7, 11/ 1999.

[224] D. Guo, "Vector Drop-on-Demand Production of Tungsten Carbide-Cobalt Tooling Inserts by Three Dimensional Printing " M.Sc, Mechanical Engineering, Massachusetts Institute of Technology, US, 2004.

[225] A. Gebhardt and J.-S. Hötter, "2 - Characteristics of the Additive Manufacturing Process," in Additive Manufacturing, ed: Hanser, 2016, pp. 21-91.

[226] A. Farzadi, M. Solati-Hashjin, M. Asadi-Eydivand, and N. A. Abu Osman, "Effect of Layer Thickness and Printing Orientation on Mechanical Properties and Dimensional Accuracy of 3D Printed Porous Samples for Bone Tissue Engineering," PLoS ONE, vol. 9, p. e108252,2014

[227] E. M. Sachs, C. Hadjiloucas, S. Allen, and H. J. Yoo, "Metal and ceramic containing parts produced from powder using binders derived from salt," ed: Google Patents, 1999.

[228] D. Brodkin, C. Panzera, A. Prasad, G. Day, and S. Borenstein, "Solid free-form fabrication methods for the production of dental restorations," ed: Google Patents, 2005.

[229] J. E. Grau, "Fabrication of Engineering Ceramic Components by the Slurry-Based Three Dimensional Printing Process," Doctor of Philosophy Partial Fulfillment of the Requirement for the Degree of PhD, Department of Materials Science and Engineering, MIT, 1998.

[230] G. Petzow and W. Huppmann, "Liquid phase sintering," Zeitschrift fuer Metallkunde, vol. 67, pp. 579-590, 1976.

[231] V. A. Invenson, Densification of Metal Powders During Sintering: Springer, 2012.

[232] S.-J. L. Kang, "Solid state sintering models and densification," in Sintering: Densification, Grain Growth and Microstructureed, 2005, p. 37.

[233] S. J. L. Kang, "5 - Liquid phase sintering A2 - Fang, Zhigang Zak," in Sintering of Advanced Materials, ed: Woodhead Publishing, 2010, pp. 110-129.

[234] R. M. German, P. Suri, and P. Seong Jin, "Review: liquid phase sintering," Journal of Materials Science, vol. 44, pp. 1-39, 01/ 2009.

[235] X. Kuang, G. Carotenuto, and L. Nicolais, "A Review of Ceramic Sintering and Suggestions on Reducing Sintering Temperatures," Advanced Performance Materials, vol. 4, pp. 257-274, 1997.

[236] C. Chen, S. Nagao, T. Sugahara, H. Zhang, J. Jiu, K. Suganuma, et al., "Effect of size and shape of Ag particles for mechanical properties of sintered Ag joints evaluated by micro-compression test," in 2017 International Conference on Electronics Packaging (ICEP), 2017, pp. 130-134.

[237] F. Gungor and N. Ay, "The effect of particle size of body components on the processing parameters of semi transparent porcelain," Ceramics International, vol. 44, pp. 10611-10620, 2018.

[238] Z. Y. Liu, T. B. Sercombe, and G. B. Schaffer, "The Effect of Particle Shape on the Sintering of Aluminum," Metallurgical and Materials Transactions A, vol. 38, pp. 1351-1357, 2007.

[239] E. Ringgaard, E. R. Nielsen, and W. W. Wolny, "Optimisation of new liquid-phase sintering aid for PZT," in 12th IEEE International Symposium on Applications of Ferroelectrics, July 21, 2000 - August 2, 2000, Honolulu, HI, United states, 2000, pp. 451-454.

[240] R. Carter, "Mechanism of Solid-state Reaction Between Magnesium Oxide and Aluminum Oxide and Between Magnesium Oxide and Ferric Oxide," Journal of the American Ceramic Society, vol. 44, pp. 116-120, 1961.

[241] M. Humenik and N. M. Parikh, "Cermets: I, Fundamental Concepts Related to Micro-structure and Physical Properties of Cermet Systems," Journal of the American Ceramic Society, vol. 39, pp. 60-63, 1956.

[242] S. Duan, E. Li, Y. Chen, B. Tang, Y. Yuan, and S. Zhang, "Low temperature sintering kinetics of BaO-0.15ZnO-4TiO2 dielectric ceramic in the presence of a liquid phase," Ceramics International, vol. 43, pp. 197-200, 2017.

[243] R. M. German and K. A. D'Angelo, "Enhanced sintering treatments for ferrous powders," International Metals Reviews, vol. 29, pp. 249-272, 1984.

[244] A. Amherd Hidalgo, R. Frykholm, T. Ebel, and F. Pyczak, "Powder Metallurgy Strategies to Improve Properties and Processing of Titanium Alloys: A Review," Advanced Engineering Materials, vol. 19, p. 1600743 (14 pp.), 2017.

[245] K. Karczewski, W. J. Stepniowski, and M. Salerno, "Amino acids aided sintering for the formation of highly porous FeAl intermetallic alloys," Materials, vol. 10, 2017.

[246] R. Calm and R. Citak, "Effect of Mg content in matrix on infiltration height in producing MgO/Al composite by vacuum infiltration method," Materials Science Forum, vol. 546-549, pp. 611-14, 2007.

[247] F. F. Lange, B. V. Velamakanni, and A. G. Evans, "Method for Processing Metal-Reinforced Ceramic Composites," Journal of the American Ceramic Society, vol. 73, pp. 388-393, 1990.

[248] B. D. Kernan, E. M. Sachs, S. M. Allen, C. Sachs, L. Raffenbeul, A. Pettavino, et al., "Homogeneous steel infiltration," Metallurgical and Materials Transactions A (Physical Metallurgy and Materials Science), vol. 36A, pp. 2815-27, 2005.

[249] A. Mortensen, "Melt infiltration of metal matrix composites," Comprehensive composite materials, vol. 3, pp. 521-524, 2000.

[250] R. L. Coble, Journal of American Ceramic Society, vol. 41, p. 55, 1958.

[251] A. Zocca, P. Lima, and J. Günster, "LSD-based 3D printing of alumina ceramics," 2017.

[252] N. Travitzky, A. Bonet, B. Dermeik, T. Fey, I. Filbert-Demut, L. Schlier, et al., "Additive Manufacturing of Ceramic-Based Materials," Advanced Engineering Materials, vol. 16, pp. 729-754, 2014.

[253] J. H. S. e. al, Appl. Opt., vol. 18, 1979.

[254] T. Do, P. Kwon, and C. S. Shin, "Process development toward full-density stainless steel parts with binder jetting printing," International Journal of Machine Tools and Manufacture, vol. 121, pp. 50-60, 2017.

[255] N. B. Crane, J. Wilkes, E. Sachs, and S. M. Allen, "Improving accuracy of powder-based SFF processes by metal deposition from a nanoparticle dispersion," Rapid Prototyping Journal, vol. 12, pp. 266-274, 2006.

[256] A. Elliott, S. AlSalihi, A. L. Merriman, and M. M. Basti, "Infiltration of Nanoparticles into Porous Binder Jet Printed Parts," American Journal of Engineering and Applied Sciences, vol. 9, 2016.

[257] P. Nandwana, A. M. Elliott, D. Siddel, A. Merriman, W. H. Peter, and S. S. Babu, "Powder bed binder jet 3D printing of Inconel 718: Densification, microstructural evolution and challenges(star, open)," 2016.

[258] N. Sa'ude, M. Ibrahim, N. A. Ismail, and R. Ibrahim, "Freeform fabrication of titanium based powder by inkjet 3D printer," in 6th International Conference on Leading Edge Manufacturing in 21st Century, LEM 2011, November 8, 2011 - November 10, 2011, Omiya Sonic City, Saitama, Japan, 2011, pp. Japan Society of Mechanical Engineers (JSME),; Manufacturing and Machine Tool Division.

[259] W. Cho, E. M. Sachs, N. M. Patrikalakis, and D. E. Troxel, "A dithering algorithm for local composition control with three-dimensional printing," Computer-aided design, vol. 35, pp. 851-867, 2003.

[260] B. Kieback, A. Neubrand, and H. Riedel, "Processing techniques for functionally graded materials," Materials Science and Engineering: A, vol. 362, pp. 81-106, 2003.

[261] C. Jianhua, Z. Xiankun, W. Yan, and Z. Qi, "Subsurface Geobody Imaging Using CMY Color Blending with Seismic Attributes," Journal of Electrical and Computer Engineering, vol. 2016, p. 9181254 (7 pp.), 2016.

[262] M. Stanić and B. Lozo, "Color and permanence issues in 3D ink-jet printing," in The 33rd International Convention MIPRO, 2010, pp. 274-277.

[263] F.-L. Yin and B.-Q. Huo, "Image Transformation for Digital Printing Machine," Applied Mechanics and Materials, vol. 401-403, pp. 180-3, 2013.

[264] D. T. M. S.N. Houde-Walter, Appl. Opt, vol. 25, 1986.

[265] e. a. M. Yamane, "Graded Index Materials by the Sol–Gel Process," SPIE Optical Engineering Press, 1993.

[266] R. Techapiesancharoenkij, "Bimetallic Bars with Local Control of Composition by Three Dimensional Printing " M.Sc, MIT, US, 2003.

[267] M. P. Paranthaman, C. S. Shafer, A. M. Elliott, D. H. Siddel, M. A. McGuire, R. M. Springfield, et al., "Binder Jetting: A Novel NdFeB Bonded Magnet Fabrication Process," JOM, vol. 68, pp. 1978-1982, 2016.

[268] J. Sun, Z. Peng, W. Zhou, J. Y. H. Fuh, G. S. Hong, and A. Chiu, "A Review on 3D Printing for Customized Food Fabrication," Procedia Manufacturing, vol. 1, pp. 308-319, 2015.

[269] A. G. E. Bassoli, L. Iuliano, and M. G. Violante, "3D printing technique applied to rapid casting," Rapid Prototyping Journal, vol. 13, pp. 148-155, 2007.

[270] V. T. D. A. Snelling, R. Kay, A. Druschitz, and C. B. Williams, "Mitigating Gas Defects in Castings Produced from 3D Printed Molds," presented at the 117th Metalcasting Congress, 2012.

[271] M. Chhabra and R. Singh, "Mathematical Modeling of Surface Roughness of Castings Produced Using ZCast Direct Metal Casting," Journal of The Institution of Engineers (India): Series C, vol. 96, pp. 145-155, April 01 2015.

[272] S. S. Gill and M. Kaplas, "Comparative study of 3D printing technologies for rapid casting of aluminium alloy," Materials and Manufacturing Processes, vol. 24, pp. 1405-1411, 2009.

[273] E. Sachs, E. Wylonis, S. Allen, M. Cima, and H. Guo, "Production of injection molding tooling with conformal cooling channels using the three dimensional printing process," Polymer Engineering & Science, vol. 40, pp. 1232-1247, 2000.

[274] A. Azhari, E. Marzbanrad, D. Yilman, E. Toyserkani, and M. A. Pope, "Binder-jet powder-bed additive manufacturing (3D printing) of thick graphene-based electrodes," Carbon, vol. 119, pp. 257-266, 2017.

[275] L. Rabinskiy, A. Ripetsky, S. Sitnikov, Y. Solyaev, and R. Kahramanov, "Fabrication of porous silicon nitride ceramics using binder jetting technology," IOP Conference Series: Materials Science and Engineering, vol. 140, p. 012023, 2016.

[276] B. Verlee, T. Dormal, and J. Lecomte-Beckers, "Density and porosity control of sintered 316L stainless steel parts produced by additive manufacturing," Powder Metallurgy, vol. 55, pp. 260-267, 2012.

[277] E. Sachs, M. Cima, J. Bredt, A. Curodeau, T. Fan, and D. Brancazio, "CAD-casting: direct fabrication of ceramic shells and cores by three dimensional printing," Manufacturing Review, vol. 5, pp. 117-26, 1992.

[278] L. Xianxian, Z. Zhaoqiang, and C. Bojun, "Influence of binder additives on the sintering of nano-3Y-TZP," Key Engineering Materials, vol. 336-338, pp. 2290-2, 2007.

[279] J.-Y. Qiu, K. Watari, Y. Hotta, Y. Kinemuchi, and K. Mitsuishi, "Grinding of agglomerate AlN powder by wet milling", pp. 45-48, 2006

[280] C. Guo, F. Lin, and W. Ge, "Study on the fabrication process of 316L stainless steel via electron beam selective melting," Jixie Gongcheng Xuebao/Journal of Mechanical Engineering, vol. 50, pp. 152-158, 2014.

[281] A. Mostafaei, E. T. Hughes, C. Hilla, E. L. Stevens, and M. Chmielus, "Data on the densification during sintering of binder jet printed samples made from water- and gas-atomized alloy 625 powders," Data in Brief, vol. 10, pp. 116-121, 2017.

[282] L. N. Dyachkova and E. E. Feldshtein, "Microstructures, Strength Characteristics and Wear Behavior of the Fe-based P/M Composites after Sintering or Infiltration with Cu–Sn Alloy," Journal of Materials Science & Technology, vol. 31, pp. 1226-1231, 2015.

[283] P. Lu, X. Xu, W. Yi, and R. M. German, "Porosity effect on densification and shape distortion in liquid phase sintering," Materials Science and Engineering: A, vol. 318, pp. 111-121, 2001.

[284] A. Lorenz, E. Sachs, and S. Allen, "Freeze-off limits in transient liquid-phase infiltration," Metallurgical and Materials Transactions A (Physical Metallurgy and Materials Science), vol. 35A, pp. 641-53, 2004.

[285] D. Impens and R. J. Urbanic, "An analysis of variation correlating post processing infiltrate types, build parameters and mechanical characteristics for binder jet built parts," in ASME 2015 International Mechanical Engineering Congress and Exposition, IMECE 2015, November 13, 2015 - November 19, 2015, Houston, TX, United states, 2015, p. American Society of Mechanical Engineers (ASME).

[286] M. Caputo, M. Krizner, and C. Virgil Solomon, "Investigation of 3D printing parameters of shape memory alloy powders," in Materials Science and Technology Conference and Exhibition 2015, MS and T 2015, October 4, 2015 - October 8, 2015, Columbus, OH, United states, 2015, pp. 1669-1675.

[287] J. Rajabi, N. Muhamad, and A. B. Sulong, "Effect of nano-sized powders on powder injection molding: a review," Microsystem Technologies, vol. 18, pp. 1941-1961, 2012.

[288] J.-W. Lee, S. Timilsina, G.-W. Kim, and J. S. Kim, "A new strategy for novel binder discovery in nano and μ powder injection molding: A metaheuristics-assisted virtual combinatorial materials search," Powder Technology, vol. 302, pp. 187-195, 2016.

[289] C. B. Williams, J. K. Cochran, and D. W. Rosen, "Additive manufacturing of metallic cellular materials via three-dimensional printing," The International Journal of Advanced Manufacturing Technology, vol. 53, pp. 231-239, 2011.

[290] J. Song, J. C. Gelin, T. Barrière, and B. Liu, "Experiments and numerical modelling of solid state sintering for 316L stainless steel components," Journal of Materials Processing Technology, vol. 177, pp. 352-355, 2006.

[291] ASTM, "standard test method for determination of tap density of metallic powders and compounds," ed, 2000.

[292] A. Al-Tounsi and M. S. J. Hashmi, "Effect of sintering temperature on the densification, shrinkage and compressive strength of stainless steel 300 series," Journal of Materials Processing Technology, vol. 37, pp. 551-557, 1993.

[293] T. Pieczonka, J. Kazior, A. Tiziani, and A. Molinari, "Dilatometric study of solid state sintering of austenitic stainless steel," Journal of Materials Processing Technology, vol. 64, pp. 327-334, 1997.

[294] C. H. Ji, N. H. Loh, K. A. Khor, and S. B. Tor, "Sintering study of 316L stainless steel metal injection molding parts using Taguchi method: final density," Materials Science and Engineering: A, vol. 311, pp. 74-82, 2001.

[295] N. Sultana and M. Wang, "Fabrication of Tissue Engineering Scaffolds Using the Emulsion Freezing/Freeze-drying Technique and Characteristics of the Scaffolds," in Integrated Biomaterials in Tissue Engineering, ed: John Wiley & Sons, Inc., 2012, pp. 63-89.

[296] D. Sin, X. Miao, G. Liu, F. Wei, G. Chadwick, C. Yan, et al., "Polyurethane (PU) scaffolds prepared by solvent casting/particulate leaching (SCPL) combined with centrifugation," Materials Science and Engineering: C, vol. 30, pp. 78-85, 2010.

[297] S. A. Poursamar, J. Hatami, A. N. Lehner, C. L. da Silva, F. C. Ferreira, and A. P. M. Antunes, "Gelatin porous scaffolds fabricated using a modified gas foaming technique: Characterisation and cytotoxicity assessment," Materials Science and Engineering: C, vol. 48, pp. 63-70, 2015.

[298] B. B. Mandal, A. Grinberg, E. Seok Gil, B. Panilaitis, and D. L. Kaplan, "High-strength silk protein scaffolds for bone repair," Proceedings of the National Academy of Sciences, vol. 109, pp. 7699-7704, May 15, 2012.

[299] P. Thomas, "Clinical and diagnostic challenges of metal implant allergy using the example of orthopaedic surgical implants: Part 15 of the Series Molecular Allergology," Allergo Journal International, vol. 23, pp. 179-185, 2014.

[300] S. Tada, R. Stegaroiu, E. Kitamura, O. Miyakawa, and H. Kusakari, "Influence of implant design and bone quality on stress/strain distribution in bone around implants: a 3-dimensional finite element analysis," International Journal of Oral & Maxillofacial Implants, vol. 18, 2003.

[301] R. Chumnanklang, T. Panyathanmaporn, K. Sitthiseripratip, and J. Suwanprateeb, "3D printing of hydroxyapatite: Effect of binder concentration in pre-coated particle on part strength," Materials Science and Engineering: C, vol. 27, pp. 914-921, 2007.

[302] M. Javaid and A. Haleem, "Additive manufacturing applications in medical cases: A literature based review," Alexandria Journal of Medicine, 2017.

[303] F.-H. Liu, R.-T. Lee, W.-H. Lin, and Y.-S. Liao, "Selective laser sintering of bio-metal scaffold," in 1st CIRP Conference on BioManufacturing, BioM 2013, March 3, 2013 - March 5, 2013, Tokyo, Japan, 2013, pp. 83-87.

[304] L. Liulan, T. Aili, Z. Huicun, H. Qingxi, and F. Minglun, "The mechanical properties of bone tissue engineering scaffold fabricating via selective laser sintering," in Life System Modeling and Simulation. International Conference, LSMS 2007, 14-17 Sept. 2007, Berlin, Germany, 2007, pp. 146-52.

[305] M. N. Cooke, J. P. Fisher, D. Dean, C. Rimnac, and A. G. Mikos, "Use of stereolithography to manufacture critical-sized 3D biodegradable scaffolds for bone ingrowth," Journal of Biomedical Materials Research Part B: Applied Biomaterials, vol. 64B, pp. 65-69, 2003.

[306] K. Kumagai, T. Asaoka, K. Furukawa, and T. Ushida, "Fabrication of scaffold for bone regeneration by taylor made stereolithography," Advances in Science and Technology, vol. 86, pp. 70-4, / 2013.

[307] L. Cuidi, G. Li, C. Fangping, and L. Changsheng, "Fabrication of mesoporous calcium silicate/calcium phosphate cement scaffolds with high mechanical strength by freeform fabrication system with micro-droplet jetting," Journal of Materials Science, vol. 50, pp. 7182-91, 11/ 2015.

[308] J. A. Inzana, D. Olvera, S. M. Fuller, J. P. Kelly, O. A. Graeve, E. M. Schwarz, et al., "3D printing of composite calcium phosphate and collagen scaffolds for bone regeneration," Biomaterials, vol. 35, pp. 4026-4034, 2014.

[309] L. Ju-Yeon, C. Bogyu, B. Wu, and L. Min, "Customized biomimetic scaffolds created by indirect three-dimensional printing for tissue engineering," Biofabrication, vol. 5, p. 045003 (9 pp.), 12/ 2013.

[310] l. Lin, b. Rong, Q. Hu, and M. Fang, "Microstructural Comparison and Analysis of Bone Scaffold Prepared by FDM and SLS Process," in 11th International Congress of the IUPESM. Medical Physics and Biomedical Engineering. World Congress 2009. Biomaterials, Cellular and Tissue Engineering, Artificial Organs, 7-12 Sept. 2009, Berlin, Germany, 2009, pp. 109-12.

[311] M. W. Sa, B. B. Nguyen, R. A. Moriarty, T. Kamalitdinov, J. P. Fisher, and J. Y. Kim, "Fabrication and evaluation of 3D printed BCP scaffolds reinforced with ZrO2 for bone tissue applications," Biotechnol Bioeng, vol. 115, pp. 989-999, Apr 2018.

[312] H.-J. Yen, C.-S. Tseng, S.-H. Hsu, and C.-L. Tsai, "Evaluation of chondrocyte growth in the highly porous scaffolds made by fused deposition manufacturing (FDM) filled with type II collagen," Biomedical Microdevices, vol. 11, pp. 615-624, 2009.

[313] X. Wang, M. Jiang, Z. Zhou, J. Gou, and D. Hui, "3D printing of polymer matrix composites: A review and prospective," Composites Part B: Engineering, vol. 110, pp. 442-458, 2017/02/01/ 2017.

[314] B. P. Hung, B. A. Naved, E. L. Nyberg, M. Dias, C. A. Holmes, J. H. Elisseeff, et al., "Three-Dimensional Printing of Bone Extracellular Matrix for Craniofacial Regeneration," ACS biomaterials science & engineering, vol. 2, pp. 1806-1816, 04/18 2016.

[315] W.-G. La, J. Jang, B. S. Kim, M. S. Lee, D.-W. Cho, and H. S. Yang, "Systemically replicated organic and inorganic bony microenvironment for new bone formation generated by a 3D printing technology," RSC Advances, vol. 6, pp. 11546-11553, 2016.

[316] T. Moloye and C. Batich, "Preparation and in vitro characterization of polycaprolactone and demineralized bone matrix scaffolds," in 2011 MRS Fall Meeting, November 28, 2011 - December 2, 2011, Boston, MA, United states, 2012, pp. 23-28.

[317] P. Tack, J. Victor, P. Gemmel, and L. Annemans, "3D-printing techniques in a medical setting: a systematic literature review," BioMedical Engineering OnLine, vol. 15, p. 115, 2016.

[318] D. Mahmoud and M. A. Elbestawi, "Lattice structures and functionally graded materials applications in additive manufacturing of orthopedic implants: a review," Journal of Manufacturing and Materials Processing, vol. 1, p. 13 (19 pp.), 12/ 2017.

[319] A. Thornton, Additive manufacturing (AM): Emerging technologies, applications and economic implications: Nova Science Publishers, Inc., 2015.

[320] W. Xiaojian, X. Shanqing, Z. Shiwei, X. Wei, M. Leary, P. Choong, et al., "Topological design and additive manufacturing of porous metals for bone scaffolds and orthopaedic implants: a review," Biomaterials, vol. 83, pp. 127-41, 03/ 2016.

[321] A. A. Zadpoor and J. Malda, "Additive Manufacturing of Biomaterials, Tissues, and Organs," Annals of Biomedical Engineering, vol. 45, 2017.

[322] J. H. G. C. Justin Nussbaum, Nathan Crane, "Evaluation of the Processing Variables in Large Area Polymer Sintering of Single Layer Components," in in Solid Freeform Fabrication, Austin, TX, 2016.

[323] B. Clarke, "Normal Bone Anatomy and Physiology," Clinical Journal of the American Society of Nephrology : CJASN, vol. 3, pp. S131-S139, 2008.

[324] H. K. Seung, P. Heng, P. G. Costas, K. L. Christine, M. J. F. Jean, and P. Dimos, "All-inkjet-printed flexible electronics fabrication on a polymer substrate by low-temperature high-resolution selective laser sintering of metal nanoparticles," Nanotechnology, vol. 18, p. 345202, 2007.

[325] L. A. Fred, L. Armin, N. Volkmar, F. H. Camila, and C. Tiago, "Selective laser sintering of Mo-CuNi composite to be used as EDM electrode," Rapid Prototyping Journal, vol. 20, pp. 59-68, 2014.

[326] D. Gu and Y. Shen, "Influence of Cu-liquid content on densification and microstructure of direct laser sintered submicron W–Cu/micron Cu powder mixture," Materials Science and Engineering: A, vol. 489, pp. 169-177, 2008.

[327] F. Dabbas, S. L. Stares, J. M. Mascheroni, D. Hotza, and G. V. Salmoria, "Selective Laser Sintering of Polyamide/Hydroxyapatite Scaffolds," in Proceedings of the 3rd Pan American Materials Congress, Cham, 2017, pp. 95-103.

[328] P. Feng, M. Niu, C. Gao, S. Peng, and C. Shuai, "A novel two-step sintering for nano-hydroxyapatite scaffolds for bone tissue engineering," Scientific Reports, vol. 4, p. 5599, 2014.

[329] J. An, J. E. M. Teoh, R. Suntornnond, and C. K. Chua, "Design and 3D Printing of Scaffolds and Tissues," Engineering, vol. 1, pp. 261-268, 2015/06/01/ 2015.

[330] S. Eosoly, D. Brabazon, S. Lohfeld, and L. Looney, "Selective laser sintering of hydroxyapatite/poly-ε-caprolactone scaffolds," Acta Biomaterialia, vol. 6, pp. 2511-2517, 2010.

[331] M. Saffarzadeh, G. J. Gillispie, and P. Brown, "Selective Laser Sintering (SLS) rapid protytping technology: A review of medical applications," in 53rd Annual Rocky Mountain Bioengineering Symposium, RMBS 2016 and 53rd International ISA Biomedical Sciences Instrumentation Symposium, April 8, 2016 - April 10, 2016, Denver, CO, United states, pp. 142-149, 2016

[332] S. Bose, S. Vahabzadeh, and A. Bandyopadhyay, "Bone tissue engineering using 3D printing," Materials Today, vol. 16, pp. 496-504, 2013.

[333] K. Maji, S. Dasgupta, K. Pramanik, and A. Bissoyi, "Preparation and characterization of gelatin-chitosan-nano-TCP based scaffold for orthopaedic application," Materials Science and Engineering: C (Materials for Biological Applications), vol. 86, pp. 83-94, 05/01 2018.

[334] M. Meskinfam, S. Bertoldi, N. Albanese, A. Cerri, M. C. Tanzi, R. Imani, et al., "Polyurethane foam/nano hydroxyapatite composite as a suitable scaffold for bone tissue regeneration," Materials Science and Engineering: C (Materials for Biological Applications), vol. 82, pp. 130-40, 2018.

[335] J. Pei, R. Jiabing, Y. Pan, Z. Lingyue, S. Xinyu, and T. Hua, "Rational design of a high-strength bone scaffold platform based on in situ hybridization of bacterial cellulose/nano-hydroxyapatite framework and silk fibroin reinforcing phase," Journal of Biomaterials Science, Polymer Edition, vol. 29, pp. 107-24, 2018.

[336] S. M. Barinov, I. V. Vakhrushev, V. S. Komlev, A. V. Mironov, V. K. Popov, A. Y. Teterina, et al., "3D printing of ceramic scaffolds for engineering of bone tissue," Inorganic Materials: Applied Research, vol. 6, pp. 316-322, 2015.

[337] I. Das, G. De, L. Hupa, and P. K. Vallittu, "Porous SiO2nanofiber grafted novel bioactive glass-ceramic coating: A structural scaffold for uniform apatite precipitation and oriented cell proliferation on inert implant," Materials Science and Engineering C, vol. 62, pp. 206-214, 2016.

[338] I.-K. Jun, Y.-H. Koh, S.-H. Lee, and H.-E. Kim, "Novel fabrication of a polymer scaffold with a dense bioactive ceramic coating layer," Journal of Materials Science: Materials in Medicine, vol. 18, pp. 1537-1542, 2007.

[339] D. M. Garcia Cruz, D. F. Coutinho, J. F. Mano, J. L. Gomez Ribelles, and M. Salmeron Sanchez, "Physical interactions in macroporous scaffolds based on poly(-caprolactone)/chitosan semi-interpenetrating polymer networks," Polymer, vol. 50, pp. 2058-2064, 2009.

[340] X. Liu, J. M. Holzwarth, and P. X. Ma, "Functionalized Synthetic Biodegradable Polymer Scaffolds for Tissue Engineering," Macromolecular Bioscience, vol. 12, pp. 911-919, 2012.

[341] S. V. Muley, A. N. Vidvans, G. P. Chaudhari, and S. Udainiya, "An assessment of ultra fine grained 316L stainless steel for implant applications," Acta Biomaterialia, vol. 30, pp. 408-19, 2016.

[342] Y. Yu, A. Neville, and D. Dowson, "Tribo-corrosion properties of cobalt-based medical implant alloys in simulated biological environments," Wear, vol. 263, pp. 1105-1111, 2007.

[343] H. Yazici, H. Fong, B. Wilson, E. E. Oren, F. A. Amos, H. Zhang, et al., "Biological response on a titanium implant-grade surface functionalized with modular peptides," Acta Biomaterialia, vol. 9, pp. 5341-52, 02/ 2013.

[344] T. Akimoto, T. Ueno, Y. Tsutsumi, H. Doi, T. Hanawa, and N. Wakabayashi, "Evaluation of corrosion resistance of implant-use Ti-Zr binary alloys with a range of compositions," Journal of Biomedical Materials Research - Part B Applied Biomaterials, vol. 106, pp. 73-79, 2018.

[345] O. Comakli, M. Yazici, T. Yetim, A. F. Yetim, and A. Celik, "Effect of Ti amount on wear and corrosion properties of Ti-doped Al2O3nanocomposite ceramic coated CP titanium implant material," Ceramics International, vol. 44, pp. 7421-7428, 2018.

[346] L. Jinwen, Z. Yong, H. Wangtu, Z. Wei, Z. Yongqing, and Z. Yusheng, "Electrochemical corrosion characteristics and biocompatibility of nanostructured titanium for implants," Applied Surface Science, vol. 434, pp. 63-72, 03/15 2018.

[347] E. J. P. Jansen, R. E. J. Sladek, H. Bahar, A. Yaffe, M. J. Gijbels, R. Kuijer, et al., "Hydrophobicity as a design criterion for polymer scaffolds in bone tissue engineering," Biomaterials, vol. 26, pp. 4423-4431, 2005.

[348] H.-Y. Mi, X. Jing, and L.-S. Turng, "Fabrication of porous synthetic polymer scaffolds for tissue engineering," Journal of Cellular Plastics, vol. 51, pp. 165-196, 2014.

[349] G. Turnbull, J. Clarke, F. Picard, P. Riches, L. Jia, F. Han, et al., "3D bioactive composite scaffolds for bone tissue engineering," Bioactive Materials, vol. 3, pp. 278-314, 2018.

[350] R. Colquhoun and K. E. Tanner, "Mechanical behaviour of degradable phosphate glass fibres and composites—a review," Biomedical Materials, vol. 11, p. 014105, 2016.

[351] S.-J. L. Kang, "1 - SINTERING PROCESSES," in Sintering, ed Oxford: Butterworth-Heinemann, 2005, pp. 3-8.

[352] V. Cannillo, P. Fabbri, and A. Sola, "Fabrication of 45S5 bioactive glass-polycaprolactone composite scaffolds," in ICCM-17 - 17th International Conference on Composite Materials, 2009.

[353] R. L. Prabhakar, S. Brocchini, and J. C. Knowles, "Effect of glass composition on the degradation properties and ion release characteristics of phosphate glass--polycaprolactone composites," Biomaterials, vol. 26, pp. 2209-18, 05/ 2005.

[354] S. Sayyar, E. Murray, B. C. Thompson, S. Gambhir, D. L. Officer, and G. G. Wallace, "Covalently linked biocompatible graphene/polycaprolactone composites for tissue engineering," Carbon, vol. 52, pp. 296-304, 02/ 2013.

[355] P. Lanlan, P. Xibo, H. Rui, W. Qianbing, and W. Jian, "Multiwall carbon nanotubes/polycaprolactone composites for bone tissue engineering application," Colloids and Surfaces B: Biointerfaces, vol. 93, pp. 226-34, 2012.

[356] L. Yihan, M. Leiguo, L. Hailang, L. Wenjia, Z. Yongjie, L. Hongchen, et al., "Integration of a calcined bovine bone and BMSC-sheet 3D scaffold and the promotion of bone regeneration in large defects," Biomaterials, vol. 34, pp. 9998-10006, 12/ 2013.

[357] C. V. M. Rodrigues, P. Serricella, A. B. R. Linhares, R. M. Guerdes, R. Borojevic, M. A. Rossi, et al., "Characterization of a bovine collagen–hydroxyapatite composite scaffold for bone tissue engineering," Biomaterials, vol. 24, pp. 4987-4997, 2003.

[358] W. D. K. a. M. Berg, Journal of Applied Physics, vol. 26, p. 1205, 1955.

[359] J. B. C. T.M. Che, R.M. Mininni, Sol–Gel Opt., vol. 1328, p. 145, 1990.

[360] A. Hoglund, M. Hakkarainen, and A.-C. Albertsson, "Degradation profile of poly(;-caprolactone)-the influence of macroscopic and macromolecular biomaterial design," Journal of Macromolecular Science, Part A: Pure and Applied Chemistry, vol. 44, pp. 1041-1046, 2007.

[361] J. Duan, Y.-n. Xie, J.-h. Yang, T. Huang, N. Zhang, Y. Wang, et al., "Graphene oxide induced hydrolytic degradation behavior changes of poly(l-lactide) in different mediums," Polymer Testing, vol. 56, pp. 220-228, 2016.

[362] H. Ming-Hsi, L. Suming, D. W. Hutmacher, J. Coudane, and M. Vert, "Degradation characteristics of poly(caprolactone)-based copolymers and blends," Journal of Applied Polymer Science, vol. 102, pp. 1681-7, 10/15 2006.

[363] J. M. Williams, A. Adewunmi, R. M. Schek, C. L. Flanagan, P. H. Krebsbach, S. E. Feinberg, et al., "Bone tissue engineering using polycaprolactone scaffolds fabricated via selective laser sintering," Biomaterials, vol. 26, pp. 4817-4827, 2005.

[364] H. F. F. a. H. L. L. G.H. Gessinger, Acta Metall, vol. 21, pp. 715-724, 1973.

[365] L. Polo-Corrales, M. Latorre-Esteves, and J. E. Ramirez-Vick, "Scaffold Design for Bone Regeneration," Journal of nanoscience and nanotechnology, vol. 14, pp. 15-56, 2014.

[366] F. Matassi, A. Botti, L. Sirleo, C. Carulli, and M. Innocenti, "Porous metal for orthopedics implants," Clinical Cases in Mineral and Bone Metabolism, vol. 10, pp. 111-115, 2013.

[367] B. V. Krishna, S. Bose, and A. Bandyopadhyay, "Low stiffness porous Ti structures for load-bearing implants," Acta Biomaterialia, vol. 3, pp. 997-1006, 2007.

[368] C. V. J., R. A. P., G. J. F., Z. Lai-Chang, and S. T. B., "Prototypes for Bone Implant Scaffolds Designed via Topology Optimization and Manufactured by Solid Freeform Fabrication," Advanced Engineering Materials, vol. 12, pp. 1106-1110, 2010.

[369] A. K. M. Khoda, I. T. Ozbolat, and B. Koc, "Designing heterogeneous porous tissue scaffolds for additive manufacturing processes," Computer-Aided Design, vol. 45, pp. 1507-1523, 2013.

[370] G. Papazetis and G. C. Vosniakos, "Direct porous structure generation of tissue engineering scaffolds for layer-based additive manufacturing," The International Journal of Advanced Manufacturing Technology, vol. 86, pp. 871-883, 2016.

[371] W. Jun, N. Aage, R. Westermann, and O. Sigmund, "Infill optimization for additive manufacturing-approaching bone-like porous structures," IEEE Transactions on Visualization and Computer Graphics, vol. 24, pp. 1127-40, 02/01 2018.

[372] X.-b. Su, Y.-q. Yang, P. Yu, and J.-f. Sun, "Development of porous medical implant scaffolds via laser additive manufacturing," Transactions of Nonferrous Metals Society of China, vol. 22, pp. s181-s187, 2012.

[373] A. A. Chen, V. L. Tsang, D. R. Albrecht, and S. N. Bhatia, "3-D Fabrication Technology for Tissue Engineering," in BioMEMS and Biomedical Nanotechnology: Volume III Therapeutic Micro/Nanotechnology, M. Ferrari, T. Desai, and S. Bhatia, Eds., ed Boston, MA: Springer US, 2007, pp. 23-38.

[374] G. C. Justin Nussbaum, Julie Harmon, Nathan Crane, "Evaluation of the Processing Variables in Large Area Polymer Sintering of Single Layer Components," in Solid Freeform Fabrication, Austin TX, 2016.

[375] M. Ziaee, E. M. Tridas, and N. B. Crane, "Binder-Jet Printing of Fine Stainless Steel Powder with Varied Final Density," JOM, vol. 69, pp. 592-6, 03/ 2017.

[376] G. Jacob, A. Donmez, J. Slotwinski, and S. Moylan, "Measurement of powder bed density in powder bed fusion additive manufacturing processes," Measurement Science and Technology, vol. 27, p. 115601 (12 pp.), 11/ 2016.

[377] T. Kokubo, H. Kushitani, S. Sakka, T. Kitsugi, and T. Yamamuro, "Solutions able to reproduce in vivo surface-structure changes in bioactive glass-ceramic A-W," J Biomed Mater Res, vol. 24, pp. 721-34, Jun 1990.

[378] S. Haeri, "Optimisation of blade type spreaders for powder bed preparation in Additive Manufacturing using DEM simulations," Powder Technology, vol. 321, pp. 94-104, 2017/11/01/ 2017.

[379] A. Bembey, A. Bushby, A. Boyde, V. Ferguson, and M. Oyen, "Hydration effects on the micro-mechanical properties of bone," Journal of Materials Research, vol. 21, pp. 1962-1968, 2006.

[380] G. L. a. J.W.Barlow, "Selective Laser Sintering of Calcium PhosphatePowders," in sff, Austin, TX, 1994.

[381] K. H. Tan, C. K. Chua, K. F. Leong, C. M. Cheah, P. Cheang, M. S. Abu Bakar, et al., "Scaffold development using selective laser sintering of polyetheretherketone–hydroxyapatite biocomposite blends," Biomaterials, vol. 24, pp. 3115-3123, 2003/08/01/ 2003.

[382] T. G. Spears and S. A. Gold, "In-process sensing in selective laser melting (SLM) additive manufacturing," Integrating Materials and Manufacturing Innovation, vol. 5, p. 2, 2016.

[383] B. M. L. Mahesh Mani, M A. Donmez, Shaw C. Feng, Shawn P. Moylan, Ronnie R. Fesperman Jr., "Measurement Science Needs for Real-time Control of Additive Manufacturing Powder Bed Fusion Processes," NIST Pubs, 2015.

[384] I. Yadroitsev, P. Bertrand, and I. Smurov, "Parametric analysis of the selective laser melting process," Applied Surface Science, vol. 253, pp. 8064-8069, 2007.

[385] N. JC, "Selective Laser Sintering: a definition of the process and empirical sintering model," PhD, The university of Texas, Austin, 1993.

[386] V. Speranza, A. Sorrentino, F. De Santis, and R. Pantani, "Characterization of the Polycaprolactone Melt Crystallization: Complementary Optical Microscopy, DSC, and AFM Studies," The Scientific World Journal, vol. 2014, p. 9, 2014.

[387] R. W. McVey, R. M. Melnychuk, J. A. Todd, and R. P. Martukanitz, "Absorption of laser irradiation in a porous powder layer," Journal of Laser Applications, vol. 19, pp. 214-224, 2007.

[388] A. B. a. E. A. Carolin Korner, "Fundamental consolidation mechanisms during selective beam melting of powders," Modelling and Simulation in Materials Science and Engineering, 2013.

APPENDIX A: COPYRIGHT PERMISSIONS

Below is the permission for use of Figure 2.2 in chapter 2.

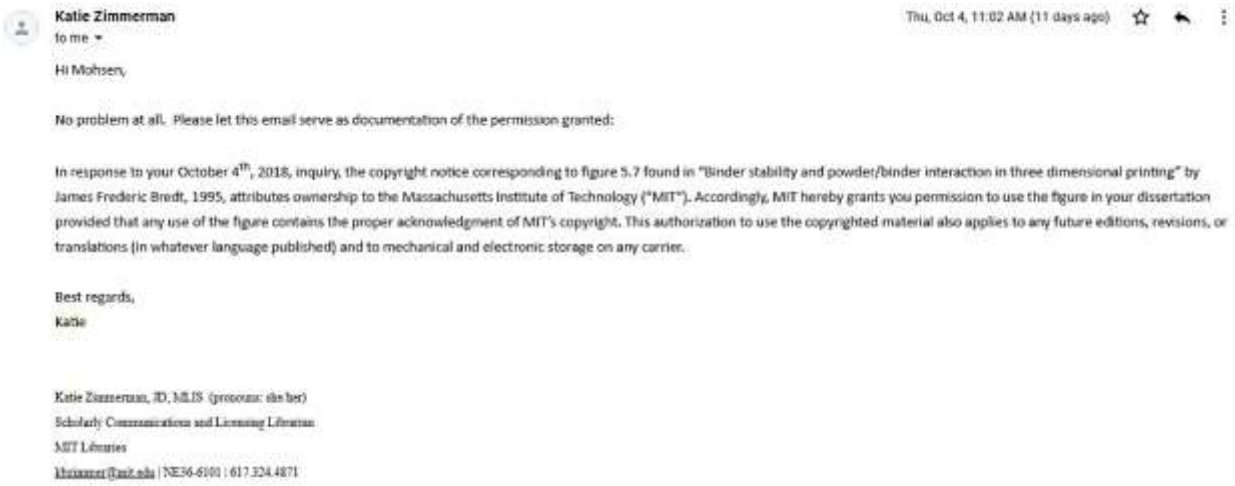

Katie Zimmerman
to me

Thu, Oct 4, 11:02 AM (11 days ago)

Hi Mohsen,

No problem at all. Please let this email serve as documentation of the permission granted:

In response to your October 4th, 2018, inquiry, the copyright notice corresponding to figure 5.7 found in "Binder stability and powder/binder interaction in three dimensional printing" by James Frederic Bredt, 1995, attributes ownership to the Massachusetts Institute of Technology ("MIT"). Accordingly, MIT hereby grants you permission to use the figure in your dissertation provided that any use of the figure contains the proper acknowledgment of MIT's copyright. This authorization to use the copyrighted material also applies to any future editions, revisions, or translations (in whatever language published) and to mechanical and electronic storage on any carrier.

Best regards,
Katie

Katie Zimmerman, JD, MLIS (pronouns: she/her)
Scholarly Communications and Licensing Librarian
MIT Libraries
kbzimmer@mit.edu | NE36-6101 | 617.324.4871

Below is the permission for use of chapter 3.

Copyright Clearance Center RightsLink®

Home | Account Info | Help

SPRINGER NATURE

Title: Binder-Jet Printing of Fine Stainless Steel Powder with Varied Final Density
Author: Mohsen Ziaee, Eric M. Tridas, Nathan B. Crane
Publication: JOM Journal of the Minerals, Metals and Materials Society
Publisher: Springer Nature
Date: Jan 1, 2016
Copyright © 2016, The Minerals, Metals & Materials Society

Logged in as:
mohsen Ziaee
Account #:
LOGOUT

Order Completed

Thank you for your order.

This Agreement between mohsen Ziaee ("You") and Springer Nature ("Springer Nature") consists of your license details and the terms and conditions provided by Springer Nature and Copyright Clearance Center.

Your confirmation email will contain your order number for future reference.

printable details

License Number	4375940563011
License date	Jun 25, 2018
Licensed Content Publisher	Springer Nature
Licensed Content Publication	JOM Journal of the Minerals, Metals and Materials Society
Licensed Content Title	Binder-Jet Printing of Fine Stainless Steel Powder with Varied Final Density
Licensed Content Author	Mohsen Ziaee, Eric M. Tridas, Nathan B. Crane
Licensed Content Date	Jan 1, 2016
Licensed Content Volume	69
Licensed Content Issue	3
Type of Use	Thesis/Dissertation
Requestor type	academic/university or research institute
Format	electronic
Portion	full article/chapter
Will you be translating?	no
Circulation/distribution	<501
Author of this Springer Nature content	yes
Title	Binder-Jet Printing of Fine Stainless Steel Powder with Varied Final Density
Instructor name	Dr. Nathan Crane
Institution name	University of South Florida
Expected presentation date	Jul 2018
Requestor Location	mohsen Ziaee United States Attn: mohsen Ziaee
Billing Type	Invoice
Billing address	mohsen Ziaee United States Attn: mohsen Ziaee
Total	0.00 USD

ORDER MORE | CLOSE WINDOW

Copyright © 2018 Copyright Clearance Center, Inc. All Rights Reserved. Privacy statement. Terms and Conditions.
Comments? We would like to hear from you. E-mail us at customercare@copyright.com

APPENDIX B: POWDER DEPOSITION SET-UP COMPONENTS

The layer formation machine (Figure A) was designed and built to form layers during the manufacturing process. The machine includes custom-made parts as well as the components available on market. The two side-by-side Z-positioners were motorized by stepper motors and moved the powder supply and the build stage within the rectangular hollow blocks. The layers are sequentially formed by moving the materials in XY-plane by means of a roller driven back and forth using a stepper motor and pulley system along the sliding rails. A 12V DC motor was employed to spin the roller to effectively spread the layers. The sequence of the movements required for layer formation and the idle time of the system - to allow scanning each layer - were synchronized by Marlin firmware and Arduino micro-controller kit.

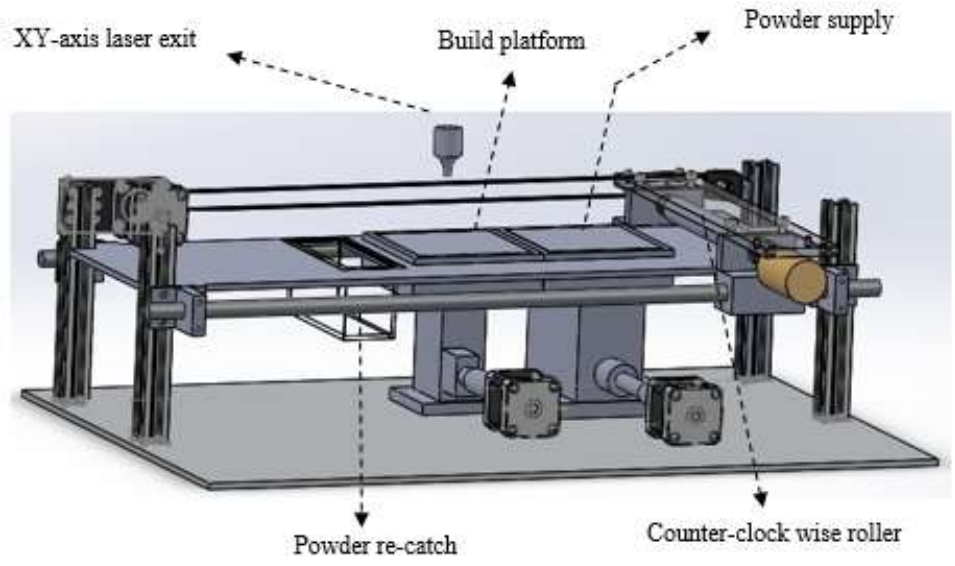

Figure A. The layout of the layer formation machine designed to allow layer-wise processing of the DBM/PCL mixtures

Upon operating the machine, the powder supply piston pushes up a sufficient amount of material to form a layer and simultaneously the build stage goes down to accommodate the fresh layer. Then the spinning roller transports the material from powder supply stage over the build platform (from right to left in the Figure A) and deposits the extra material in the powder re-catch to be retrieved. Then the roller retracts to move out of the laser exit way. Afterwards, the laser scans the 2D pattern based on the sliced CAD model. This process is repeated for all the layers until the physical model of the 3D computer model of the part is built. This appendix lists the components of the layer formation machine (Table A) and provides the drawings of the key custom-made components.

Table A. Bill of materials for the automated layer formation machine

No.	Item	Source
1	Top plate for motorized positioners	Custom-made
2	The intermediate plate for the build Z-positioner	
3	The intermediate plate for the powder supply piston	
4	Baseplate	
5	Shield plate	
6	Hollow square blocks	
7	Sliding rails	
8	Roller	
9	Roller support	
10	Roller to roller support attachment	
11	Belt to roller support attachment	
12	Hollow rectangular blocks	
13	The base plate to the shield plate connecting bars	
14	The connecting piece of the roller to the roller support	
15	The belt to roller support attachment	
16	The rail to pillars attachment piece	
17	Stepper motor to pillars connecting piece	
18	Powder re-catch	
19	Black angle corner connector	Openbuilds
20	Stepper motor	
21	Tee nut	
22	V-Slot 20×20 linear bars	

Table A (Continued)

No.	Item	Source
23	Belt	Openbuilds
24	Idle pulley	
25	Timing pulley	
26	Attachment plates	
27	Micro-switch	Omron
28	Linear bushings with pillow blocks	Misumi
29	Sliding rods	
30	12V DC motor	Zheng
31	Flexible coupling	Ebay

The limited space in the laser cutting machine and the small clearance over the powder bed necessitated to design and build some components for the set-up. The drawing of the customized components are presented in this appendix. For the all following components, the raw material is 6061 Aluminum and the dimensions shown on the drawings are in inches unless otherwise is stated.

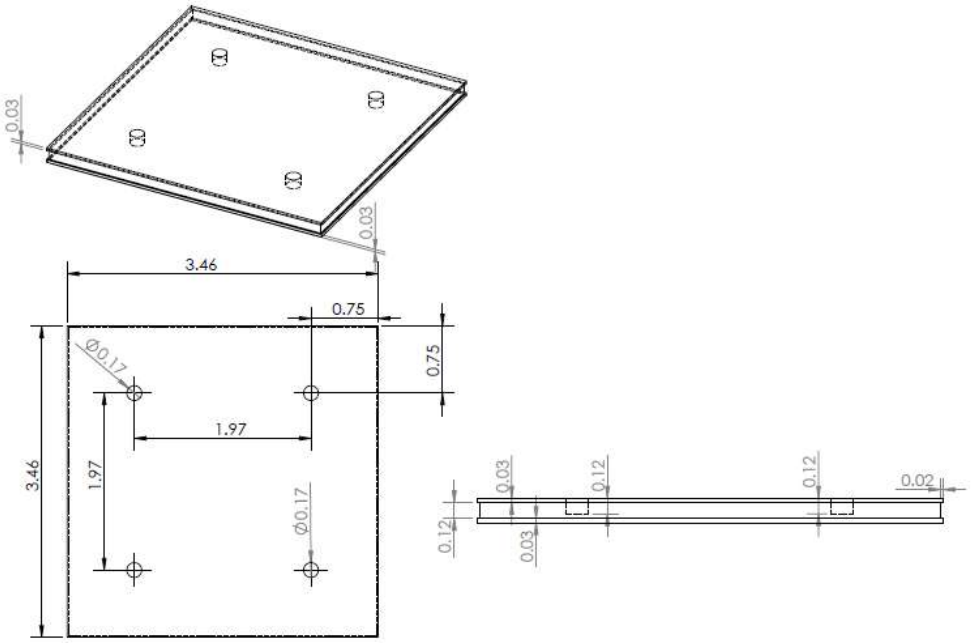

Figure B. The top plate for the motorized Z-positioners.

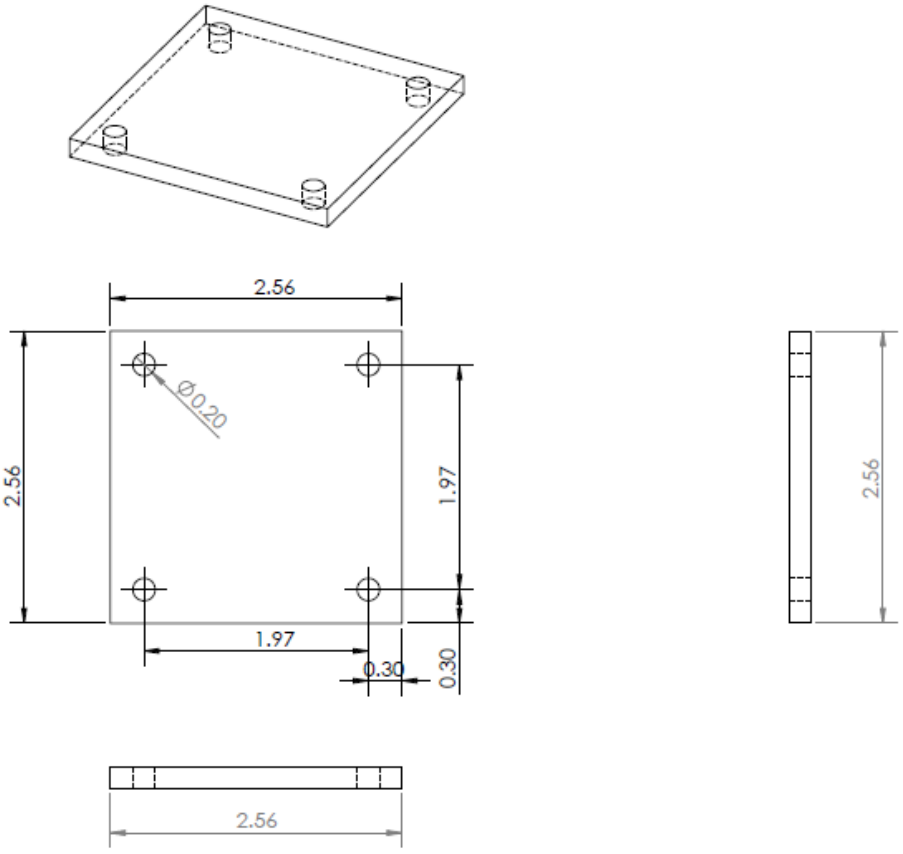

Figure C. The intermediate plate for the build Z-positioner.

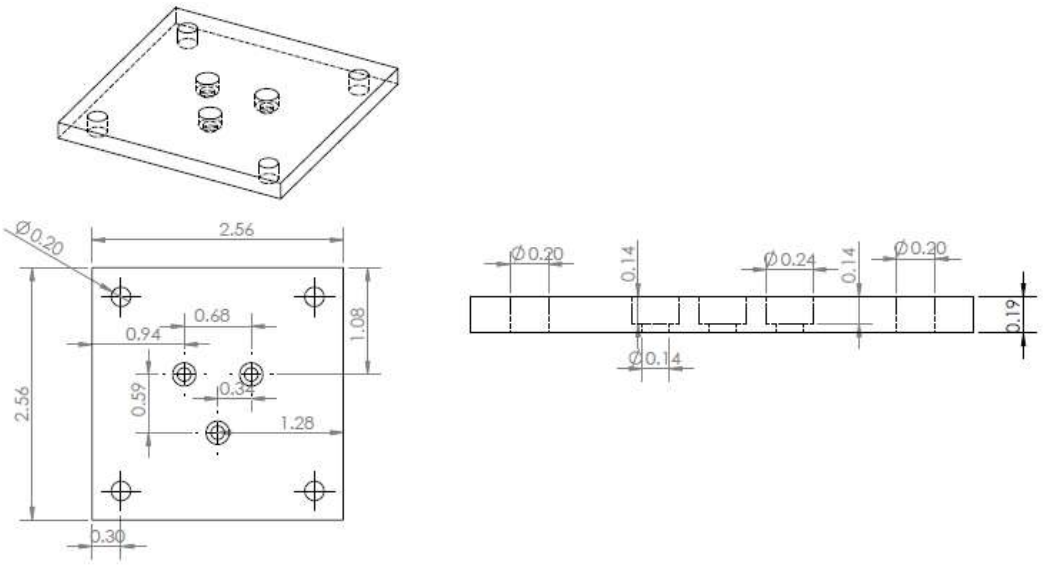

Figure D. The intermediate plate for the powder supply piston

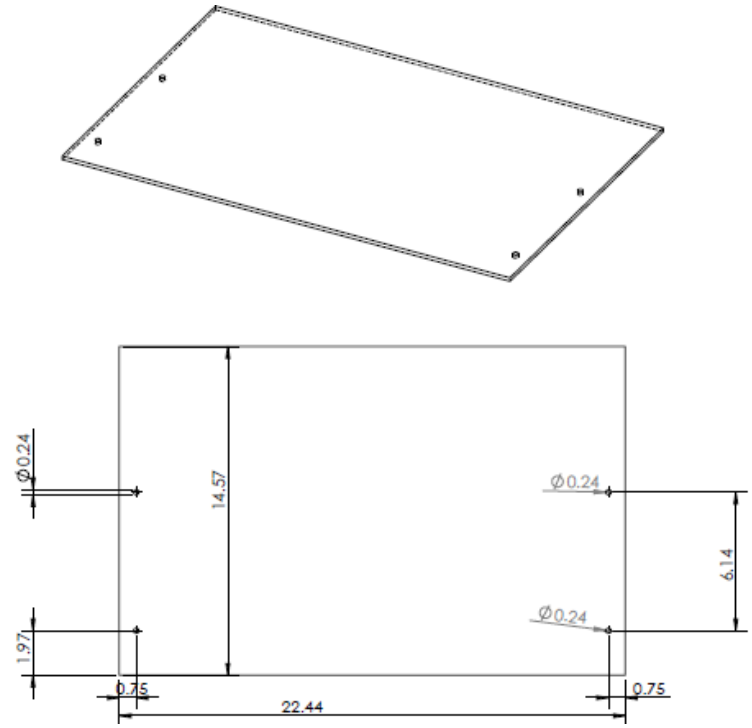

Figure E. The baseplate of the powder deposition machine made out of an Aluminum plate of 0.19 inches thick.

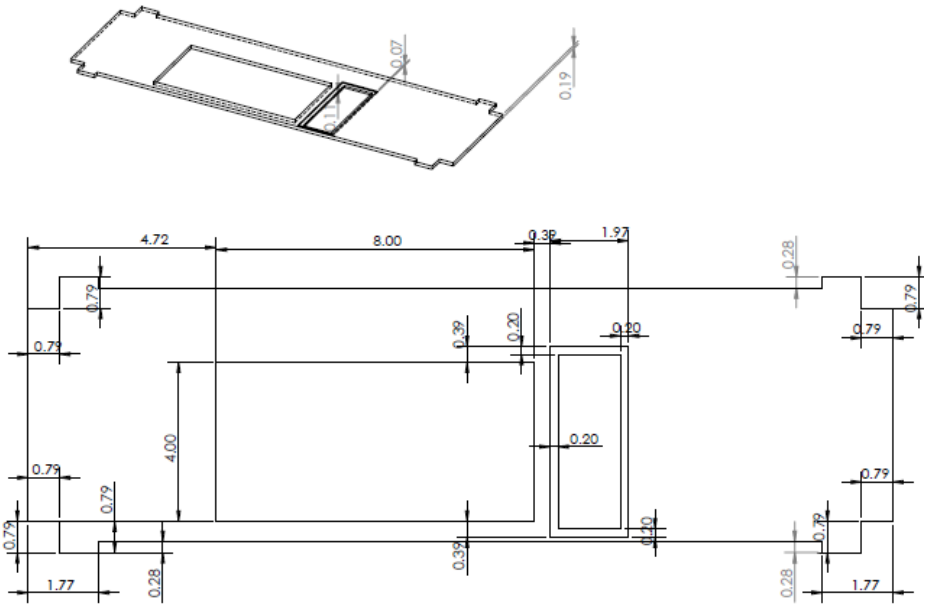

Figure F. The design of the shield plate with the thickness of 0.19 inches.

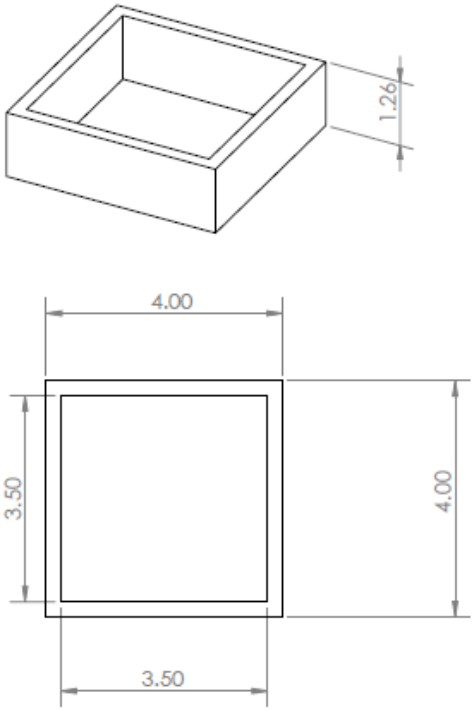

Figure G. The hollow square blocks that welded to the shield plate wherein the pistons move up and down.

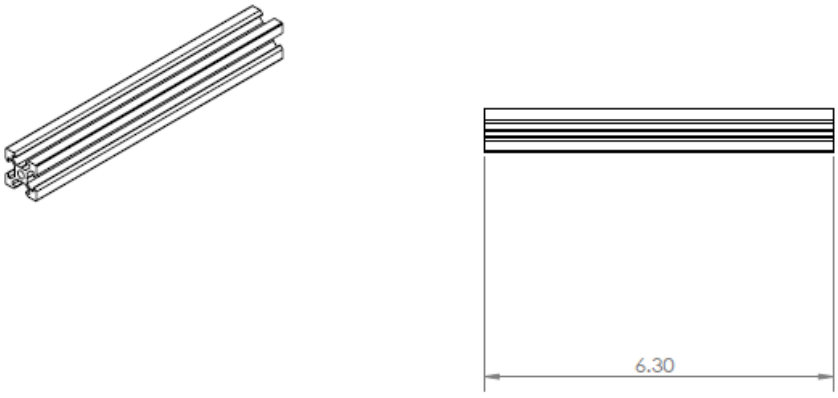

Figure H. The V-slot 20×20 linear bars used to connect the base plate to the shield plate of the set-up.

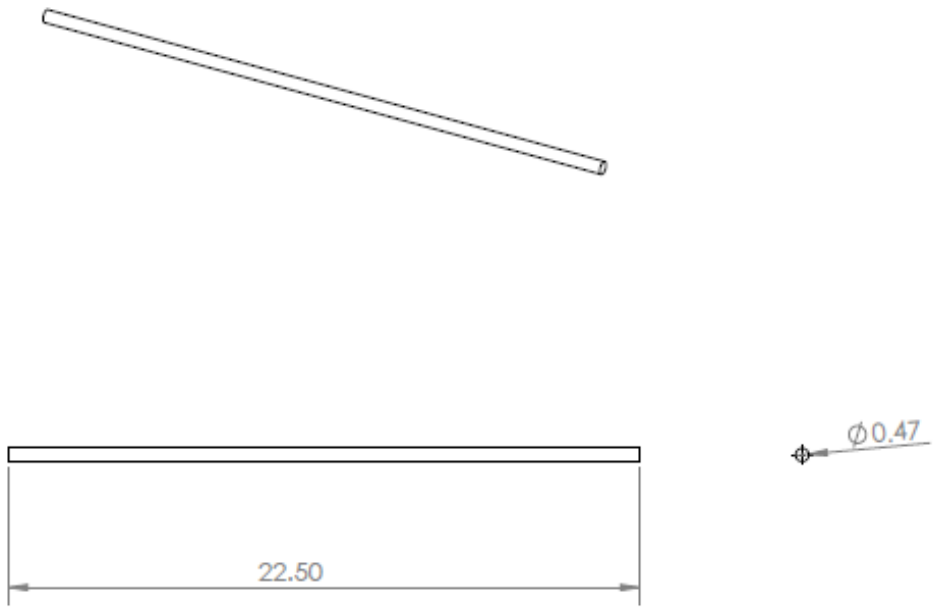

Figure I. The sliding rails prepared to guide the spreading device over the shield plate.

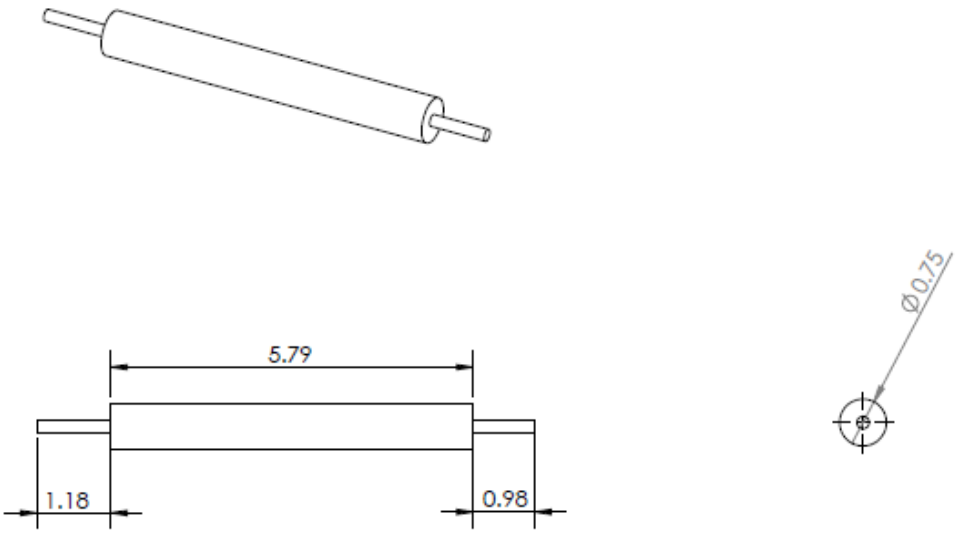

Figure J. The mirror-like steel rod machined to be used as a spreading tool.

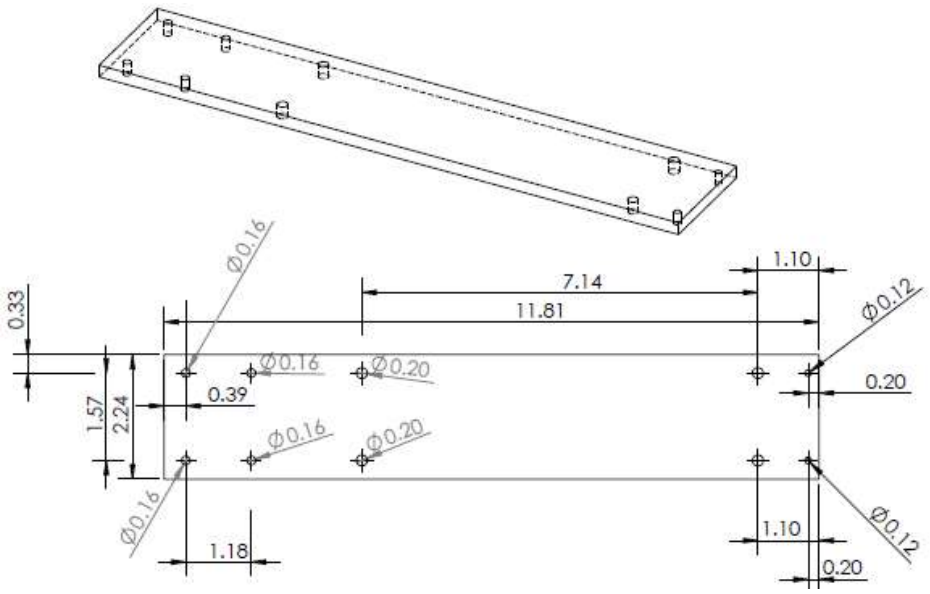

Figure K. The dimensions of an Aluminum plate of 0.19 inches thick, used to prevent uneven movement of the roller.

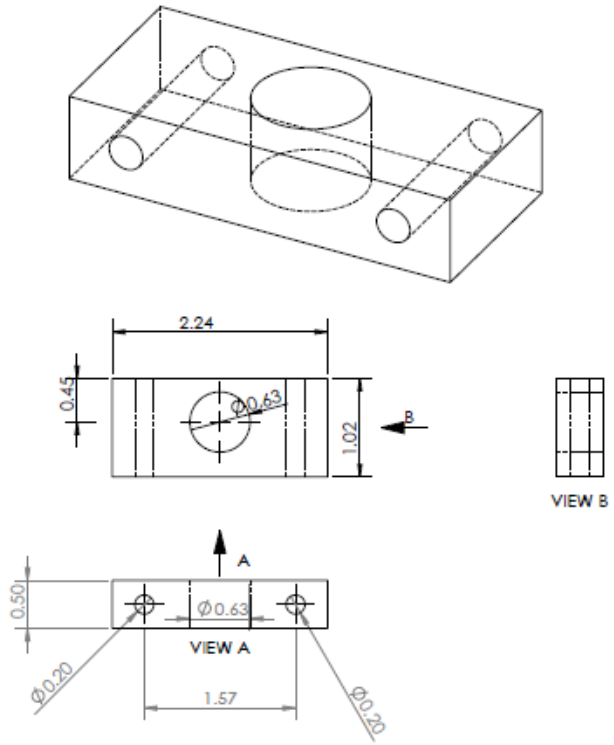

Figure L. The connecting piece of the spinning roller to the roller support.

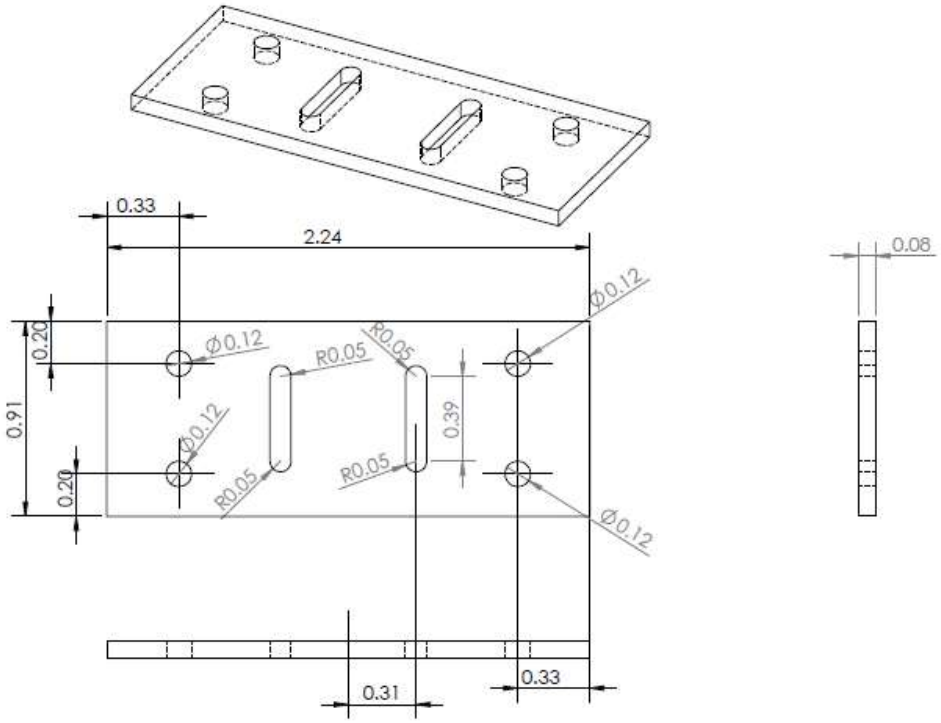

Figure M. The layout of the belt to roller support attachment.

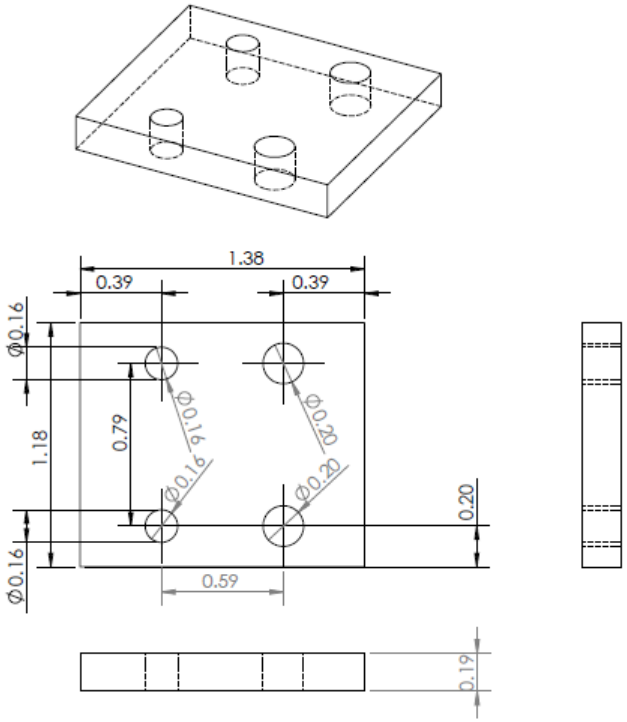

Figure N. The rail to the pillars attachment piece.

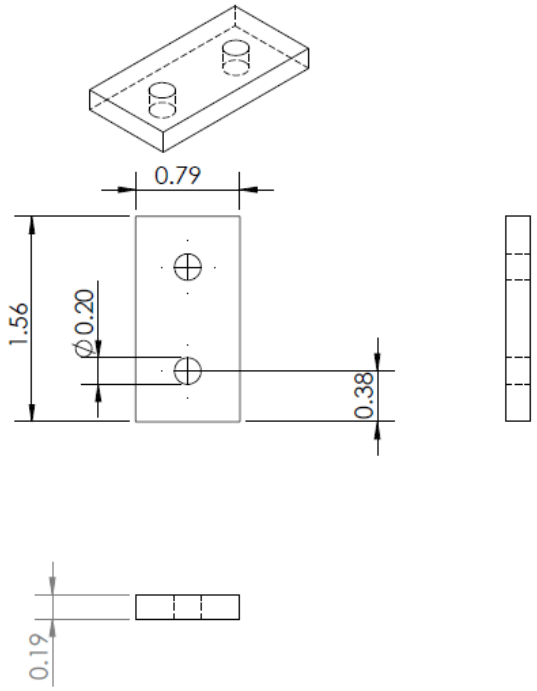

Figure O. Stepper motor to pillars connecting piece.

APPENDIX C: G-CODE FOR RUNNING POWDER DEPOSITION SET-UP

```
;Layer 1
G90
G1 y5 z2.5 f200
G4 S1
G1 X15 f200
G1 X0  f200
G4 S185
;Layer 2
G90
G1 y8.5 z5 f200
G4 S1
G1 X15 f200
G1 X0 f200
G4 S185
;Layer 3
G90
G1 y12 z7.5 f200
G4 S1
G1 X15 f200
G1 X0 f200
```

```
G4 S185
;Layer 4
G90
G1 y15.5 z10 f200
G4 S1
G1 X15 f200
G1 X0 f200
G4 S185
;Layer 5
G90
G1 y19 z12.5 f200
G4 S1
G1 X15 f200
G1 X0 f200
G4 S185
;Layer 6
G90
G1 y22.5 z15 f200
G4 S1
G1 X15 f200
G1 X0 f200
G4 S185
;Layer 7
```

```
G90
G1 y26 z17.5 f200
G4 S1
G1 X15 f200
G1 X0 f200
G4 S185
;Layer 8
G90
G1 y29.5 z20 f200
G4 S1
G1 X15 f200
G1 X0 f200
G4 S185
;Layer 9
G90
G1 y33 z22.5 f200
G4 S1
G1 X15 f200
G1 X0 f200
G4 S185
;Layer 10
G90
G1 y36.5 z25 f200
```

G4 S1

G1 X15 f200

G1 X0 f200

G4 S185

;Layer 11

G90

G1 y40 z27.5 f200

G4 S1

G1 X15 f200

G1 X0 f200

G4 S310

;Layer 12

G90

G1 y43.5 z30 f200

G4 S1

G1 X15 f200

G1 X0 f200